Development of a Dynamic Positioning System for an Emergency Recovery and Rescue Vessel

Nikolaos Kouretas

Diploma Thesis

School of Naval Architecture and Marine Engineering
National Technical University of Athens

Supervisor: Assistant Professor G. Papalambrou

Committee Members:

Professor G. Grigoropoulos
Professor G. Zarafonitis

February 2019

Acknowledgements

This thesis concludes my five years of studies at the School of Naval Architecture and Marine Engineering of the National Technical University of Athens. It has been, without doubt, a great academic journey, where i gained great knowledge in multiple engineering fields and further developed my soft skills.

The work described in this thesis was carried out at the Laboratory of Marine Engineering (LME) at the School of Naval Architecture and Marine Engineering of the National Technical University of Athens, under the supervision of Assistant Professor George Papalambrou.

I owe my greatest appreciation to my thesis supervisor, Assistant Professor George Papalambrou, for giving me the opportunity to work on a topic, which required a combination of both knowledge in marine engineering and skills in computer programming and microcontroller design, which i enjoy as a hobby. I would also like to thank him for his patience, continuous support and immense knowledge in control engineering. His guidance helped me in all the time working on this thesis.

I would like to thank Supertoys Boats and Mr. Vassilios Mentogiannis for the collaboration on the thesis's subject. While working together, I gained hands-on experience on the techniques of installing and testing vessel equipment on board.

I would also like to thank Mr. Nikolaos Planakis, researcher at LME and fellow naval engineer, for the fruitful discussions on my initial approach to dynamic positioning and controlling.

Finally, i express my sincere gratitude to my family, for the unceasing encouragement, support and motivation throughout my studies.

Abstract

In this thesis, the feasibility of implementing an alternative dynamic positioning system design into a high-speed rescue vessel with no blades or potential harmful gear, is investigated. The vessel will be ultimately given to the Hellenic Coast Guard for further enhancing their rescuing operations. The work described can be divided into two main parts. The first part is concentrated in building a simulation model, comprised of a vessel model, environmental loads model and a PID controller, which will be simulated using the MatLab Simulink environment, so as to confirm the potential application of the system proposed. The simulation scenarios are defined based on the typical weather conditions that are encountered during dynamic positioning operations in open seas.

The second part is devoted to preparing a smaller test boat, which will be used for testing the alternative DP system design before installing it on the final vessel. This part's targets are, firstly, to properly install the DP system on board, and secondly, to build a measuring device, named as data logger, which will include an inertial measurement unit (IMU). The device will be programmed and calibrated, in order to install it on board and measure the position and heading of the vessel during the initial sea experiments. It was decided to omit the use of a GPS unit at this stage, in order to exploit the possibilities of position estimation, only with the aid of small sensors installed on board.

Περίληψη

Στην παρούσα διπλωματική εργασία, εξετάζεται η εφικτότητα εγκατάστασης ενός εναλλακτικού συστήματος δυναμικής σταθεροποίησης θέσης σε ένα ταχύπλοο σκάφος, χωρίς πτερύγια ή πιθανώς επικίνδυνο εξοπλισμό. Το σκάφος θα δοθεί, εν τέλει, στην Ελληνική Ακτοφυλακή, για περαιτέρω ενίσχυση των επιχειρήσεων διάσωσης. Η εργασία μπορεί να διαχωρισθεί σε δύο κύρια μέρη. Το πρώτο μέρος επικεντρώνεται στην κατασκευή ενός μοντέλου προσομοίωσης, το οποίο αποτελείται από ένα μοντέλο σκάφους, μοντέλο περιβαλλοντικών διαταραχών και ελεγκτή PID, για τα οποία η προσομοίωση θα πραγματοποιηθεί στο περιβάλλον MatLab Simulink, έτσι ώστε να πιστοποιηθεί η δυνατότητα εγκατάστασης του συστήματος. Τα σενάρια προσομοίωσης έχουν ορισθεί, με βάση τις τυπικές περιβαλλοντικές διαταραχές που υφίστανται στις συγκεκριμένες εφαρμογές.

Το δεύτερο μέρος είναι αφιερωμένο στην προετοιμασία ενός μικρότερου δοκιμαστικού σκάφους, το οποίο θα χρησιμοποιηθεί για τη δοκιμή του εναλλακτικού συστήματος, πριν εγκατασταθεί στο τελικό σκάφος. Οι στόχοι αυτού του μέρους είναι, πρώτον, να εγκατασταθεί πλήρως το σύστημα σταθεροποίησης και, δεύτερον, να κατασκευασθεί ένα μετρητικό όργανο, ονομαζόμενο data logger, το οποίο περιέχει ένα IMU. Το μετρητικό όργανο θα προγραμματισθεί, με στόχο να τοποθετηθεί επί του σκάφους, ώστε να μετρά τη θέση και την πορεία πλεύσης, κατά τη διάρκεια των πειραμάτων. Σε αυτό το στάδιο, αποφασίστηκε να μη γίνει χρήση συστήματος, GPS, ώστε να διερευνηθεί η δυνατότητα εκτίμησης θέσης, μόνο με τη βοήθεια μικρών αισθητήρων, εγκατεστημένων επί του σκάφους.

Abbreviations

I²C Inter-Integrated Circuit.

CAD Computer Aided Design.

DOF Degrees Of Freedom.

DP Dynamic Positioning.

ECEF Earth Centered Earth Fixed.

ECI Earth Centered Inertial.

GPS Global Positioning System.

GUI Graphical User Interface.

IMU Inertial Measurement Unit.

LQG Linear-Quadratic-Gaussian.

LQR Linear Quadratic Regulator.

MEMS Microelectromechanical Systems.

MPC Model Predictive Control.

NED North-East-Down.

PCB Printed Circuit Board.

PID Proportional-Integral-Derivative.

RAO Response Amplitude Operator.

SCL Serial Clock.

SDA Serial Data.

SNAME Society of Naval Architects and Marine Engineers.

SPI Serial Peripheral Interface.

Contents

List of Figures

List of Tables

Chapter 1

Introduction

1.1 Historical View and Motivation

Dynamic positioning systems have been implemented in sea operations since the 1960s. The first applications were designed for large drilling vessels, which had to be kept stationary and maintain a fixed heading in order to successfully perform their tasks in deep waters. The vessel's control was achieved through conventional PID controllers in cascade with simple filters, commonly a low-pass filter, which was capable of excluding the high frequency components of sea waves as explained in [8].

The second age of dynamic-positioning schemes came in the 1970s when model-based LQG control was implemented in operations. This was introduced by Balchen [2] and further developed by Grimble [12], with many publications later on. Their models, although computationally heavier, allowed for more accurate approach towards the problem. The initial implementations used gain-scheduling approaches and later on the extended kalman filter, a technique which is common even in current solutions and not only in shipping industry. Since then, extended research in the 1990s and 2000s has led to the use of nonlinear controllers and estimators which adapt better to the nonlinear characteristics of vessel dynamics. Nowadays, as technology has vastly advanced, dynamic positioning is not only common in all types of commercial vessels but even in small crafts and yachts.

The versatile nature of dynamic positioning makes it a field of constant research, while it is a fundamental part towards the successful design of unmanned vessels, something that is currently a trending aspect for the shipping industry overall. Big projects are currently under development, namely the partnership of Rolls-Royce with Google, to bring an autonomous vessel by 2020 for cargo transport or passenger shipping, which will make use of Google's Cloud machine learning engine to extend the artificial intelligence algorithms for detecting, identifying and tracking the objects the vessel will encounter, [22]. Moreover, the ReVolt ship concept by DNV GL has been developed that proposes the use of an unmanned, fully battery powered and autonomous ship for short trading routes. This concept has been researched in collaboration with NTNU, [1].

The available open-source technologies, low-cost hardware for implementation and the current trending projects as well as the future perspective of dynamic positioning are the main motivators for this study.

1.2 Literature Review

Extended research has been conducted on the topic of dynamic positioning and several different approaches towards controlling have been proposed. Specifically, in [18], it has been verified that it is possible to control a speed-craft vessel only with the use of a PID controller and linear vessel model, without any wave filtering. Moreover, in [1], a PID controller was again used with success, coupled with an error-state Kalman filter. What's more, [29] and [27], have addressed the problem of dynamic positioning by using a model-predictive controller (MPC), whereas [7] presented the same concept but extended, to fit a nonlinear vessel model.

In [26], the simulation of an LQ controller installed on board of a surface effect ship, is elaborated. Also, another LQR approach is presented in [13] for DP, with three different models, which include actuator dynamics and integral action. An unconventional technique for controlling is presented in [14], where the vessel position stabilization is achieved by forcing the heading of the vessel to be towards the mean environmental loads vector, copying the motion of a pendulum. Finally, in [30], the concept of a neural network is used in conjunction with an adaptive controller based on Lyapunov back-stepping method, where the target of the neural network is to estimate the unknown nonlinear motion function of a remotely operated vehicle (ROV), under dynamic positioning.

1.3 Problem Description

This thesis constitutes part of a large European-founded project, named LINCOLN (Lean Innovative Connected Vessels), which aims to develop added-value specialized vessels that are able to run requested services for marine sectors in the most effective, efficient, economic valuable and eco-friendly way, [15]. Part of this project is to develop an emergency response and rescue vessel (ERRV), which is shown in Figure 1.1. NTUA is collaborating with Supertoys Boats, a boat trader in Greece, who is one of the partners in the project, in order to implement a dynamic positioning system on the vessel, which will ultimately be given to the Hellenic Coast Guard for further enhancing rescuing operations.

Figure 1.1: Supertoys Evolution boat for ERRV concept

1.4 Contributions

Based on the predefined project goal, the contributions of this thesis can be summarized by the following list:

- Implement an alternative design of a dynamic positioning system, with no blades or potentially harmful gear for the people being rescued
- Derive a preliminary mathematical model for the description of vessel dynamics
- Model environmental forces that are dominant in dynamic positioning operations
- Design a PID controller as a first step towards vessel controlling
- Simulate all the aforementioned elements in a closed loop using MatLAB
- Install the alternative DP system into a small test boat for concept evaluation
- Build a data logger with a simple Inertial Measurement Unit (IMU) for measuring position and heading of the small boat during initial sea trials

1.5 Thesis Outline

- **Chapter 2** introduces the basic principles of dynamic positioning, as well as the core parts that consist the full vessel control system. Moreover, the required coordinate reference frames for building and evaluating a mathematical simulation are defined.
- **Chapter 3** presents the mathematical modeling required for the simulations. A ship model is extracted based on ship's 6-DOF equations of motion as presented in [8] as well as the environmental forces acting on the vessel.
- **Chapter 4** gives an insight about the hardware equipment that will be installed and tested on a small boat to evaluate dynamic positioning feasibility. What's more, the sensor (IMU) that will be implemented inside the data logger for the initial sea tests is introduced and the process of calibration is explained.
- **Chapter 5** presents the designing process of a PID controller that encapsulates the dynamics of the vessel. Also, a reference model required for the simulation process is extracted, together with any other PID concept enhancements.
- **Chapter 6** presents the results of the simulation for the defined operating scenarios, as well as the results of the conducted sea trial.
- **Chapter 7** presents the concluding thoughts about this thesis's targets based on the simulation results and the suggested future work for the next steps of the project.

1.6 Notation

In this thesis, the SNAME notation (1950) will be used for analyzing ship's motions in six degrees of freedom, as depicted in Figure 1.2 and Table 1.1.

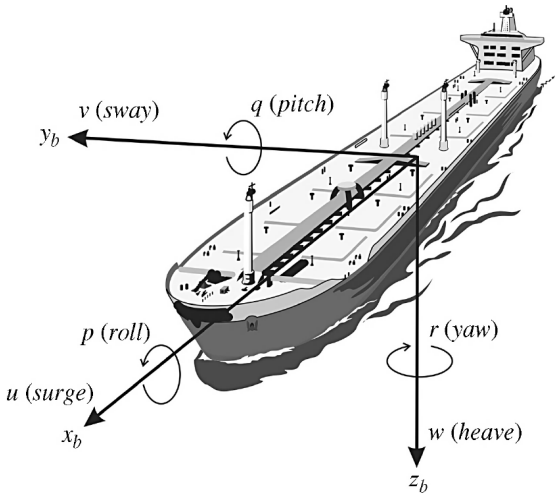

Figure 1.2: 6-DOF velocities in body-fixed reference frame $\{b\}$

Table 1.1: SNAME (1950) notation for marine vessels

DOF		Forces and moments	Linear and angular velocities	Position/ Euler angles
1	motion - x direction (surge)	X	u	x
2	motion - y direction (sway)	Y	v	y
3	motion - z direction (heave)	Z	w	z
4	rotation about x axis (roll)	K	p	ϕ
5	rotation about y axis (pitch)	M	q	θ
6	rotation about z axis (yaw)	N	r	ψ

Based on Table 1.1, the general motion of a vessel in 6 DOF can be described by the following vectors, which will be used in this thesis for the mathematical model formulation.

$$\boldsymbol{\eta} = [\, x, y, z, \phi, \theta, \psi \,]^T$$
$$\boldsymbol{\nu} = [\, u, v, w, p, q, r \,]^T$$
$$\boldsymbol{\tau} = [\, X, Y, Z, K, M, N \,]^T$$

Chapter 2

Principles of Dynamic Positioning

2.1 System Description

A dynamic positioning system can be described as a set of dedicated modules installed on board, with each one of them having a specific task to complete. All these modules are constantly interacting, transmitting information between one another in order to achieve the main operational target, which is the positional stabilization of the vessel. A schematic overview of all the modules is shown in Figure 2.1 and a brief description of each component is further given.

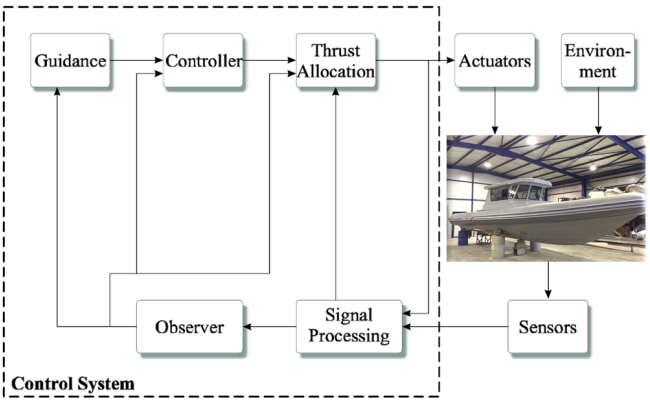

Figure 2.1: Schematic overview of a dynamic positioning system and its components

Controller

In position keeping applications, the controller is responsible for deriving the control signal which will be fed to the thrust allocation algorithm. This control signal is usually the required force in each of the motion directions involved in dynamic positioning, that is surge, sway and yaw. Moreover, the control law under which this signal is finally produced varies depending on the demands of the application. Specifically, in most cases a conventional feedback controller is using the position and velocity estimates from the observer and produces a signal based on the sum of those estimates and the reference input of the user. Additionally, it is common to further enhance the control signal by incorporating a feed-forward controller which accounts for wind disturbance and acts proactively before a wind gust has acted randomly upon the vessel.

Guidance

The guidance system usually consists of an advanced algorithm for vessel path calculation. This gives the option to the operator for tracking the vessel's trajectory during operations as well as entering the desired route to follow based on external incorporated maps, which are useful during low speed maneuvers and docking. Additionally, for countering sudden changes that might rise in position and velocity estimations, the guidance module is also smoothing the reference input to the controller in order to minimize the possibility of control saturation.

Observer

The concept of an observer is introduced in advanced guidance and positioning systems. In sea operations, its main objective is to reconstruct the position, heading and velocities of the vessel based on a motion mathematical model, and thus filtering out the high-frequency wave components which should not be compensated by the actuators. This is due to the fact that they cause excessive mechanical wear to the gear and in general extend the scope of dynamic positioning. Also, an observer can act as the main source of position and heading estimation, in cases where one or more of vessel's sensors malfunction and readings become unavailable (dead reckoning).

Signal Processing

The signal processing module is constantly monitoring the signals received from the vessel's sensors and actively performs quality testing ensuring no wild points, frozen signals or signal drift is entering the observer and finally the controller. Additionally, since the sensors are not transmitting their values in a unified frame but rather the frame depends upon the sensor's principal of operation and installation position, all the required geometrical transformations between the relevant coordinate frames are performed inside the signal processing unit.

Thrust Allocation

Thrust allocation is the final module of a dynamic positioning control system, in which the control signal derived from the controller is fed. This module is responsible for mapping the controller's demands in force and moment to set-points for the actuators installed on board. These set-points depend on the type of actuation used and typically are propeller speed, azimuth angle or rudder angle. Furthermore, this mapping should be done in an optimal manner, and thus optimization techniques are usually deployed in order to find the best-fit solution to the problem. The cost-function for optimization depends on the demands of each application and usually is considered to be the minimization of fuel consumption or electrical power levels on the actuators involved.

Apart from the aforementioned modules that form the control system, when simulations are performed for a dynamic positioning scheme, the following parameters should be also modeled for successfully building a complete frame for calculations.

Ship Dynamics

In a simulation, the actual vessel is missing and thus a sufficient model of it should be built, which yields as closely as possible the same motion scheme. In order to achieve that, ship motion theory should be taken into consideration, and specifically the six degrees of freedom equations of motion for a moving vessel. Due to the fact that the equations involved are strongly coupled, simplifications are made in most cases, assuming plane symmetries and ideal positions of center of gravity and center of buoyancy. In any case, the final mathematical model should encapsulate the vessel's motions in an adequate manner for the operational target that is set.

Environment

Similarly to ship dynamics, simulations do not involve real waves. Spectrum analysis for ocean waves is a dominant field of research with many representations for developing seas, fully-developed seas and swells, and thus wave modeling greatly depends on the application and operational target. The main environmental forces that should be taken into account when modeling a dynamic positioning system are due to ocean waves, wind and undersea currents.

Sensors and Actuators

The actuators a ship has installed need to be modeled in order to account for specific limitations posed by their operation. Specifically, when a control set-point is fed to an actuator from the thrust allocation algorithm, the resultant force is not acting instantly on the hull but is rather delayed based on the dynamics of the actuator. These dynamics are usually modeled by including rate limits, geometrical limits and delays into the simulation. Regarding vessel's sensors, the two most used in dynamic positioning operations are a gyroscopic compass and a GPS, which feed the heading and position of the vessel to the control system, respectively. When including these sensors inside a simulation loop, it is common to add a random white noise to the measurement fed to the system, similarly to what is happening in real world operations, where the actual measurements suffer from external noise.

All the aforementioned modules of a dynamic positioning system will be included in the simulations of this thesis and their modeling is analyzed in the following chapters.

2.2 Reference Frames

In vessel navigation, the values of parameters required for a specific operation are obtained through a wide complex of sensors installed on-board, with each one of them having different working principles. Due to this fact, it is mandatory that appropriate reference frames are defined, so the vessel operator or even a computer understands correctly the values that are being transmitted. In general, a reference frame is a predefined coordinate system of either two or three dimensions that is used to define the motion of said coordinate system relative to another coordinate system. Usually, one coordinate system is fixed to the navigating object and another one to the world the object is navigating in. When all systems are defined, the relation between two or more frames can be defined as a set of translational and rotational transformations.

2.2.1 Vessel Reference Frames

The main reference frame that constitutes the basis of terrestrial navigation is the ECI-frame $x_i y_i z_i$, shown in Figure 2.2, which is assumed inertial when compared with the remote fixed stars that is defined relative to. Its origin is located at the center of the Earth. Additionally, the ECEF frame $x_e y_e z_e$, is defined as a rotation of the ECI frame around the z axis, while x and y axes rotate around the z axis with the rotational speed of the Earth ω_e. Although ECEF frame is not inertial, it is generally assumed to be due to the negligible rotational speed of the Earth, depending always on the scope of the operation. Since the main focus in this thesis is an IMU and not a GPS, which transmits position data in the ECEF frame with the aid of satellites, and dynamic positioning operations are limited to a small geographic area, where the Earth's curvature doesn't affect navigation, these two reference frames will be not taken into account.

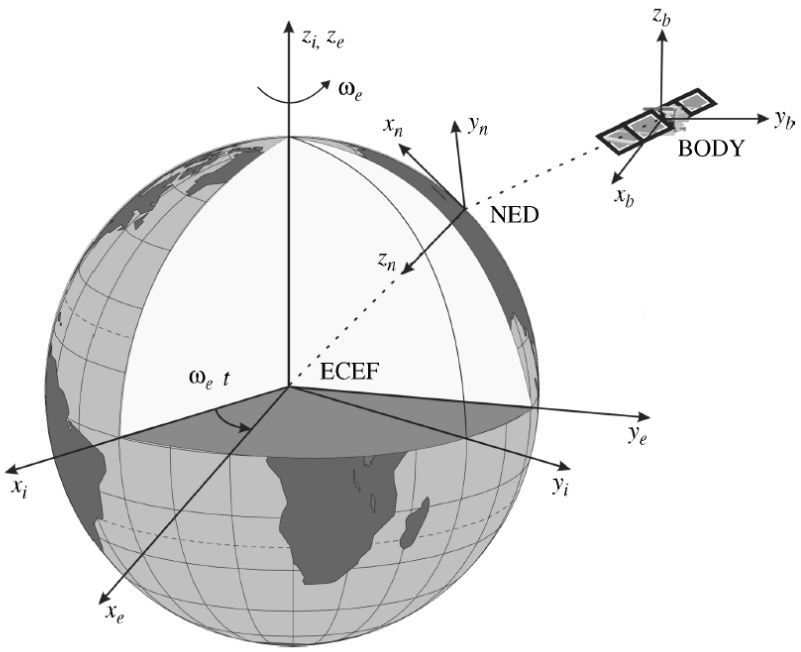

Figure 2.2: Coordinate system frames ECEF, ECI, NED, BODY used for navigation [8]

In this project, the following geographic reference frames will be used as part of navigation by means of compass and IMU sensor data.

NED

The NED coordinate system $\{n\} = (x_n, y_n, z_n)$ with origin o_n is defined relative to the ECEF frame (see Figure 2.2) and is the most commonly used reference system. Usually, it is defined as the tangent plane on the surface of the Earth, following the objects movement but with axes pointing in different directions than the body-fixed axes. The x axis points towards true North, the y axis points towards East and the z axis points downwards normal to the Earth's surface. The relation between NED and ECEF is obtained through two angles l and μ, known as longitude and latitude, respectively.

For marine craft dynamic positioning operations, changes in longitude and latitude are considered to be very small, and thus negligible. A fixed tangent plane on the Earth's surface is used for navigation, known as flat Earth navigation. At such cases, $\{n\}$ can be denoted as an inertial reference frame.

BODY

The BODY reference frame $\{b\} = (x_b, y_b, z_b)$ is a moving coordinate frame fixed to the vessel. The origin o_b is usually chosen to coincide with a point amidships in the waterline. The position and orientation of the vessel are described relative to the inertial reference frame $\{n\}$ while the linear accelerations and angular velocities of the vessel are expressed in the body-fixed coordinate system $\{b\}$. Finally, the body axes x_b, y_b, z_b are chosen to coincide with the principal axes of inertia and are defined as:

- x_b - longitudinal axis (directed from aft to fore)
- y_b - transversal axis (directed to starboard)
- z_b - normal axis (directed from top to bottom)

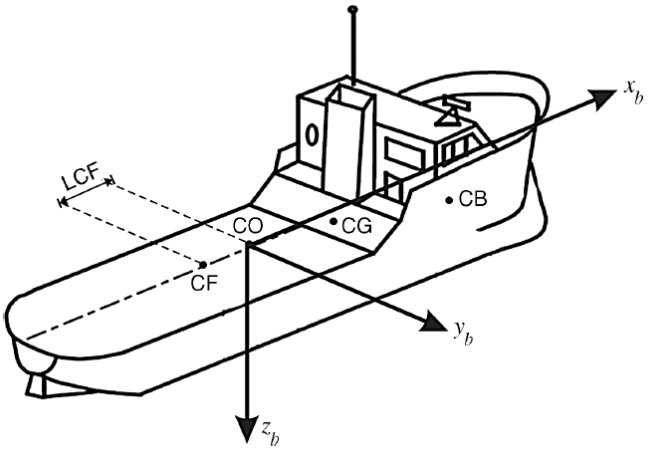

Figure 2.3: Body-fixed coordinate system $\{b\}$ [8]

Additionally, the four hull points shown in Figure 2.3, are defined below and will be used for building the mathematical model of the vessel for simulations, since they are the origins for defining specific matrices included in the model. In order to reduce the complexity of transformations, CO is decided to be the final reference point under which all the calculations will take place. In such case, the distance of each actuator is constant and does not depend on vessel's loading or operational condition.

- CG: Center of gravity
- CB: Center of buoyancy
- CO: Point coinciding with the vessel's midship section
- CF: Center of floatation

2.2.2 Transformations

The two reference frames that have been defined in the previous section need to have a direct mathematical relation in order to transform the measured data from one to another and perform the required calculations. Both the NED and BODY frames are considered to be lying on the horizontal plane, on the close region of operation of the vessel, where the Earth's curvature, as mentioned before, is ignored. As a result, the transformation of coordinates between these two frames can be simply done by means of a rotation matrix. Additionally, in dynamic positioning, roll ϕ and pitch θ angles are negligible and will not be included in the simulations, and thus the rotation matrix is built based only on the yaw angle ψ.

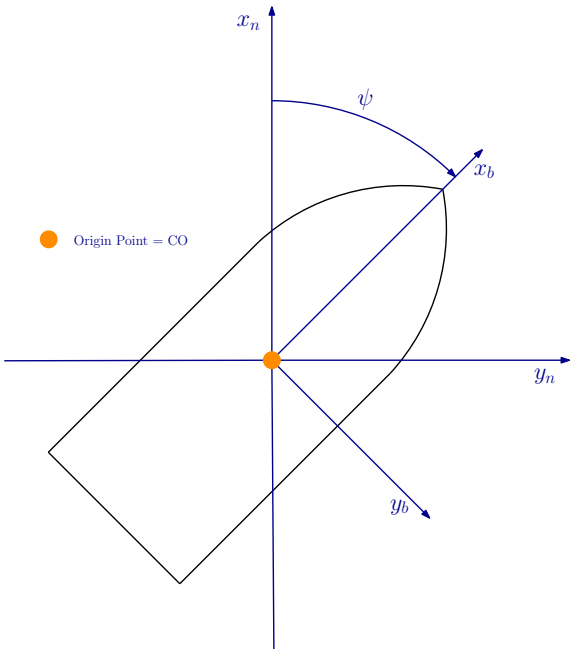

Figure 2.4: Inertial NED $\{n\}$ and BODY frame $\{b\}$

Rotation Matrix

The rotation matrix, in general, is an element of the *special orthogonal group of order 3*, which is defined as [28]:

$$SO(3) = \{R|R^T \in \mathbb{R}^{3x3}, \quad R \quad is \quad orthogonal \quad and \quad det(R) = 1\} \tag{2.1}$$

which again is a subset of the *orthogonal group of order 3*, defined as:

$$O(3) = \{R|R^T \in \mathbb{R}^{3x3}, \quad RR^T = R^T R = I\} \tag{2.2}$$

Consequently, the rotation matrix for defining the transformation vectors and coordinates between NED and BODY frame, can be composed by the yaw angle ψ, as shown in Figure 2.4. Positive rotation angle is defined based on right-hand rule and the relevant axes. For a 3-DOF problem, which is the case of a dynamic positioning system, the transformation from BODY to NED frame is accomplished through the rotation matrix, defined as:

$$\boldsymbol{J}_b^n(\psi) = \begin{bmatrix} cos(\psi) & -sin(\psi) & 0 \\ sin(\psi) & cos(\psi) & 0 \\ 0 & 0 & 1 \end{bmatrix} \tag{2.3}$$

Moreover, based on linear algebra, the transpose matrix of $\boldsymbol{J}_b^n(\psi)$, expressed as $(\boldsymbol{J}_b^n(\psi))^T = \boldsymbol{J}_n^b(\psi)$ can be used to define a rotation from NED to BODY coordinate frames. As a result the two following equations can be used for transforming the velocities measured from sensors on board and consequently in the body-fixed frame, to the vessel's position in NED frame that will be fed to the controller. These equations are known as the kinematic equations of motion for a vessel performing dynamic positioning.

$$\dot{\boldsymbol{\eta}} = \boldsymbol{J}_b^n(\psi)\boldsymbol{\nu} \tag{2.4}$$

$$\boldsymbol{\nu} = \boldsymbol{J}_n^b(\psi)\dot{\boldsymbol{\eta}} \tag{2.5}$$

where $\boldsymbol{\eta}$ and $\boldsymbol{\nu}$ are defined in Chapter 1.

2.3 Euler Angles

Euler angles provide a way to represent the 3-D orientation of an object using a combination of three rotations about different axes. In the simulations, only the rotation about yaw axis will be taken into account, as explained in the previous paragraph. But when deriving the algorithm for the IMU that estimates position and heading in real scenarios, all three angles, roll, pitch and yaw need to be included so as to derive a more accurate estimate. Consequently, the matrices for such case are presented below.

Moreover, the sequence under which the rotation about each axis is performed, leads to different rotational matrices. Here, the sequence mostly adapted to aviation and terrestrial navigation is analyzed and used, that is first yaw, then pitch and finally roll. Lastly, two virtual intermediate coordinate frames will be used to clarify the defined rotations.

Starting from the NED frame $\{n\}$, a vector rotation by ψ degrees leading to the intermediate frame 1 $\{u_1\}$ is achieved by multiplying by the matrix:

$$\boldsymbol{R}_n^{u1} = \begin{bmatrix} cos(\psi) & sin(\psi) & 0 \\ -sin(\psi) & cos(\psi) & 0 \\ 0 & 0 & 1 \end{bmatrix} \tag{2.6}$$

Continuing, a second rotation by θ degrees in pitch direction from the intermediate frame $1\{u_1\}$ to the intermediate frame 2 $\{u_2\}$, is achieved by multiplying by the matrix:

$$\boldsymbol{R}_{u1}^{u2} = \begin{bmatrix} cos(\theta) & 0 & -sin(\theta) \\ 0 & 1 & 0 \\ sin(\theta) & 0 & cos(\theta) \end{bmatrix} \tag{2.7}$$

Finally, a third rotation by ϕ degrees in roll direction from the intermediate frame 2 $\{u_2\}$ to the BODY frame, is achieved by multiplying by the matrix:

$$\boldsymbol{R}_{u2}^{b} = \begin{bmatrix} 1 & 0 & 0 \\ 0 & cos(\phi) & sin(\phi) \\ 0 & -sin(\phi) & cos(\phi) \end{bmatrix} \tag{2.8}$$

Combining the above rotations, the total rotation matrix transforming a vector from NED to BODY frame is:

$$\boldsymbol{R}_n^b(\phi,\theta,\psi) = \begin{bmatrix} c(\psi)c(\theta) & c(\theta)s(\psi) & -s(\theta) \\ c(\psi)s(\phi)s(\theta) - c(\phi)s(\psi) & c(\phi)c(\psi) + s(\phi)s(\psi)s(\theta) & c(\theta)s(\phi) \\ s(\phi)s(\psi) + c(\phi)c(\psi)s(\theta) & c(\phi)s(\psi)s(\theta) - c(\psi)s(\phi) & c(\phi)c(\theta) \end{bmatrix} \tag{2.9}$$

where c(.) and s(.), denote the cos and sin function, respectively.

Following the transformations in the opposite direction, one can obtain a vector from BODY to NED frame.

In a different scenario, where the obtained angular rates from the gyroscope that is fixed on the body, are required to be transformed to Euler angle rates, a different approach is required. Since each rotation from BODY to NED or NED to BODY frames is performed about a different axis, the total angular rate transformation is achieved as shown below:

$$\begin{bmatrix} p \\ q \\ r \end{bmatrix} = \begin{bmatrix} \dot{\phi} \\ 0 \\ 0 \end{bmatrix} + \boldsymbol{R}_{u2}^{b} \begin{bmatrix} 0 \\ \dot{\theta} \\ 0 \end{bmatrix} + \boldsymbol{R}_{u2}^{b} \boldsymbol{R}_{u1}^{u2} \begin{bmatrix} 0 \\ 0 \\ \dot{\psi} \end{bmatrix} = \boldsymbol{J}^{-1} \begin{bmatrix} \dot{\phi} \\ \dot{\theta} \\ \dot{\psi} \end{bmatrix} \tag{2.10}$$

Inverting matrix J, the final equation for obtaining Euler angle rates $\dot{\phi}, \dot{\theta}, \dot{\psi}$ from body frame rates p,q,r, is:

$$\begin{bmatrix} \dot{\phi} \\ \dot{\theta} \\ \dot{\psi} \end{bmatrix} = \boldsymbol{J} \begin{bmatrix} p \\ q \\ r \end{bmatrix} = \begin{bmatrix} 1 & sin(\phi)tan(\theta) & cos(\phi)tan(\theta) \\ 0 & cos(\phi) & -sin(\phi) \\ 0 & sin(\phi)sec(\theta) & cos(\phi)sec(\theta) \end{bmatrix} \begin{bmatrix} p \\ q \\ r \end{bmatrix} \tag{2.11}$$

$$\Rightarrow \begin{bmatrix} \dot{\phi} \\ \dot{\theta} \\ \dot{\psi} \end{bmatrix} = \begin{bmatrix} p + qsin(\phi)tan(\theta) + rcos(\phi)tan(\theta) \\ qcos(\phi) - rsin(\phi) \\ qsin(\phi)sec(\theta) + rcos(\phi)sec(\theta) \end{bmatrix} \tag{2.12}$$

Observing equation (2.12), leads to a common issue that is introduced when using Euler angles for such transformations. That is, for this rotation sequence, when pitch angle θ approaches values of $\pm 90°$, sec function is approaching infinity values, causing the calculations to fail. But in the case of vessel, such angles are impossible to be encountered during normal operation and thus there is no need for correction.

Chapter 3

Mathematical Modeling

When developing control systems that interact with real world dynamics, it is often helpful to derive a mathematical model which is an approximated description of the physical phenomena. This enables simulations of a variety of scenarios, where system performance can be tested and improved solely, without the interference of external factors present only in a small range of operational conditions. Additionally, the computational cost of the simulations is greatly reduced, thus making the controller modeling simpler and more robust.

In naval architecture, ship's motions can be studied by using either maneuvering or seakeeping theory. In maneuvering theory, ship's hydrodynamic coefficients are considered to be frequency independent, whereas in seakeeping theory they are computed as a function of the wave excitation frequency based on hull geometry and mass distribution. Both methods have linear and non-linear model representations in 6 DOF. Moreover, one can unify both theories which enables time-domain simulation of a marine craft. In such case, care must be taken so as not to account for hydrodynamic effects twice, as both theories consider some of them.

3.1 Vessel Model

According to Fossen, [8], the equations of motions can be represented in a vectorial setting, suitable for computer implementation and controller design which also includes the physical properties of both aforementioned theories. The vectorial model is expressed in the BODY $\{b\}$ and NED $\{n\}$ frames, with the appropriate kinematic transformations between these two. Considering the full 6 DOF model representation, the basic motion equation is given below:

$$\boldsymbol{M}\dot{\boldsymbol{\nu}} + \boldsymbol{C}(\boldsymbol{\nu})\boldsymbol{\nu} + \boldsymbol{D}(\boldsymbol{\nu})\boldsymbol{\nu} + \boldsymbol{g}(\boldsymbol{\eta}) + \boldsymbol{g}_0 = \boldsymbol{\tau} + \boldsymbol{w} \tag{3.1}$$

Since dynamic positioning is a two dimensional problem in the horizontal plane, only 3 DOF are required to express the motions of the vessel, specifically surge, sway and yaw. In the following sections, the various terms of equation (3.1) are explained, while also specific parameters are omitted, in order to build an adequate initial mathematical vessel model for the simulations. Additionally, the mathematical model's matrices will be analyzed, with the body fixed reference frame origin coinciding with a point amidships, defined as CO in section [2.2.1]. This makes it simpler to refer to any matrix at any point, given the fact that center of gravity depends on vessel's loading condition.

3.1.1 Inertia Matrix M

The inertia matrix M is the sum of the rigid-body inertia matrix and the added-mass inertia matrix, defined as:

$$\boldsymbol{M} = \boldsymbol{M}_{RB} + \boldsymbol{M}_{A} \tag{3.2}$$

The rigid-body inertia matrix includes the actual mass of the vessel and also the moments of inertia around the defined body frame axes with respect to the vessel's center of buoyancy. In 6 DOF the matrix is composed as below:

$$\boldsymbol{M}_{RB} = \begin{bmatrix} m & 0 & 0 & 0 & mz_{bg} & -my_{bg} \\ 0 & m & 0 & -mz_{bg} & 0 & mx_{bg} \\ 0 & 0 & m & my_{bg} & -mx_{bg} & 0 \\ 0 & -mz_{bg} & my_{bg} & I_x & -I_{xy} & -I_{xz} \\ mz_{bg} & 0 & -mx_{bg} & -I_{yx} & I_y & -I_{yz} \\ -my_{bg} & mx_{bg} & 0 & -I_{zx} & -I_{zy} & I_z \end{bmatrix} \tag{3.3}$$

where m is the vessel's mass, $\boldsymbol{r}_g^b = (x_{bg}, y_{bg}, z_{bg})$ is the distance vector between the vessel's center of buoyancy and center of gravity and the rest terms are moments or products of inertia around the center of buoyancy.

Regarding dynamic positioning, this matrix can be greatly reduced in complexity. Firstly, the terms referring to motions except surge, sway and yaw are not required. Secondly, by choosing the origin of the body-fixed coordinate system to be the center of gravity, the terms including the distance vector $\boldsymbol{r}_g^b$ can also be omitted. Lastly, the body axes can be chosen to coincide with the principal axes of inertia, thus the remaining products of inertia are zero. By applying these simplifications, the resultant inertia matrix is shown below:

$$\boldsymbol{M}_{RB}^{CG} = \begin{bmatrix} m & 0 & 0 \\ 0 & m & 0 \\ 0 & 0 & I_z^{CG} \end{bmatrix} \tag{3.4}$$

The added mass matrix $\boldsymbol{M}_A$ includes the inertia of the surrounding fluid, and contributes to equation (3.2) only when the vessel is accelerating relative to the water mass. In general, the hydrodynamic added mass depends on the frequency of motion due to water surface effects and can be calculated considering different approaches, such as 2-D potential strip theory (e.g.Newman, 1977), 3-D potential panel methods (e.g. WAMIT application) or even semi-empirical methods (e.g. Imlay, 1961). All these methods exceed the scope of this thesis and are only given for reference.

According to Fossen [9], the added mass matrix can be approximated by a constant frequency independent matrix based on the following assumption: the vessel has port-starboard symmetry, and thus the vessel's surge motion can be decoupled from the rest motions. In this case, such assumption is valid and the final form of the added mass matrix for 6 DOF is as shown below:

$$\boldsymbol{M}_A^{CB} = -\begin{bmatrix} X_{\dot{u}} & 0 & 0 & 0 & 0 & 0 \\ 0 & Y_{\dot{v}} & 0 & Y_{\dot{p}} & 0 & Y_{\dot{r}} \\ 0 & 0 & Z_{\dot{w}} & 0 & Z_{\dot{q}} & 0 \\ 0 & K_{\dot{v}} & 0 & K_{\dot{p}} & 0 & K_{\dot{r}} \\ 0 & 0 & M_{\dot{w}} & 0 & K_{\dot{q}} & 0 \\ 0 & N_{\dot{v}} & 0 & N_{\dot{p}} & 0 & K_{\dot{r}} \end{bmatrix} \tag{3.5}$$

The notation of SNAME (1950) is followed for the hydrodynamic derivatives introduced in equation (3.5). The hydrodynamic derivatives are defining a correlation between the developing force or moment along an axis due to an acceleration induced in the same or different axis direction. In general, hydrodynamic derivatives can be acquired by different methods, such as model testing in towing tanks, computer ship motions analysis using hydrodynamic simulations or regression analysis of statistical data of similar hull forms. Below, an example is given as explanation to the definition of the hydrodynamic derivative.

The hydrodynamic added mass force X along the x body axis due to an acceleration $\dot{u}$ in the x direction is written as:

$$X = -X_{\dot{u}}.\dot{u}, \qquad X_{\dot{u}} = \frac{\partial X}{\partial \dot{u}} \tag{3.6}$$

Similarly to the rigid-body matrix, if the dynamic positioning motions are considered (3 DOF), equation (3.5) is further simplified as following:

$$\boldsymbol{M}_A^{CB} = -\begin{bmatrix} X_{\dot{u}} & 0 & 0 \\ 0 & Y_{\dot{v}} & 0 \\ 0 & 0 & N_{\dot{r}} \end{bmatrix} \tag{3.7}$$

Finally, the two final matrices will be translated to have their origin reference point amidships. This is achieved by the following matrix transformations:

$$\boldsymbol{M}_{RB}^{CO} = \boldsymbol{H}(\boldsymbol{r}_{cg}^b)^T \boldsymbol{M}_{RB}^{CG} \boldsymbol{H}(\boldsymbol{r}_{cg}^b) \tag{3.8}$$

$$\boldsymbol{M}_A^{CO} = \boldsymbol{H}(r_{cb}^b)^T \boldsymbol{M}_A^{CB} \boldsymbol{H}(\boldsymbol{r}_{cb}^b) \tag{3.9}$$

where the following matrices define the distance between center of gravity CG and center of buoyancy CB with the point CO amidships, respectively.

$$\boldsymbol{r}_{cg}^b = \begin{bmatrix} x_g \\ y_g \\ z_g \end{bmatrix}, \qquad \boldsymbol{r}_{cb}^b = \begin{bmatrix} x_b \\ y_b \\ z_b \end{bmatrix} \tag{3.10}$$

$$\boldsymbol{H}(\boldsymbol{r}_{cg}^b) = \begin{bmatrix} 1 & 0 & -y_g \\ 0 & 1 & x_g \\ 0 & 0 & 1 \end{bmatrix}, \qquad \boldsymbol{H}(\boldsymbol{r}_{cb}^b) = \begin{bmatrix} 1 & 0 & -y_b \\ 0 & 1 & x_b \\ 0 & 0 & 1 \end{bmatrix} \tag{3.11}$$

The final matrices that will be implemented in the simulations are shown below.

$$\boldsymbol{M}_{RB}^{CO} = \begin{bmatrix} m & 0 & 0 \\ 0 & m & mx_g \\ 0 & mx_g & I_z^{CG} + mx_g^2 \end{bmatrix} \tag{3.12}$$

$$\boldsymbol{M}_{A}^{CO} = -\begin{bmatrix} X_{\dot{u}} & 0 & 0 \\ 0 & Y_{\dot{v}} & Y_{\dot{r}} \\ 0 & Y_{\dot{r}} & N_{\dot{r}} \end{bmatrix} \tag{3.13}$$

Regarding the term $I_z^{CG} + mx_g^2$ in the rigid-body matrix, it will be approximated, based on equation (3.14), as stated in the hydrostatic theory of [8]:

$$I_z^{CG} + mx_g^2 = I_z^{CO} = m(0.25L_{BP})^2 \tag{3.14}$$

where $R_{66} = 0.25L_{BP}$ is the common approximation for the radius of gyration in yaw for small craft vessels.

All the hydrodynamic derivatives included in the added mass matrix, will be taken from a similar vessel used in many projects at NTNU, Viknes 830, for which extended model tests have been carried out. This is considered to be a good initial step for parameter identification in this project's dynamic positioning system implementation.

3.1.2 Coriolis-centripetal matrix C

This matrix contains the terms which describe the coriolis effect and centripetal force induced in the system, due to the fact that the body fixed frame is not inertial and as a result the required force to achieve the same acceleration in this frame of reference is different than that in an inertial frame. Furthermore, the coriolis effect is present on both the rigid mass of the vessel and the water added mass described in the previous section. For a surface vessel, having port-starboard symmetry, homogeneous mass distribution and the body fixed frame origin is located amidships, the coriolis-centripetal matrix is given for 3-DOF as:

$$\boldsymbol{C}(\boldsymbol{\nu}) = \boldsymbol{C}_{RB}(\boldsymbol{\nu}) + \boldsymbol{C}_{A}(\boldsymbol{\nu}) \tag{3.15}$$

$$\boldsymbol{C}_{RB}(\boldsymbol{\nu}) = \begin{bmatrix} 0 & -mr & -mx_g r \\ mr & 0 & 0 \\ mx_g r & 0 & 0 \end{bmatrix} \tag{3.16}$$

$$\boldsymbol{C}_{A}(\boldsymbol{\nu}) = \begin{bmatrix} 0 & 0 & Y_{\dot{v}} v_r + Y_{\dot{r}} r \\ 0 & 0 & -X_{\dot{u}} u_r \\ -Y_{\dot{v}} v_r - Y_{\dot{r}} r & X_{\dot{u}} u_r & 0 \end{bmatrix} \tag{3.17}$$

Dynamic positioning only focuses on station keeping and sometimes low speed maneuvering, thus the vessel's velocity is zero or very small. As a result, the coriolis term will be removed from the basic model equation without much loss of precision.

3.1.3 Damping Matrix D

According to Fossen [8], the damping matrix encapsulates all the dissipating forces present on the hull from different hydrodynamic phenomena including wave drift damping, potential damping, damping due to vortex shedding, lifting forces and skin friction. All these terms contribute to both linear and quadratic damping and since it is difficult to make a clear distinction between them, a convenient way to express the total hydrodynamic damping is as:

$$\boldsymbol{D}(\boldsymbol{\nu}) = \boldsymbol{D}_L + \boldsymbol{D}_n(\boldsymbol{\nu}) \tag{3.18}$$

where $\boldsymbol{D}_L$ is the linear part and $\boldsymbol{D}_n(\nu)$ the nonlinear part of total damping.

Assuming port-starboard symmetry, surge can be decoupled from the rest motions and with the body fixed frame origin point amidships (point CO), the linear matrix takes the following form:

$$\boldsymbol{D}_L^{CO} = -\begin{bmatrix} X_u & 0 & 0 & 0 & 0 & 0 \\ 0 & Y_v & 0 & Y_p & 0 & Y_r \\ 0 & 0 & Z_w & 0 & Z_q & 0 \\ 0 & K_v & 0 & K_p & 0 & K_r \\ 0 & 0 & M_w & 0 & M_q & 0 \\ 0 & N_v & 0 & N_p & 0 & N_r \end{bmatrix} \tag{3.19}$$

Reducing the above matrix to the required 3 DOF needed for dynamic positioning, we obtain:

$$\boldsymbol{D}_L^{CO} = -\begin{bmatrix} X_u & 0 & 0 \\ 0 & Y_v & Y_r \\ 0 & N_v & N_r \end{bmatrix} \tag{3.20}$$

The diagonal terms of matrix (3.20) are modeled according to seakeeping theory damping forces coefficients matrix B, as shown below, while the rest terms are calculated based on the matrices defined for Viknes boat.

$$-X_u = B_{11v} \tag{3.21}$$

$$-Y_v = B_{22v} \tag{3.22}$$

$$-N_r = B_{66v} \tag{3.23}$$

Based on Fossen [8], under the assumption that the vessel is a second order system for stabilization, the above linear viscous damping terms can be modeled as following:

$$B_{11v} = \frac{m + A_{11}(0)}{T_{surge}} \tag{3.24}$$

$$B_{22v} = \frac{m + A_{22}(0)}{T_{sway}} \tag{3.25}$$

$$B_{66v} = \frac{I_z + A_{66}(0)}{T_{yaw}} \tag{3.26}$$

where $T_{surge}, T_{sway}, T_{yaw}$ are considered time constants for each motion, which are dependent on the natural periods of the vessel T_n and relative damping ratio ζ, according to equation (3.27):

$$T = \frac{T_n}{8\pi\zeta} \tag{3.27}$$

As a starting point, the values for the time constants are chosen to be the values of the Viknes boat, as shown below:

$$T_{surge} = T_{sway} = T_{yaw} = 10\,[s] \tag{3.28}$$

Moreover, the added mass coefficients under zero-frequency are derived as a function of vessel's mass m and radius of gyration r, [8]. Specifically:

$$A_{11}(0) = 0.1m \tag{3.29}$$

$$A_{22}(0) = 0.4m \tag{3.30}$$

$$A_{66}(0) = 0.5mr^2 \tag{3.31}$$

Finally, the nonlinear term $\boldsymbol{D}_n(\boldsymbol{\nu})$ is considered to encapsulate two independent phenomena, which are the nonlinear surge damping and cross-flow drag. Regarding dynamic positioning, these terms exceed the scope of a simplified linear study and thus are omitted.

3.1.4 Additional Terms

The rest of the terms included in equation (3.1) are defined below:

- $\boldsymbol{g}(\boldsymbol{\eta})$ - Hydrostatic forces acting upon the vessel due to buoyancy.
- $\boldsymbol{g}_0$ - Gravity force, which is always acting in the center of gravity and depends upon local gravitational acceleration vector.
- $\boldsymbol{\tau}$ - Actuator forces, which depend up the setup of the dynamic positioning system and will be further analyzed in the next chapter.
- w - Environmental forces due to waves, wind and ocean currents acting upon the hull and need to be countered.

In the linearized motion equation for dynamic positioning, restoring $\boldsymbol{g}(\boldsymbol{\eta})$ and gravity $\boldsymbol{g}_0$ forces are neglected, since they merely affect the horizontal plane motions surge, sway and yaw.

Based on the above assumptions, the simplified form of equation (3.1) that will be used in the simulations, is shown below:

$$\boldsymbol{M}^{CO}\dot{\boldsymbol{\nu}} + \boldsymbol{D}_L^{CO}\boldsymbol{\nu} = \boldsymbol{\tau} + \boldsymbol{w} \tag{3.32}$$

3.2 Environmental Loads Model

As mentioned in the first chapter, the main target of a dynamic positioning system is to maintain the vessel's position and heading despite the environmental forces acting upon the hull. In the process of accurately building realistic simulation scenarios, one needs to define these forces. The next sections describe the main environmental phenomena and resultant forces that need to be taken into consideration, specifically ocean waves and currents as well as wind. Furthermore, the mathematical models used in the simulations are defined and explained. Lastly, the phenomena will be modeled separately for increased accuracy and not in a combined way, which is sometimes opted in control applications.

3.2.1 Waves

Ocean waves are a complex phenomenon and their modeling depends heavily on the operational target of an application, in this case a vessel equipped with a dynamic positioning system. In control applications, the wave-induced forces can be modeled as the sum of first-order and second-order forces, based on the principal of superposition, as shown below:

$$\boldsymbol{\tau}_{wave} = \boldsymbol{\tau}_{wave1} + \boldsymbol{\tau}_{wave2} \tag{3.33}$$

The first-order forces, $\boldsymbol{\tau}_{wave1}$, are the result of the wave-frequency (WF) motion which is observed as zero-mean oscillatory motion, whereas second-order forces, $\boldsymbol{\tau}_{wave2}$, are wave drift forces that are slowly varying over time. When designing a control system, the two aforementioned wave force components need to be countered in different ways. The oscillatory component is usually compensated by using a cascaded notch and low-pass filter to exclude the undesired frequencies, since their is no direct need for dampening while the wave drift forces are removed by using integral action [8].

Generally, waves are described by their frequency spectra $S(\omega)$, which is further defined by the following parameters:

- The significant wave height H_s, which is the mean wave height of one-third of the highest waves
- The modal period T_0, also known as peak period T_p, which is the highest period noted between wave components

Over the years, spectral analysis has yielded many models, capable of defining the sea-state for either developing or fully-developed seas as well as swells, e.g Bretschneider spectrum, Pierson-Moskowitz spectrum, Jonswap spectrum. In order to calculate the wave-induced forces and vessel's motions based on a sea-state, one needs to firstly define the motion and force RAOs of the vessel. RAOs can be considered as the black box that translate a sea state to the required motion or force, as depicted in Figures 3.1, 3.2. These are generally calculated through model towing tests or with hydrodynamic code.

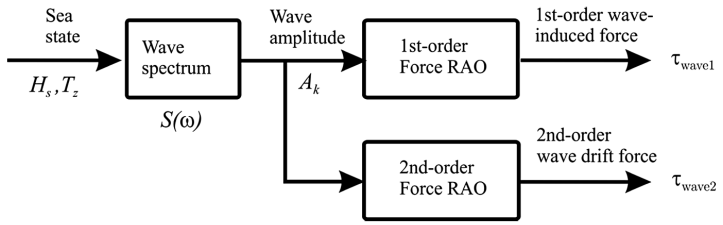

Figure 3.1: Wave-induced forces deriving from a sea-state based on force RAOs [8]

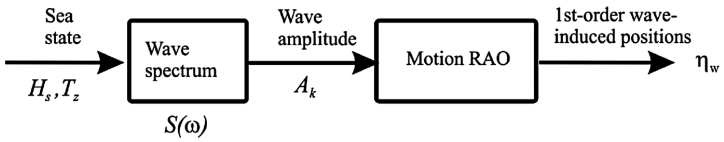

Figure 3.2: Wave-induced positions deriving from a sea-state based on motion RAO [8]

An alternative method for modeling the sea-state in control applications where the main goal is to determine system robustness and closed-loop performance is shown in the next Figure 3.3 and analyzed. This method is simpler yet efficient and eliminates the direct need of hydrodynamic computations, and thus it will be implemented in the simulations.

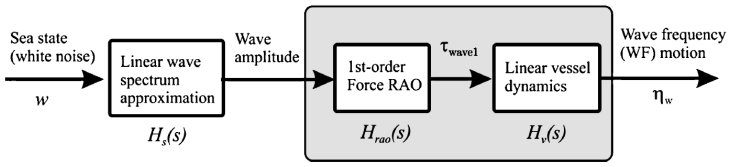

Figure 3.3: Linear approximation for computation of wave-induced positions [8]

The basic concept of this method is that the total motion of a vessel can be derived using again the principle of linear superposition where the first-order wave-frequency motion, $\boldsymbol{\eta}_w$, is added to the vessel's low frequency motion, $\boldsymbol{\eta}$, as shown in equation (3.34):

$$\boldsymbol{y} = \boldsymbol{\eta} + \boldsymbol{\eta}_w \tag{3.34}$$

The generalized wave-frequency position vector η_w, is defined as:

$$\boldsymbol{\eta}_w = \boldsymbol{K}\boldsymbol{H}_s(s)\boldsymbol{w}(s) \tag{3.35}$$

where:

- K is a constant tunable gain which encapsulates the response of the motion RAOs and the linear vessel dynamics in cascade, based on the following equation:

  $$\boldsymbol{K} \approx \boldsymbol{H}_{rao}(s)\boldsymbol{H}_v(s) \tag{3.36}$$

  where $\boldsymbol{H}_{rao}(s)$ is the wave amplitude-to-force transfer function and $\boldsymbol{H}_v(s)$ is the force-to-motion transfer function.

  According to Fossen [8], this gain will be tuned for each DOF, so as the simulations yield realistic results of position signals. Specifically, the signals for surge and sway should have magnitude of $\pm 1[m]$ and the signal for yaw should have magnitude of $\pm 5 - 10 degrees$

- $w(s)$ is a zero-mean Gaussian white noise process with unity spectral power

- $\boldsymbol{H}_s(s) = diag\left[h_1(s), h_2(s), h_6(s)\right]$ is a diagonal matrix containing linear approximations of the wave spectrum $S(\omega)$. For each DOF there will be a transfer function. This modeling proposition was firstly proposed by Balchen et al. (1976) [2] that was redefined with another damping term λ by Sælid et al. (1983) [24], for better fitting to the shape of the Pierson-Moskowitz spectrum. The wave spectrum can be approximated by a second-order system of relative degree one, as:

  $$h(s) = \frac{K_w s}{s^2 + 2\lambda\omega_0 s + \omega_0^2} \tag{3.37}$$

The gain constant K_w is defined in a more convenient way as:

$$K_w = 2\lambda\omega_0\sigma \tag{3.38}$$

where σ is a constant describing the wave intensity, λ is a damping coefficient and ω_0 is the peak wave frequency. Consequently, determination of h(s) relies on modeling the aforementioned parameters.

For this study, the Pierson-Moskowitz Spectrum will be used for wave modeling, which is given by equation (3.39):

$$S(\omega) = A\omega^{-5}exp\big(-B\omega^{-4}\big) \tag{3.39}$$

where A,B are spectrum's coefficients, given as:

$$A = 8.1\ 10^{-3}g^2 \tag{3.40}$$

$$B = 0.74\Big(\frac{g}{V_{19.4}}\Big)^4 = \frac{3.11}{H_s} \tag{3.41}$$

where $g = 9.8055m/s^2$ is the gravitational acceleration, $V_{19.4}$ is the wind speed at a height of 19.4 m above the sea surface and H_s is the significant wave height. The relationship between $V_{19.4}$ and H_s is based on the assumption that the waves can be represented by Gaussian random processes and that $S(\omega)$ is narrow banded.

In order to fully determine the spectrum $S(\omega)$, the only unknown parameter is the significant wave height. This will be defined based on Table 3.1, depicting the observed wave height in accordance with sea state description, as given by [20], where only sea states for viable dynamic positioning operations are included.

Table 3.1: Observed wave height based on sea state, Price and Bishop [20]

Sea state code	Description of sea	Wave height observed [m]
2	Smooth (wavelets)	0.1 - 0.5
3	Slight	0.5 - 1.25
4	Moderate	1.25 - 2.5
5	Rough	2.5 - 4.0

The modal frequency ω_0 for the PM spectrum is obtained by requiring:

$$\left(\frac{dS(\omega)}{d\omega}\right)_{\omega=\omega_0} = 0 \tag{3.42}$$

Solving equation (3.42), we obtain:

$$\omega_0 = \sqrt[4]{\frac{4B}{5}} \tag{3.43}$$

The values of significant height H_s and peak frequency ω_0 that will be used in the simulations are shown in Table 3.2. All the results are based on the wave height observed from Table 3.1 for each sea state code.

Table 3.2: Significant wave height H_s and peak frequency ω_0 for PM spectrum

Sea state code	Significant wave height H_s [m]	Peak frequency ω_0 [rad/s]
2	0.489	1.8
3	1.304	1.1
4	2.465	0.8
5	4.382	0.6

Observing η_w from equation (3.35), it can be rewritten for a single degree of freedom as:

$$\eta_w = K\xi(s) \tag{3.44}$$

$$\xi(s) = h(s)\, w(s) \tag{3.45}$$

The power spectral density function for $\xi(s)$, with unity power white noise, is computed as:

$$P_{\xi\xi}(\omega) = \left|h(j\omega)\right|^2 \tag{3.46}$$

For the case of h(s) of equation (3.37), this yields [8]:

$$P_{\xi\xi}(\omega) = \frac{4(\lambda\omega_0\sigma)^2\omega^2}{\left(\omega_0^2 - \omega^2\right)^2 + 4\left(\lambda\omega_0\omega\right)^2} \tag{3.47}$$

The target, here, is to derive an approximation of $S(\omega)$ by appropriately fitting $P_{\xi\xi}(\omega)$ to the relevant frequency range. In this study, an approximation is derived by using the nonlinear least squares method in the MatLab optimization toolbox.

The maximum value of $P_{\xi\xi}(\omega)$ should be obtained for $\omega = \omega_0$, which yields:

$$P_{\xi\xi}(\omega_0) = S(\omega_0) \Rightarrow \sigma^2 = max\, S(\omega) \tag{3.48}$$

$$\Rightarrow \sigma = \sqrt{\frac{A}{\omega_0^5} exp\Big(- \frac{B}{\omega_0^4}\Big)} \tag{3.49}$$

Regarding λ, the results of the nonlinear least square fitting method are depicted in Table 3.3, based on the peak frequency of PM spectrum for the sea states of Table 3.2:

Table 3.3: σ and λ values for spectrum fitting using NLS method

Sea state code	λ	σ
2	0.2567	0.1087
3	0.2564	0.3724
4	0.2563	0.8256
5	0.2562	1.6947

Observing Table 3.3, λ values are not dependent on the significant weight height H_s, something that is also stated in [8] but was shown here for a complete overview. Consequently, a constant value of $\lambda = 0.26$ will be used for all the sea states. Regarding σ values, depending on the sea state, the value of Table 3.3 will be used as shown.

At this point, all the required parameters of equation (3.37) have been derived, and thus wave modeling will be based on the aforementioned equations. Finally, the next Figure 3.4 shows $P_{\xi\xi}(\omega)$ fitted to the PM spectrum $S(\omega)$ for the case of a peak frequency equal to $\omega_0 = 0.8\,[rad/s]$, as an example for visual observation of the method.

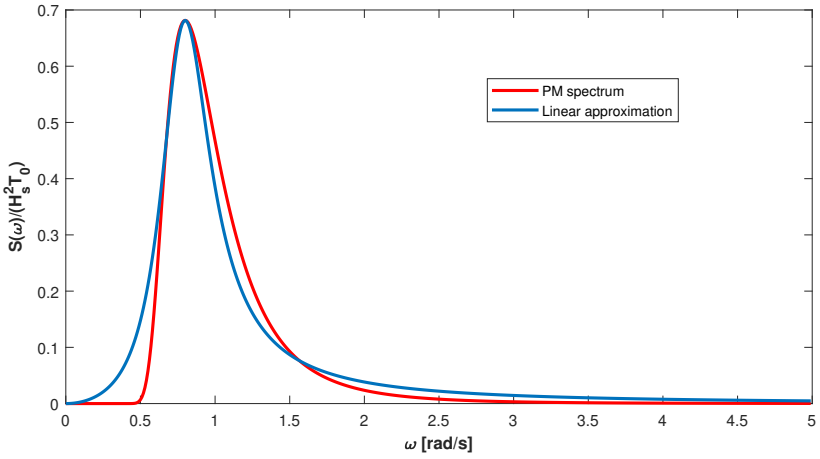

Figure 3.4: $P_{\xi\xi}(\omega)$ function fitted to PM spectrum using NLS method

3.2.2 Wind

Wind is defined as the movement of air relative to the surface of the Earth. It usually consists of several components and is modeled as the sum of a mean wind value and a random fluctuating component, known as wind gust. The two main wind sensors a vessel is equipped with are an anemometer and a weather vane, which measure wind's speed and direction, respectively. The main vessel parameters contributing to the resulting wind force are the hull's frontal and lateral projected area.

Vessel's speed while in DP operation does not heavily impact the true wind direction. Thus, the equations for calculating wind forces in 3 DOF will be derived considering the vessel at rest. Under zero speed assumption, we obtain:

$$\boldsymbol{\tau}_{wind} = \begin{bmatrix} X_{wind} \\ Y_{wind} \\ N_{wind} \end{bmatrix} = \begin{bmatrix} qC_X(\gamma_w)A_{Fw} \\ qC_Y(\gamma_w)A_{Lw} \\ qC_N(\gamma_w)A_{Lw}L_{OA} \end{bmatrix} \tag{3.50}$$

The dynamic pressure of the apparent wind is given as:

$$q = \frac{1}{2}\rho_a V_w^2 \tag{3.51}$$

where ρ_a is the air density at 15°C given as $\rho_a = 1.225[kg/m^3]$

Regarding the mean velocity profile V_m, it is assumed to satisfy a boundary-layer profile, according to [17] and Bretschneider theory, given by equation (3.52):

$$V_m(h) = V_{10}(h/10)^{\alpha} \tag{3.52}$$

where $V_{10}\,[knots]$ is the wind velocity 10 m above the sea surface and is given by Table 3.4 based on the Beaufort scale, h [m] is the height above the sea surface, which is selected to be 2 m for vessel operations and $\alpha = 1/7$.

Table 3.4: Beaufort Scale (Price and Bishop, 1974 [20])

Beaufort number	Wind description	Wind Speed [knots]
0	Calm	0 - 1
1	Light air	2 - 3
2	Light breeze	4 - 7
3	Gentle breeze	8 - 11
4	Moderate breeze	12 - 16
5	Fresh breeze	17 - 21

The coefficients $C_X(\gamma_w), C_Y(\gamma_w), C_N(\gamma_w)$ are usually computed using a referencing height of h=10m and then converted to a different height. At this stage of model building, although the operational height is different than the referencing, the coefficients calculated at h=10m will be used. Furthermore, these coefficients strongly depend on some geometrical characteristics of the vessel in operation as well as the wind angle of attack γ_w. The relation between vessel heading ψ, wind direction (going to) in n reference frame β_w and wind angle of attack γ_w, is given by equation (3.53) and depicted in Figure 3.5.

$$\gamma_w = \psi - \beta_w - \pi \tag{3.53}$$

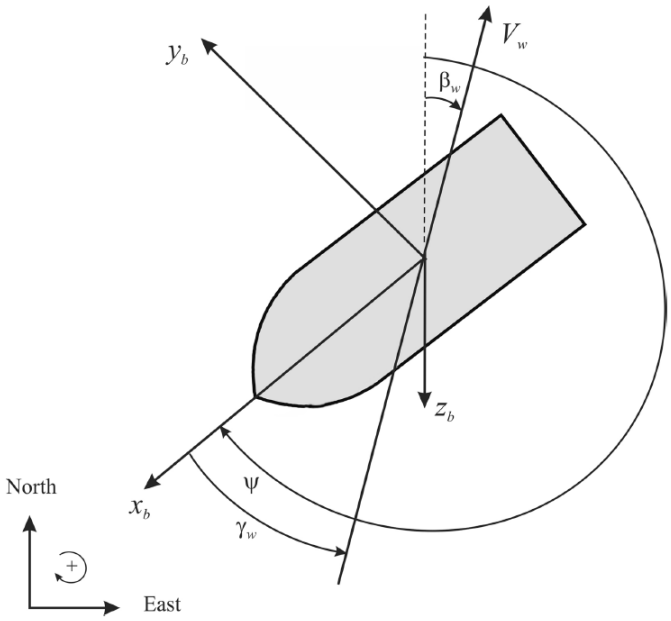

Figure 3.5: Wind speed V_w, wind direction β_w, vessel heading ψ and wind angle of attack γ_w relative to bow, Fossen [8]

Many theories have been proposed for the computation of wind coefficients, with each one focusing on a different vessel type. In this thesis, the equations under the concept proposed by Blendermann in [4], considering the flow over a Helmholtz-Kirchhoff plate, will be used as it applies on all vessel types. Specifically, there are three parameters for the loading functions: longitudinal and transverse resistance parameter CD_l and CD_t, respectively, as well as cross-force parameter δ. For a speed boat, the values of these parameters are summarized in Table 3.5:

Table 3.5: Coefficients of transverse and longitudinal resistance and cross-force

Vessel Type	CD_t	$CD_{l_{AF}}(0)$	$CD_{l_{AF}}(\pi)$	δ
Speed Boat	0.90	0.55	0.60	0.60

where $CD_{l_{AF}}(0)$ will be used for $|\gamma_w| \leq \pi/2$ and $CD_{l_{AF}}(\pi)$ for $|\gamma_w| > \pi/2$ based on the equation:

$$CD_l = CD_{l_{AF}}(\gamma_w)\frac{A_{Fw}}{A_{Lw}} \tag{3.54}$$

After measuring the required hull areas we obtain:

- Frontal Area : $A_{Fw} = 4.61\,[m^2]$
- Lateral Area : $A_{Lw} = 14.82\,[m^2]$

The final equations for the calculation of wind coefficients are given below:

$$C_X(\gamma_w) = -CD_{l_{AF}}(\gamma_w)\frac{cos(\gamma_w)}{1-\frac{\delta}{2}(1-\frac{CD_l}{CD_t})sin^2(2\gamma_w)} \tag{3.55}$$

$$C_Y(\gamma_w) = CD_t\frac{sin(\gamma_w)}{1-\frac{\delta}{2}(1-\frac{CD_l}{CD_t})sin^2(2\gamma_w)} \tag{3.56}$$

$$C_N(\gamma_w) = \left[\frac{s_L}{L_{OA}} - 0.18(\gamma_w - \frac{\pi}{2})\right] C_Y(\gamma_w) \tag{3.57}$$

where s_L is the distance between the center of the lateral projected area A_{L_w} and the waterline, defined as: $s_L = 1.38\,[m]$, assuming vessel operating draft T= 0.551 [m].

The resultant coefficients of equations (3.55), (3.56), (3.57), calculated specifically for the Evolution vessel's hull, and for angle of attack between 0 and 180 degrees are presented in diagrams 3.6, 3.7, 3.8.

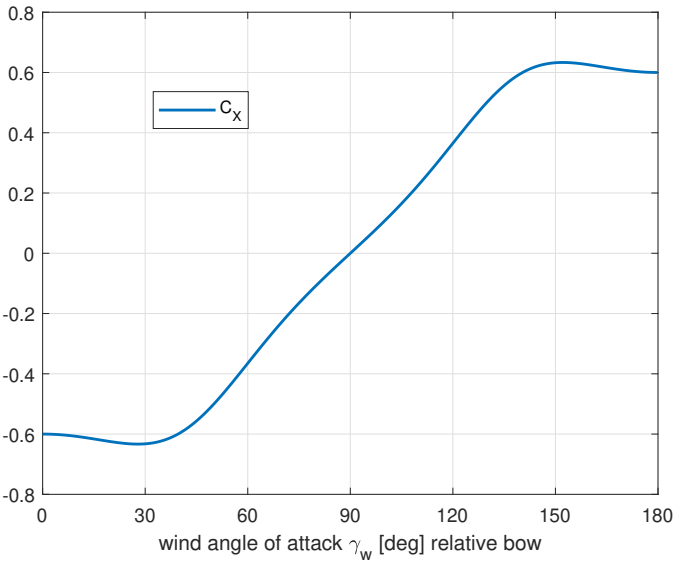

Figure 3.6: C_X wind coefficient for angle of attack in range [0,180] degrees

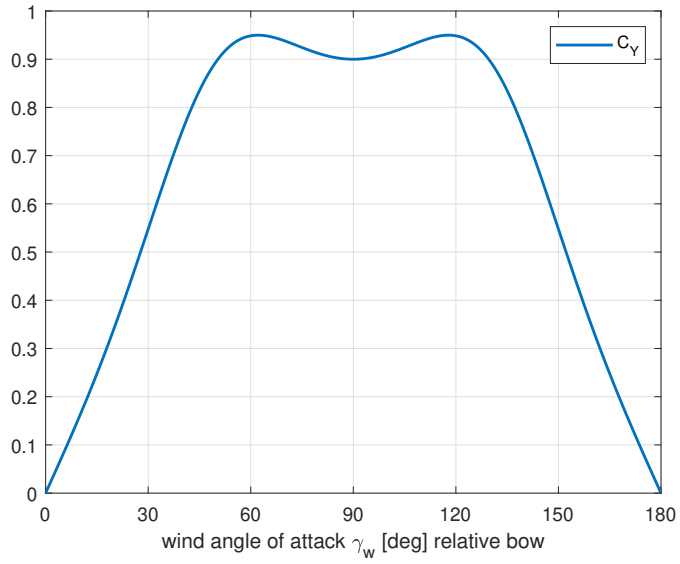

Figure 3.7: C_Y wind coefficient for angle of attack in range [0,180] degrees

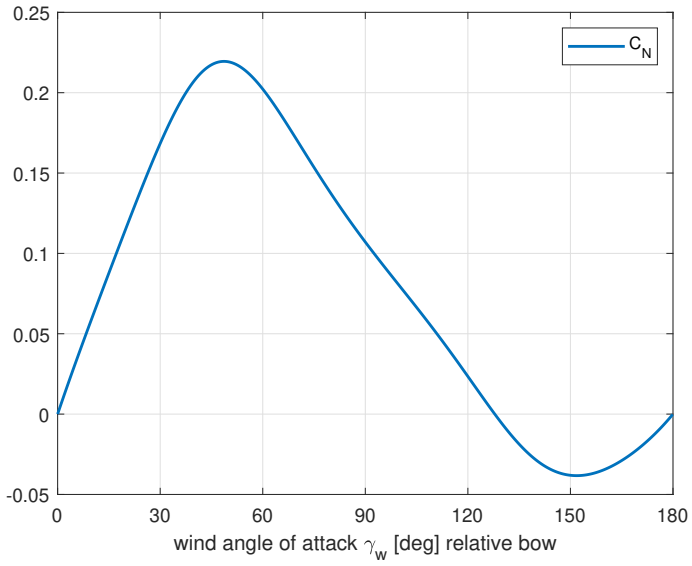

Figure 3.8: C_N wind coefficient for angle of attack in range [0,180] degrees

3.2.3 Sea Currents

Currents will be implemented in the simulations as a 2-D non-rotational current, given by matrix 3.58 in the NED frame:

$$\dot{\boldsymbol{\eta}}_c = \begin{bmatrix} V_c\, cos(\beta_c) \\ V_c\, sin(\beta_c) \\ 0 \end{bmatrix} \tag{3.58}$$

where V_c and β_c are the current's velocity and direction (going to), respectively.

Matrix 3.58 is transformed into a vector represented in the BODY frame, as:

$$\boldsymbol{\nu}_c = \boldsymbol{J}_n^b(\psi) \begin{bmatrix} V_c\, cos(\beta_c) \\ V_c\, sin(\beta_c) \\ 0 \end{bmatrix} \tag{3.59}$$

Finally, the current's velocity vector will be deducted from the vessel's velocity vector, as shown in equation (3.60), which is a modified version of equation (3.32). This is going to be the final kinetic equation of the simulation model.

$$\boldsymbol{M}^{CO}\dot{\boldsymbol{\nu}} + \boldsymbol{D}_L^{CO}(\boldsymbol{\nu} - \boldsymbol{\nu}_c) = \boldsymbol{\tau} + \boldsymbol{w} \tag{3.60}$$

Chapter 4

Boat Hardware Equipment

4.1 Thrust System

The main required aspect of the thrust system that will be implemented on the vessel is, as stated in the beginning, that there are no parts exposed, such as blades, which can be potentially harmful during the aforementioned rescuing operations at sea. For this reason, it was decided to not equip the vessel with the standard bow thruster systems that are commonly used. Instead, a system comprised of a centrifugal water pump and water ejection nozzles will be tested. Due to the fact that the alternation of the way that thrust is produced changes the variables of the system and even the limitations of it, the proposed thrust system will be firstly implemented and evaluated on a small test boat, which has an overall length of 5 meters and is shown in Figure 4.1.

Figure 4.1: HJDP-1 test boat for initial DP sea trials

As far as the water pump thrust system is considered, the Jet-Thruster JT-30 compact system manufactured by Holland Marine Parts [19] was selected to be installed. In general, this company offers solutions for maneuvering boats inside docks. According to the manufacturer, this system has no propeller blades exposed, while its installation is flexible and easy. The main system parts are shown in Figure 4.2, and the basic working principle is further explained, with each part shown separately in Figure 4.3.

Figure 4.2: Exploded diagram of Jet-Thruster JT-30 compact system

A centrifugal water pump paired with an electrical 3kW DC motor (a) is continuously supplying the piping network with water. The water exiting the pump is split through a 2-way outlet (b) to 3-way electrically controlled valves (c). These valves are centrally operated by a controller (d) and the user determines which of them open. When a valve opens, the water coming through the selected direction is finally ejected from a nozzle (f) that is fitted at the hull's boundaries. Consequently, a resultant force is acting upon the vessel, depending on the nozzle's installation location, which contributes to the vessel's motions during dynamic positioning. As a safety precaution, before each nozzle exit, ball-valves (e) are fitted, which are controlled by hand, in case there is direct need to close a water exit.

(a) Pump-motor unit

(b) 2-way outlet

(c) 3-way valve

(d) Controller

(e) Ball Valve

(f) Nozzle

Figure 4.3: Jet-Thruster JT-30 system parts detailed

The following Figures 4.4, 4.5, 4.6, 4.7, show the setup of the system and the nozzle installation position, inside the test boat. Two main factors were taken into account while installing the equipment. Firstly, the pump should be placed under the vessel's operating waterline so as there is always water present inside the impeller. Secondly, the nozzles should be installed just above the waterline.

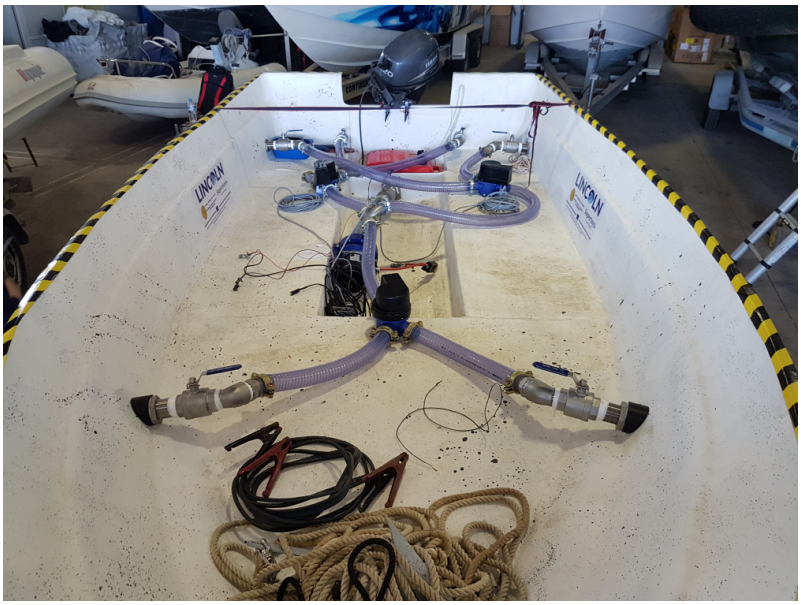

Figure 4.4: Installation of JT-30 system on small test boat (1/4)

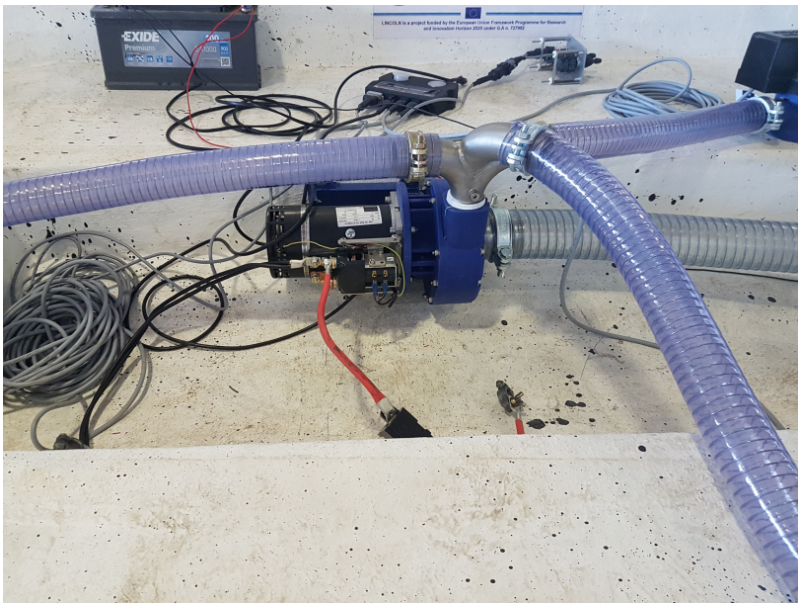

Figure 4.5: Installation of JT-30 system on small test boat (2/4)

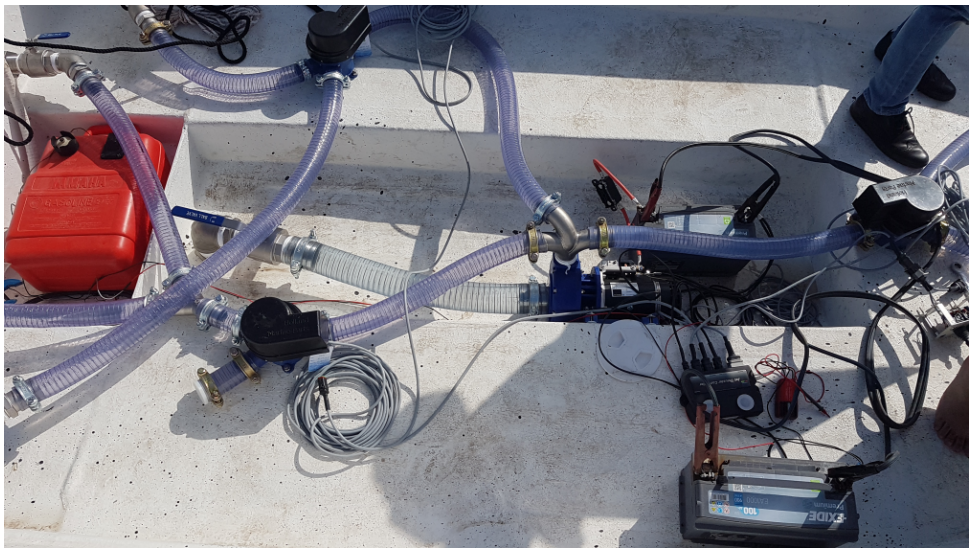

Figure 4.6: Installation of JT-30 system on small test boat (3/4)

Figure 4.7: Installation of JT-30 system on small test boat (4/4)

4.2 Sensors

4.2.1 Sensor Selection

Nowadays, inertial measurement technology is being used in many different science fields, since prices have dropped while the benefits remain the same. By using simple IMU sensors that are fixed on an object, one can get fast readings of the object's accelerations, angular and linear position. This is achieved through a process called dead reckoning, in which the calculation of an object's position is based on a previously determined position or fix and the current speed of the object. In dynamic positioning operations, it is critical to accurately define vessel's position. Due to the fact that GPS readings are suffering from internal lag between the sensor and the data transmission satellites and also the estimated position exceeds in general the acceptable error in DP operations, in this thesis the vessel's position will be estimated with the aid of an IMU sensor solely.

The IMU that will be used during the tests on the small boat is a 9-DOF sensor which is embedded on a simple breakout board manufactured by Sparkfun Electronics [6], shown in Figure 4.8.

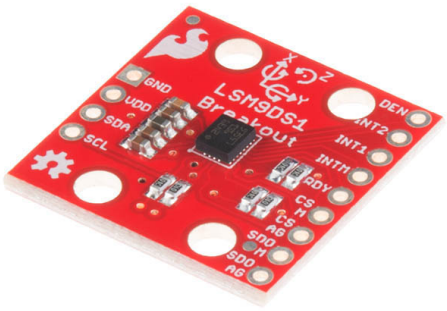

Figure 4.8: Sparkfun 9-DOF IMU - LSM9DS1

The key components of the LSM9DS1 chipset featured on this IMU are the following:

- 3D digital linear accelerometer with acceleration sensing capability up to 16 g
- 3D digital gyroscope with angular rate sensing capability up to 2000 degrees per second
- 3D digital magnetometer with magnetic field sensing capability up to 16 gauss

It is clear from the above limits that this sensor is capable of encapsulating the system dynamics consisted of the vessel and the surrounding environment. Moreover, the embedded magnetometer will be used to estimate the vessel's heading by building a digital compass from the transmitted magnetic field readings.

4.2.2 Communication

The sensor manufacturer states in the product's datasheet that the values transmitted from the device are in digital raw 16-bit data form, converted from analog readings by the embedded analog to digital converter. Moreover, two communication protocols are offered for data transmission. It was decided to use the I^2C communication interface instead of the SPI, since it very easy to implement, requiring minimum cable usage and also any new I^2C sensors that might be needed to be added in the future can be connected using the same cables.

The main device which will handle the communication and receive the transmitted values is chosen to be a Raspberry Pi 3 B+, which is a single board computer having an ARM microprocessor as core component and is widely used as a solution in embedded systems. The basic configuration is shown in Figure 4.9. Furthermore, the procedure for data transmission is elaborated.

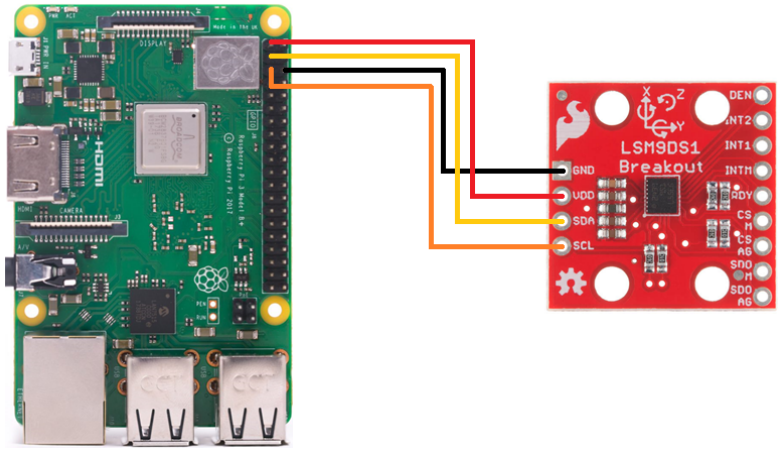

Figure 4.9: I^2C - Device Configuration

I^2C Protocol

I^2C is a serial protocol for a two-wire interface. The communication makes use of the Serial DAta (SDA) and Serial CLock (SCL) pins of the connected devices/sensors. The SCL pin provides the serial clock, in order to transmit data under an accurate time frame and the SDA pin provides the path for serial data transmission. Additionally, any sensor connected to the interface has a unique identification hexadecimal address, so as to be distinguished during data transmission. The default addresses for LSM9DS1 are 0x6B for the accelerometer and gyroscope and 0x1E for the magnetometer. Before the communication starts the SCL and SDA are both kept high by pull-up resistors. When the communication between the RPi 3 B+ (master device) and the LSM9DS1 (slave device) starts, the start condition is created. This is achieved by making SDA low, (Figure 4.10). Then the serial clock (SCL) begins to generate clock pulses and the first byte is sent by the master. This first byte contains the 7-bit address of the slave's register, in which data need to be pulled and a read/write bit. All these addresses are defined in the chip's datasheet.

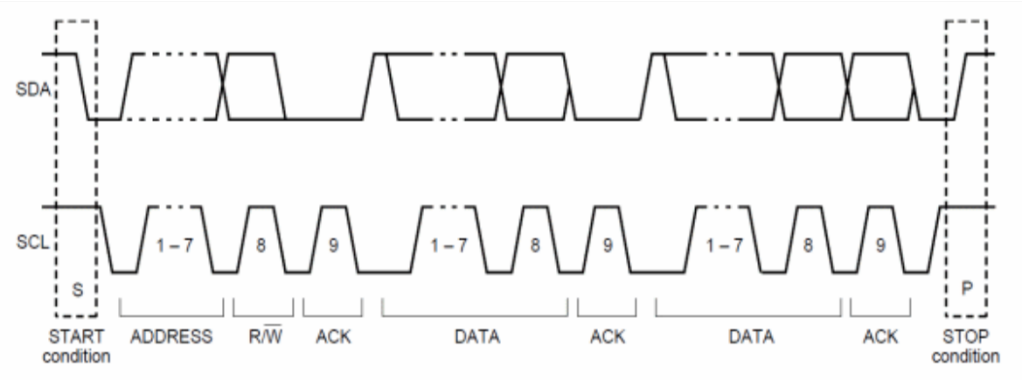

Figure 4.10: I^2C - Device Configuration

When the read/write bit is 0 the master will write to the slave and when the bit is 1 the master will read from the slave. The bits are always sent when the serial clock is high. When the serial clock is low the bit values are allowed to change. The number of bytes sent is not limited, but each byte must be followed by an acknowledge bit, ACK, (Figure 4.10). When the master is done writing/reading, then the stop condition is created (STOP). This process continues until the master decides to terminate the serial communication.

4.2.3 Digital Compass

A traditional magnetic compass consists of a small, lightweight magnet balanced on a nearly friction-less pivot point, as shown in Figure 4.11. The magnet is generally called a needle. The Earth's magnetic field will cause the needle to point to the magnetic North. The angle difference between true North and magnetic North is called declination and depends upon the region in which the compass is used.

Figure 4.11: Traditional magnetic compass

Local earth magnetic field H has a fixed component H_h on the horizontal plane pointing to the Earth's magnetic North. This component, consisting of the vectors X_h and Y_h can be measured by the magnetometer's sensing axes X_M and Y_M, as shown in Figure 4.12.

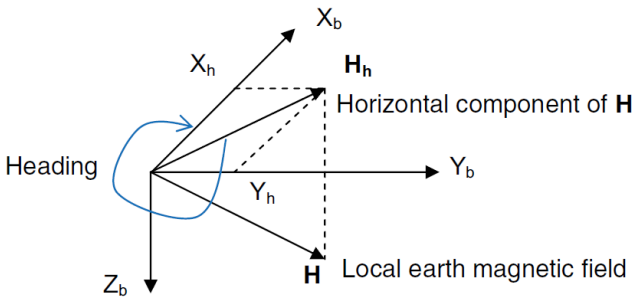

Figure 4.12: Local Earth magnetic field and heading calculation

Then the heading angle can be calculated as:

$$Heading = arctan(Y_h/X_h) \tag{4.1}$$

When the device body X_b axis is parallel to H_h, which is pointing towards magnetic North, then $X_h = max$ and $Y_h = 0$ so that $heading = 0°$. Rotating the device clockwise on the horizontal plane, the heading increases. When $X_h = 0$ and $Y_h = min$, then $heading = 90°$, and so on.

In a sea environment, where the IMU is installed on board, the vessel will never be exactly parallel to the horizontal plane, and thus the above readings will be inaccurate and fluctuate. As a result, an alternative method will be adapted for measuring heading, where the roll and pitch angles are taken into account.

Tilt compensation

When the measuring device is tilted, pitch and roll angles are not equal to 0°, as depicted in Figure 4.13. By measuring pitch and roll angles with a filter that combines the angle estimates of the accelerometer and gyroscope, the magnetic sensor readings X_M, Y_M and Z_M, will be compensated to obtain X_h and Y_h, using equations 4.2, 4.3:

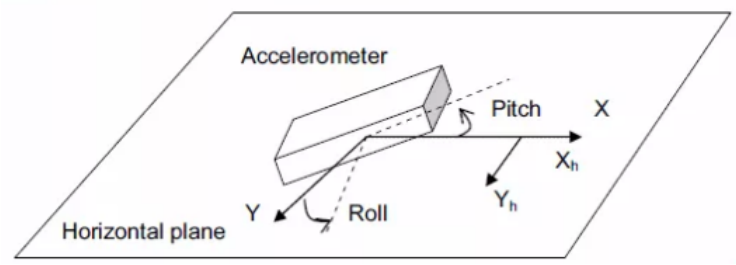

Figure 4.13: Tilt-compensated heading calculation

$$X_h = X_M cos(\theta) + Z_M sin(\theta) \tag{4.2}$$

$$Y_h = X_M sin(\phi) sin(\theta) + Y_M cos(\phi) - Z_M sin(\phi) cos(\theta) \tag{4.3}$$

After calculating X_h and Y_h, heading is obtained again from equation (4.1).

4.2.4 Calibration

Sensor accurate calibration is a critical stage of the data acquisition process. In this case, vessel's controlling will highly depend on the readings received from the IMU. As stated in previous paragraphs, in dynamic positioning, it is essential to keep track of vessel's position and orientation. Position will be estimated on each iteration by double integrating the acceleration readings on x and y axes, after removing the gravitational acceleration component. As far as angle estimation is considered, both the accelerometer and gyroscope readings will be combined to get a result. Heading will be calculated by the digital compass.

In general, the measurements from an 9-DOF IMU for one of the defined body axes, are the sum of the true value, sensor offset b and noise w. This is expressed in equations (4.4), (4.5), (4.6) :

- Accelerometer:

$$a_{imu} = a_{true} + b_{acc} + w_{acc} \tag{4.4}$$

- Gyroscope:

$$\omega_{imu} = \omega_{true} + b_{gyro} + w_{gyro} \tag{4.5}$$

- Magnetometer:

$$m_{imu} = m_{true} + b_{mag} + w_{mag} \tag{4.6}$$

The reading errors of the sensors derive from the fact that MEMS technology is not the most accurate method for determining the state of an object. Lower implementation cost means simpler manufacturing process and less precision. But, depending on the application, all these hardware errors can be minimized to the point where there is no critical divergence from the operational target. Such is the case of position and heading estimation for a vessel in dynamic positioning.

In the next paragraphs, the methods of excluding the constant offset from each sensor are explained. In addition, a Kalman filter is proposed that will be used for filtering the measurements being susceptible to noise. The following diagram 4.14 depicts the overall calibration process and filtering techniques that will finally estimate vessel's position and heading in the NED frame.

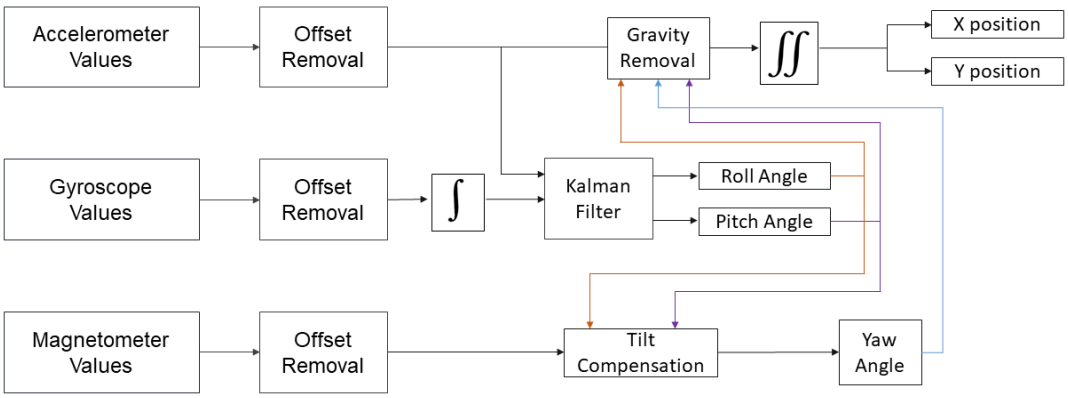

Figure 4.14: Calibration flow diagram

In general, offset is defined as the output value of a sensor when the device is lying still on the horizontal plane and no forces or moments are acting on any axis, as shown in the following figure. Note that the axes proposed in Figure 4.15 are also shown upon the PCB of Figure 4.9 for positioning the device according to the defined vessel axes. For each of the sensors, offset compensation is achieved differently.

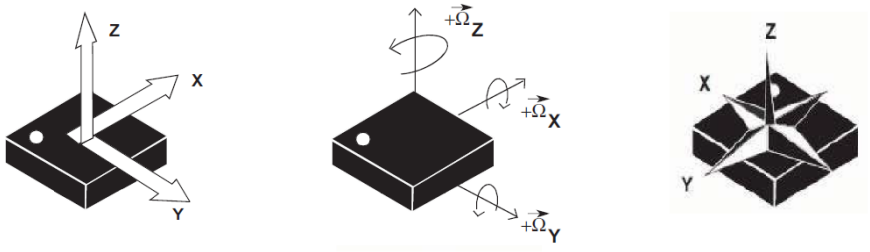

Figure 4.15: LSM9DS1 device - measuring coordinate system

Accelerometer Offset

An accelerometer that is left flat upon a horizontal plane, measures specific force only upon the vertical to plane axis, specifically the z axis, where gravity vector is present. In this position, the offset of x and y axes is defined as the mean average of 100 measured values, while the accelerometer is not moving. In order to measure the z-axis offset, the device is tilted 90 degrees so as the z axis is lying on the horizontal plane now and the z offset is again the mean average of 100 measured values. Moreover, the offset that is calculated for an axis, e.g. the x axis, is different when the vertical to horizontal plane axis is the y axis than when is the z axis. So the true offset value for each axis is calculated as shown below:

$$\text{x - offset} = [(\text{mean offset - z vertical}) + (\text{mean offset - y vertical})]/2$$
$$\text{y - offset} = [(\text{mean offset - z vertical}) + (\text{mean offset - x vertical})]/2$$
$$\text{z - offset} = [(\text{mean offset - x vertical}) + (\text{mean offset - y vertical})]/2$$

This procedure should be followed on every initialization of the measuring device and the resulting values be stored and subtracted from the accelerometer values on each iteration. It should be noted that offsets can slightly change, since the environment and mainly temperature influence the results. In advanced systems, temperature compensation needs to be also included but in the case of dynamic positioning is not obligatory. The following Figures 4.16, 4.17, 4.18, depict the acceleration on each axis when there is no movement or gravity acting on it, before and after offset removal.

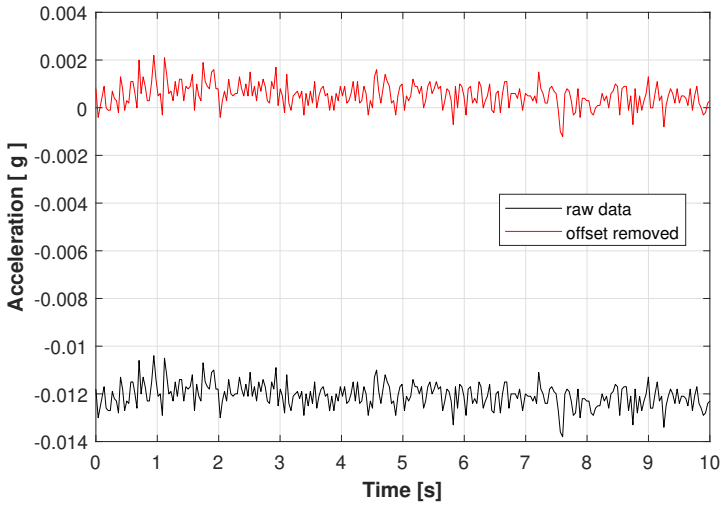

Figure 4.16: X-axis accelerometer - offset removal

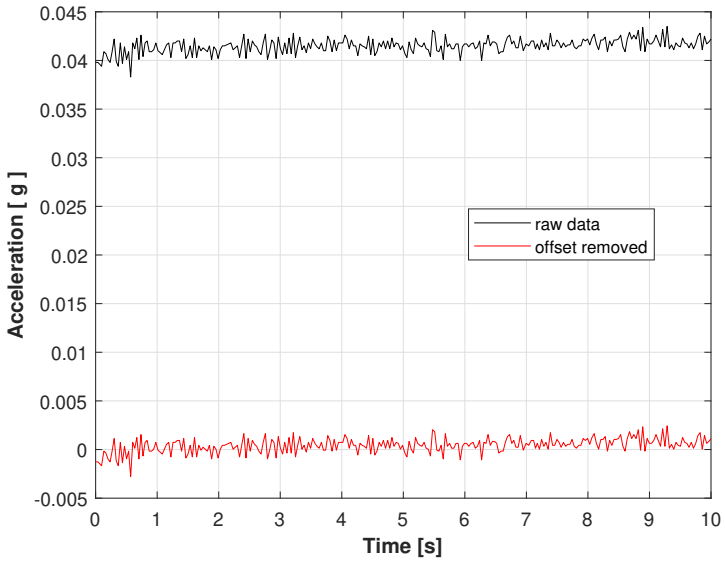

Figure 4.17: Y-axis accelerometer - offset removal

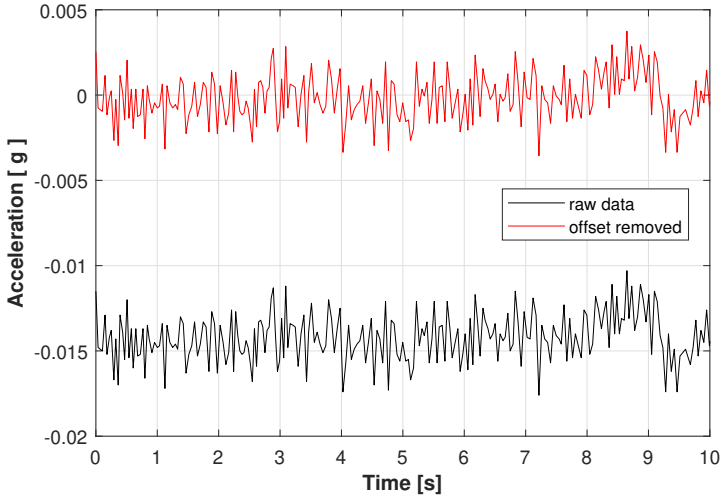

Figure 4.18: Z-axis accelerometer - offset removal

Gyroscope Offset

Similarly to the accelerometer, the gyroscope offset is defined while the device is locked in place without moving. But in this case no axes rotations are required. With the device still and without rotating, the mean average of 100 measurements on each axis defines the constant offset. Deviation due to temperature changes is again present but not critical for the operation of a vessel. The following Figures 4.19, 4.20, 4.21, depict the estimation of rotational speed for each axis before and after subtracting the gyroscope offset on each iteration, while the device is locked and not moving.

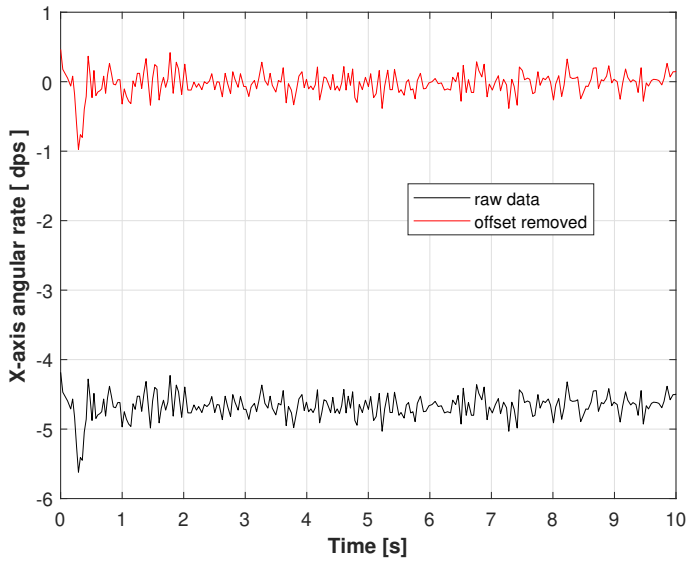

Figure 4.19: X-axis gyroscope - offset removal

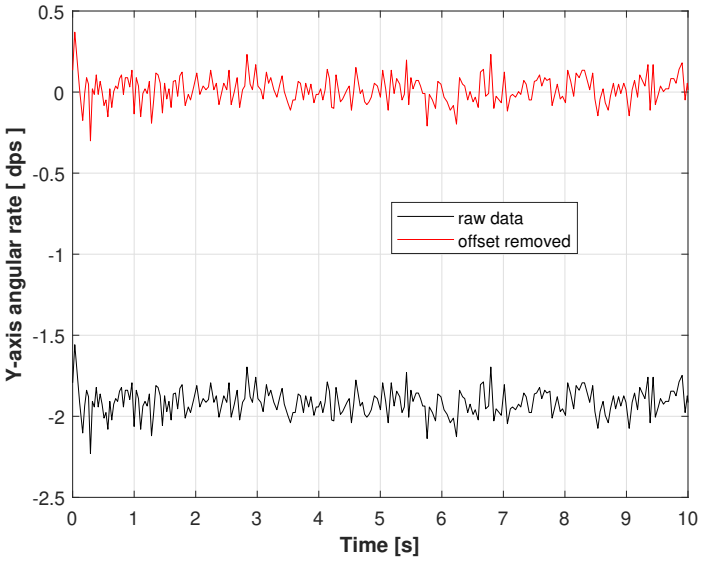

Figure 4.20: Y-axis gyroscope - offset removal

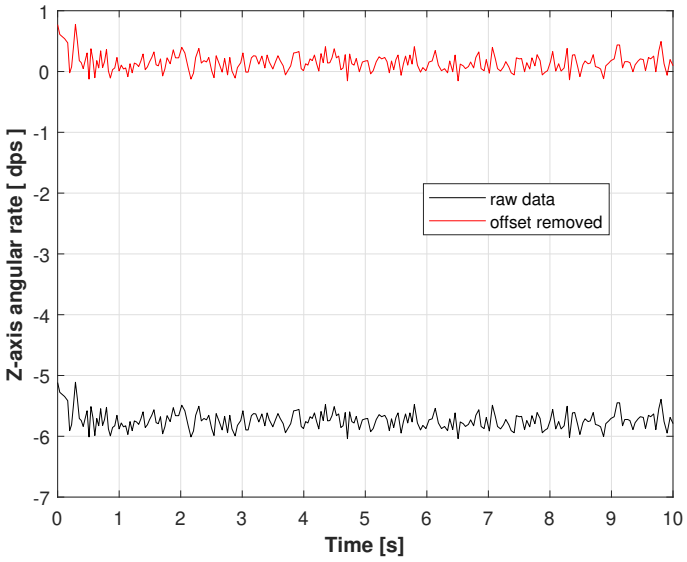

Figure 4.21: Z-axis gyroscope - offset removal

Magnetometer Offset

The magnetometer will only be used to determine orientation and for that it needs to sense the magnetic field of the Earth and return the values to the digital compass. The Earth's magnetic field strength ranges between approximately $25\mu T$ and $65\mu T$. Most electrical devices contain components that interact with this field and introduce disturbances. These disturbances can be divided into two groups, the hard iron losses and the soft iron losses. The hard iron losses are due to the device's permanently magnetized components and soft iron losses are due to local geomagnetic field inducting currents. The hard iron losses are easy to be calculated and compensated, because they are constant regardless of orientation and position of the device, and thus are treated as magnetometer's constant offset.

In order to calculate the magnetometer's offset, the procedure described next is followed. The device is instantiated and configured to transmit raw magnetic field values. By rotating the device 360 degrees on one axis at a time and for all x,y,z axes, the maximum and minimum raw magnetic field values are written down. After completing the aforementioned rotations, the mean value of the maximum and minimum measurements per axis is extracted. This mean value is the hard iron offset that will be subtracted from each future measurement during operation.

This procedure should be followed only once when the final system is created and all the electronics are placed. Lastly, the IMU should be placed inside the electronics box in a separate location from any other devices or components with alternating magnetic fields. A digital magnetometer that has been properly calibrated for hard iron losses, gives measurements which are centered around the plane origin point, as shown below in Figure 4.22, for x-y plane.

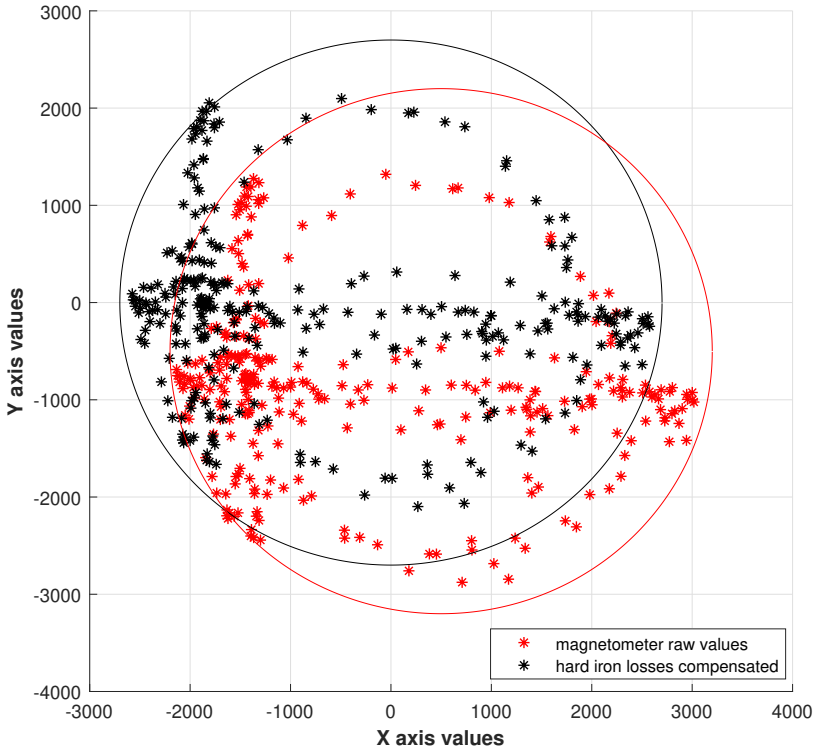

Figure 4.22: Magnetomer - hard iron losses compensation

Regarding soft iron losses, their impact on heading estimation is low and can only change if any magnetic device comes near the sensor and affect the magnetic field calculations. There are two final steps required for calibrating the magnetometer readings. Firstly, the positive side for x-axis is alternated to match that of the vessel's body axes. In that way, when the vessel's bow points towards magnetic North, the yaw angle will be 0 degrees. Secondly, the final heading value is corrected by the declination angle, which is different for each region that the vessel is operating. For the region around Athens in Greece, the declination angle correction is :

$$\text{Declination angle} = +\ 4.47^{\circ}$$

Below, in Figure 4.23, the heading angle is shown, when the device is pointing towards 95 degrees, approximately towards East, while pitch and roll angles are applied in the range of ± 10 degrees. It can be noted that the application of tilt compensation, greatly enhances the results, with only $\pm 2^{\circ}$ deviation from the actual value. Considering the capabilities of an IMU and the increased noise that affects precision, the present deviation is within acceptable values.

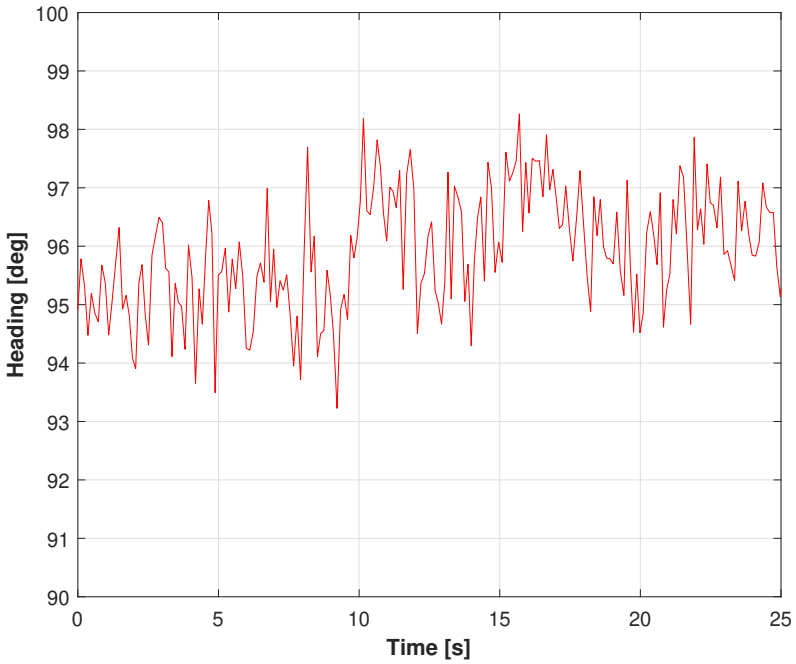

Figure 4.23: Device heading recorded with tilt compensation

Angle estimation using the accelerometer

The accelerometer can be used to estimate pitch and roll angles, simply by calculating the angle the gravity vector has with the horizontal plane, using trigonometry. Additionally, no transformation from BODY to NED is required since these calculations are directly measuring pitch and roll angles on the inertial NED frame. The following equations (4.7), (4.8), derive the roll and pitch angles:

$$\hat{\phi}_{acc} = arctan\Big(\frac{a_y}{\sqrt{a_x^2 + a_z^2}}\Big).\frac{180}{\pi} \tag{4.7}$$

$$\hat{\theta}_{acc} = arctan\Big(\frac{-a_x}{\sqrt{a_y^2 + a_z^2}}\Big).\frac{180}{\pi} \tag{4.8}$$

where a_x, a_y, a_z are the accelerations on x,y and z axis, respectively.

Although possible, acquiring pitch and roll angles solely from accelerometer readings is not advised. Accelerometers suffer extensively from noise in their readings, which leads to unnecessary spikes in their measurements. What's more, any external acceleration apart from gravitational acceleration, distorts the above calculations and the estimated angles are not trustworthy anymore. The solution of using a low-pass filter is possible, and thus will give a much cleaner estimate. But it will introduce a significant lag in the system, something that is not favorable. Instead, the above estimates can be directly fed into an advanced filter, e.g a Kalman filter, which is presented in a next paragraph.

Angle estimation using the gyroscope

The gyroscope is measuring the rotational speed for each of the body axes. Consequently, roll and pitch angles can be estimated by the gyroscope by integrating the rotational speed over the time period between each iteration. But the angles are calculated with respect to the BODY frame, and thus a rotational transformation needs to be applied, since the position and angles of the vessel need to be expressed in the NED frame.

The angle transformations that need to be performed, are presented in Section 2.3, under the concept of Euler angles. After having defined the Euler angle rates, integration of the results leads to the vessel angles in the NED frame. The significant disadvantage of this method is that the gyroscope measurements are heavily drifting, leading to false measurements about the vessel's orientation. As a result, direct use of them is not suggested. But, the gyroscope results will be also included in the equations of the Kalman filter.

Kalman Filter

The Kalman filter is a type of observer or state estimator which tries to minimize a quadratic cost function. It is highly preferred over other filters since it also takes into account the dynamics of the controlled system and not only the sensor measurements. In general, it addresses the problem of state estimation $\boldsymbol{x} \in \Re^n$ of a discrete-time controlled process that is governed by the following linear stochastic difference equation (4.9):

$$\boldsymbol{x}_k = \boldsymbol{A}\boldsymbol{x}_{k-1} + \boldsymbol{B}\boldsymbol{u}_{k-1} + \boldsymbol{w}_{k-1} \tag{4.9}$$

with sensor measurement $\boldsymbol{z} \in \Re^m$ defined as:

$$\boldsymbol{z}_k = \boldsymbol{C}\boldsymbol{x}_k + \boldsymbol{\nu}_k \tag{4.10}$$

where $\boldsymbol{x}_k$ is the system's state vector and $\boldsymbol{u}_k$ the input vector, at time step k.

The random variables $\boldsymbol{w}_k$ and $\boldsymbol{\nu}_k$ represent the process and measurement noise, respectively. They are assumed to be zero mean Gaussian white noise, independent of one another and with probability distributions:

$$p(w) \sim N(0, Q) \tag{4.11}$$

$$p(\nu) \sim N(0, R) \tag{4.12}$$

where Q and R are covariance matrices of the process and measurement noise, respectively. Q is set to relate the uncertainty of the model dynamics, with large values denoting that the model is inaccurate. R is set depending mainly on the sensors that are used in the system and noise-specific parameters are usually available from the sensor manufacturer's datasheet. Again, large values denote greater sensor noise levels.

Finally, A,B and C are system matrices. The n x n matrix A relates the current system state at step k with the states in the previous step k-1. The n x 1 matrix B relates the optional control input $\boldsymbol{u} \in \Re^l$ to the states $\boldsymbol{x}$. The m x n matrix C in the measurement equation relates the states x to the measurement $\boldsymbol{z}_k$. In practice, matrices A and C might change with each time step, but here it is assumed that they are time invariant.

The Kalman filter estimates a process by using a form of feedback control, [3]. The filter itself makes a prediction of the process state at some time k and then obtains feedback by means of noisy measurements from the sensors. Under this working principle, the filter equations can be categorized into two groups: time update and measurement update equations. The time update equations are responsible for projecting forward in time the current state to obtain an *a priori* estimate for the next time step k. The measurement update equations are responsible for giving the feedback, which is a new measurement for the *a priori* estimate, in order to obtain an improved *a posteriori* estimate. This concept is depicted in Figure 4.24.

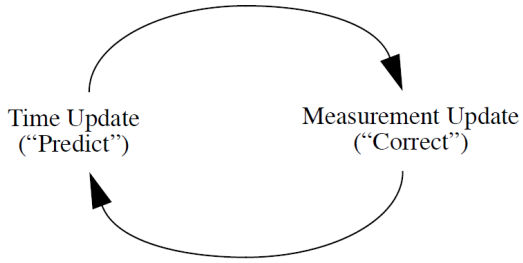

Figure 4.24: Discrete Kalman filter cycle

The *a priori* state estimate at step k given knowledge of the process prior to step k is defined as: $\hat{\boldsymbol{x}}_k^- \in \Re^n$. The *a posteriori* state estimate at step k given the measurement $\boldsymbol{z}_k$ is defined as: $\hat{\boldsymbol{x}}_k \in \Re^n$. Then, the *a priori* and *a posteriori* estimate errors can be defined as:

$$\boldsymbol{e}_k^- = \boldsymbol{x}_k - \hat{\boldsymbol{x}}_k^- \tag{4.13}$$

$$\boldsymbol{e}_k = \boldsymbol{x}_k - \hat{\boldsymbol{x}}_k \tag{4.14}$$

Finally, the *a priori* estimate error covariance is :

$$\boldsymbol{P}_k^- = E[\boldsymbol{e}_k^-(\boldsymbol{e}_k^-)^T] \tag{4.15}$$

and the *a posteriori* estimate error covariance:

$$\boldsymbol{P}_k = E[\boldsymbol{e}_k \boldsymbol{e}_k^T] \tag{4.16}$$

The main target of the filter is to provide an estimate of the state matrix at time step k. This is achieved by equation (4.17):

$$\hat{\boldsymbol{x}}_k = \hat{\boldsymbol{x}}_k^- + \boldsymbol{K}(\boldsymbol{z}_k - \boldsymbol{C}\hat{\boldsymbol{x}}_k^-) \tag{4.17}$$

The difference $(\boldsymbol{z}_k - \boldsymbol{C}\hat{\boldsymbol{x}}_k^-)$ is called measurement innovation and reflects the discrepancy between the predicted measurement $\boldsymbol{C}\hat{\boldsymbol{x}}_k^-$ and the actual measurement $\boldsymbol{z}_k$. The matrix K is known as Kalman gain, which is optimally chosen depending on what should the filter trust more, the measurement or the system dynamics model. After defining all the necessary variables, the Kalman filter equations for time and measurement updates are presented below:

Time Update - Predict

$$\hat{\boldsymbol{x}}_k^- = \boldsymbol{A}\hat{\boldsymbol{x}}_{k-1} + \boldsymbol{B}\boldsymbol{u}_{k-1} \tag{4.18}$$

$$\boldsymbol{P}_k^- = \boldsymbol{A}\boldsymbol{P}_{k-1}\boldsymbol{A}^T + \boldsymbol{Q} \tag{4.19}$$

Measurement Update - Correct

$$\boldsymbol{K}_k = \boldsymbol{P}_k^- \boldsymbol{C}^T (\boldsymbol{C}\boldsymbol{P}_k^- \boldsymbol{H}^T + \boldsymbol{R})^- 1 \tag{4.20}$$

$$\hat{\boldsymbol{x}}_k = \hat{\boldsymbol{x}}_k^- + \boldsymbol{K}_k(\boldsymbol{z}_k - \boldsymbol{C}\hat{\boldsymbol{x}}_k^-) \tag{4.21}$$

$$\boldsymbol{P}_k = (\boldsymbol{I} - \boldsymbol{K}_k\boldsymbol{C})\boldsymbol{P}_k^- \tag{4.22}$$

In order to implement the filter in the project's case, the first step is to define the state matrix x as well as the system matrices A,B and C. Ideally, the system matrices should include the dynamics of the vessel, as explained in [8], but in this case, many parameters of the mass and linear damping matrices are taken from another vessel, and thus are not useful. Consequently, a more general approach will be followed to build the filter, detailed in [25], considering only the characteristics of the IMU sensors, as explained below:

- The varying gyro bias at every time step causes drift and needs to be eliminated
- An updated estimate of angular position can be derived from the gyroscope's angular rates, properly transformed into the NED frame
- Initial estimates of angular position can be provided by the accelerometer

All these lead to the following definition of system states, control input and measurements:

$$\boldsymbol{x}_k = \begin{bmatrix} \hat{\phi}_k \\ b_{\hat{\phi}_k} \\ \hat{\theta}_k \\ b_{\hat{\theta}_k} \end{bmatrix} \tag{4.23}$$

$$\boldsymbol{u}_k = \begin{bmatrix} \dot{\phi}_{G_k} \\ \dot{\theta}_{G_k} \end{bmatrix} \tag{4.24}$$

$$\boldsymbol{z}_k = \begin{bmatrix} \hat{\phi}_{accel_k} \\ \hat{\theta}_{accel_k} \end{bmatrix} \tag{4.25}$$

where all the variables are explained below:

- $\hat{\phi}_k, \hat{\theta}_k$: roll and pitch angle filter estimates
- $b_{\hat{\phi}_k}, b_{\hat{\theta}_k}$: roll and pitch angle estimate bias
- $\dot{\phi}_{G_k}, \dot{\theta}_{G_k}$: roll and pitch angles from gyroscope integration
- $\hat{\phi}_{accel_k}, \hat{\theta}_{accel_k}$: roll and pitch angles from accelerometer

Additionally, the system matrices are defined as:

$$\boldsymbol{A} = \begin{bmatrix} 1 & -\Delta t & 0 & 0 \\ 0 & 1 & 0 & 0 \\ 0 & 0 & 1 & -\Delta t \\ 0 & 0 & 0 & 1 \end{bmatrix} \tag{4.26}$$

where Δt is the time step between each iteration that the algorithm is running.

$$\boldsymbol{B} = \begin{bmatrix} \Delta t \\ 0 \\ \Delta t \\ 0 \end{bmatrix} \tag{4.27}$$

$$\boldsymbol{C} = \begin{bmatrix} 1 & 0 & 0 & 0 \\ 0 & 0 & 1 & 0 \end{bmatrix} \tag{4.28}$$

Regarding Kalman filter matrices P, Q and R, they are initialized having the following form:

$$\boldsymbol{P} = \begin{bmatrix} 1 & 0 & 0 & 0 \\ 0 & 1 & 0 & 0 \\ 0 & 0 & 1 & 0 \\ 0 & 0 & 0 & 1 \end{bmatrix} \tag{4.29}$$

$$\boldsymbol{Q} = \begin{bmatrix} 1 & 0 & 0 & 0 \\ 0 & 1 & 0 & 0 \\ 0 & 0 & 1 & 0 \\ 0 & 0 & 0 & 1 \end{bmatrix} \tag{4.30}$$

$$\boldsymbol{R} = \begin{bmatrix} 1 & 0 \\ 0 & 1 \end{bmatrix} \tag{4.31}$$

The initial state of the IMU, and thus the vessel, is considered to be flat on the horizontal plane with no roll or pitch angle. This leads to the initial estimation of state matrix as:

$$\hat{\boldsymbol{x}}_0 = \begin{bmatrix} 0 \\ 0 \\ 0 \\ 0 \end{bmatrix} \tag{4.32}$$

From this point and on, the algorithm will cycle through equations (4.18) to (4.22), whenever new sensor measurements for roll and pitch angles are available, resulting in a new estimate for the state matrix.

The following Figures 4.25, 4.26, show the pitch and roll angles, calculated over a time period with three different methods: accelerometer data only, gyroscope data only and Kalman filter. It is obvious that when using only the accelerometer, the measurements suffer from increased noise, while any added acceleration to the gravity vector, distorts the results. On the other hand, when the gyroscope is only used, the measurements are heavily drifting, even after bias subtraction. It can be clearly noted that when the device is left to rest on the horizontal plane, pitch and roll angles are extremely different than zero. Finally, sensor fusion with the aid of a Kalman filter improves the results, by keeping only the positive aspects of each sensor and excluding unnecessary spikes or large deviations.

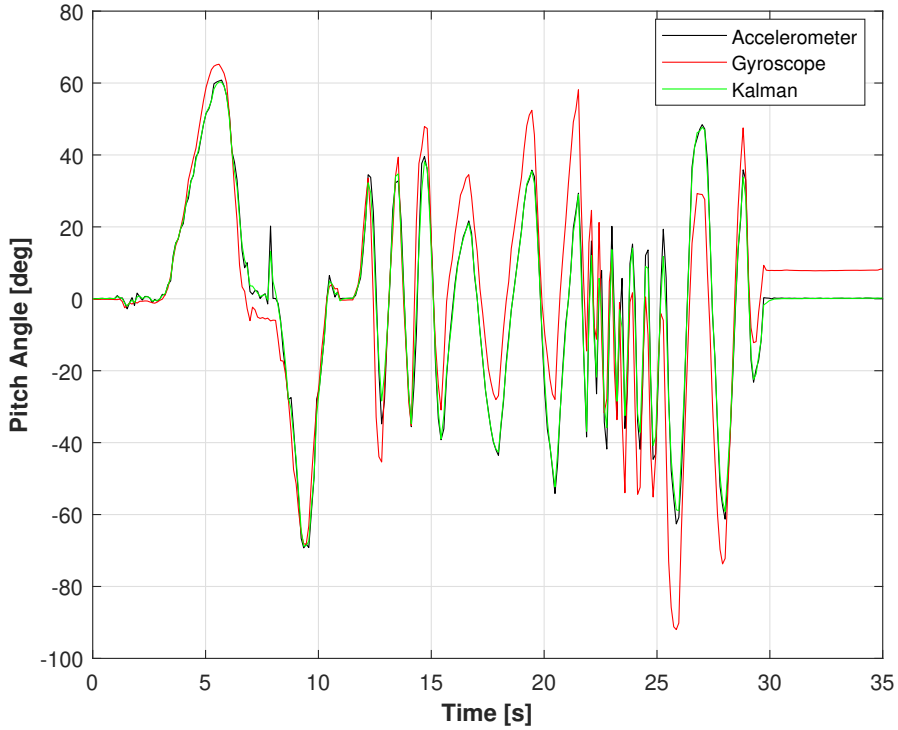

Figure 4.25: Pitch angle estimation with three different methods

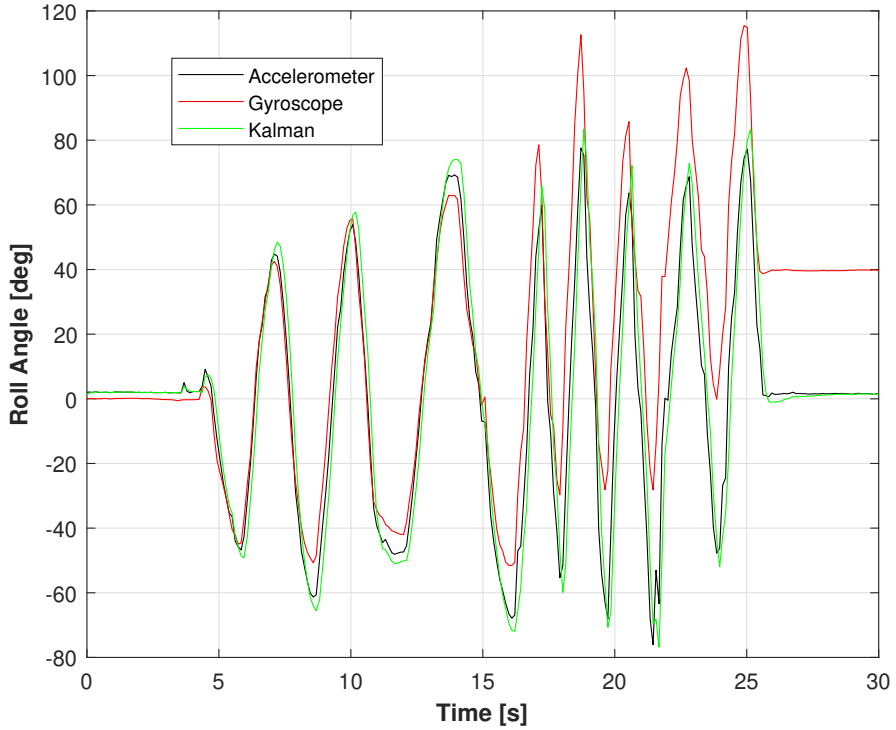

Figure 4.26: Roll angle estimation with three different methods

Position Estimation

Estimating the position of the vessel is achieved, as shown in Figure 4.14, by double integrating the accelerometer readings, after properly excluding acceleration due to gravity. True body acceleration $\boldsymbol{a}_b$ can be obtained in the NED frame by equation (4.33):

$$\boldsymbol{a}_b = \boldsymbol{R}_b^n \boldsymbol{a}_m + \begin{bmatrix} 0 \\ 0 \\ g \end{bmatrix} \tag{4.33}$$

where $\boldsymbol{a}_m$ is the measured sensor acceleration, $g = 9.8055 m/s^2$ is gravitational acceleration and $\boldsymbol{R}_b^n$ is the transformation matrix from BODY to NED frame according to Section 2.3.

After obtaining true body acceleration, double integrating the values, results in the distance the vessel has moved in each axis in the NED frame.

4.3 Data Logger

Boat sea trials will require a device to capture and store vessel's motions, while testing the dynamic positioning equipment and further modifying the controlling algorithm. Consequently, a data logger was developed, named the "black box", in which all of the functions presented in the previous paragraphs were included. The development of the data logger was separated in two phases: construction of container box and programming of data log application. The main features of the data logger container box are shown in the following Schematic 4.27 and detailed in Table 4.1.

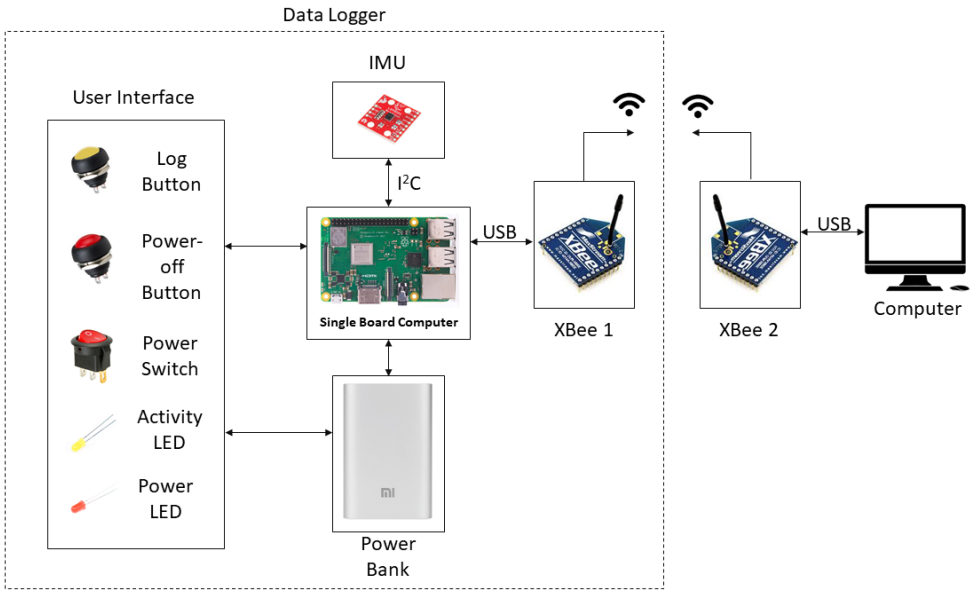

Figure 4.27: Data Logger Schematic

Table 4.1: Data Logger Features

Raspberry Pi 3 Model B+
Xiaomi 10000mAh power bank
Sparkfun LSM9DS1 9-DOF IMU
XBee Wireless Communication Pair
Waterproof User Interface Buttons
Simple LEDs and power switch

All the components are housed inside a splash proof plastic container, which was designed using 3-D CAD software as shown in Figure 4.28. The construction was made with the aid of a 3D printer, using PLA (Polylactic Acid) thermoplastic, to suit the custom space requirements and provide a fast result. The upper part of the logger, Figure 4.29, features two buttons for data logging and shutting down the device, each with an activity LED while a switch powers on/off the device. The whole device is powered by a power bank (Figure 4.27) that can last for approximately 1 day of operation.

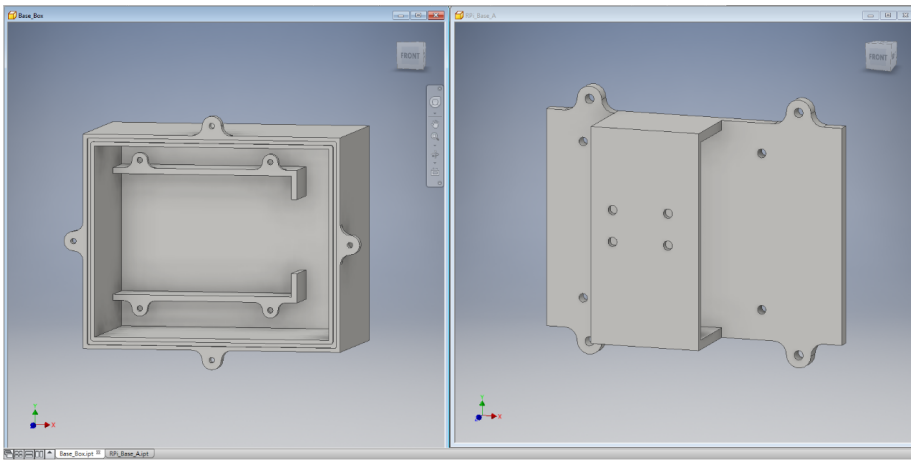

Figure 4.28: 3-D CAD of data logger

As the power bank is the heaviest component, it is placed at the bottom of the container in a compartment that secures its movement. Then a plate holds the single board computer and the IMU chip, as shown in Figure 4.30. The splash proof feature is achieved through an o-ring sealing between the cover and the box. The cover plate closes with four size 3 allen bolts.

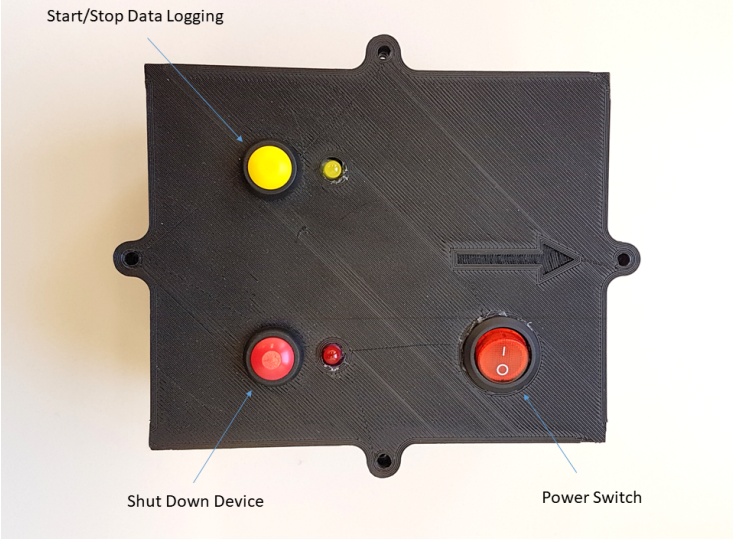

Figure 4.29: Top view of data logger with user interface buttons

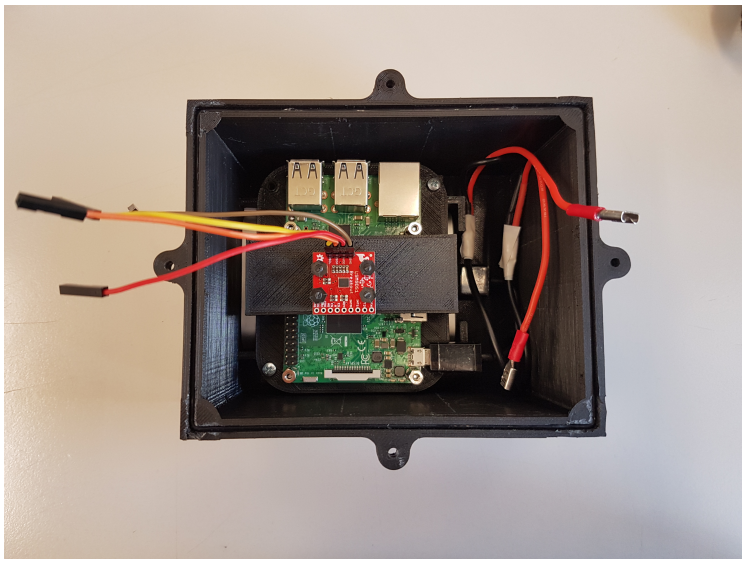

Figure 4.30: Internal view of data logger, with IMU (red) and Raspberry Pi (green)

Up to this point the operation of the data logger relies on the user interface that is provided on top of the container box. As an alternative method, a pair of wireless data transmission modules, named XBee modules, are also installed, extending the capabilities of the black box. XBees are widely used in applications where there is a requirement for communication and no viable cable solution possible. The installed modules operate through serial interface with the device they are connected to and between one another under IEEE 802.15.4 radio communication protocol. Moreover, one module is installed inside the container box which will be fixed on the vessel and the other one is connected to a computer at shore. As a result, the recorded data can be immediately sent and plotted to a computer for visual observation.

The final part required to complete the development of the IMU data logger is the programming code. All the required scripts and final application were written in Python language using the Linux environment. The application establishes communication between the XBee modules and also between the sensors and the Raspberry Pi while it effectively stores the motion data that are available at each time step in the micro SD-card that is embedded within. All the functions and calibration steps that were presented in the previous paragraphs are included in the code and performed on initial start up and whenever required. Lastly, a simple GUI was created in order to make the application user-friendly and also provide a faster way for tuning the controller.

Chapter 5

Controller Design

The main target of a control algorithm is to drive or maintain the controlled system in a desired operational state. In dynamic positioning, the desired state can be one of the following:

- Fixed position and heading above the sea floor
- Fixed heading
- Fixed distance from another vessel or object
- Fixed position relative to the combined weather force vector, known as weather-vaning

In order to achieve one of the above states, an appropriate controller design meeting the requirements of the system needs to be selected. The first option is usually a PID controller, which is easy to implement in any system, as it basically relies on the measured process variable and not on the knowledge of the underlying process itself. The biggest challenge, though, is to achieve adequate tuning of the controller gain parameters, which requires experience and proper understanding of the system dynamics.

Furthermore, advanced controller designs can be used such as MPC or LQR. These controller types require full knowledge of the underlying process and rely heavily on an accurate mathematical model. Additionally, MPC is dependent on full system state knowledge, so if a state is not directly measurable from sensors, observers need to be also implemented in the system, and thus the complexity of the controller is increased.

In this thesis, since the mathematical model derived for the vessel is greatly reduced in terms and linearized as well as dependent on parameters from another vessel, a PID controller design will be implemented in the system, based on the aforementioned reasons.

5.1 PID Theory

The concept of a PID controller is based upon the minimization of the error value between a measured system state value and a desired value, usually defined by the operator. The following block diagram 5.1 depicts the core parts of a feedback PID control loop.

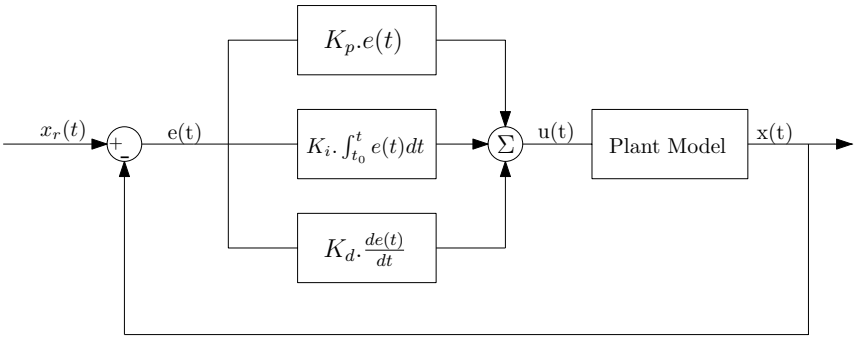

Figure 5.1: PID controller loop with feedback

The current process state x(t) is usually measured from sensors installed in the system, in case of a vessel, a GPS and a compass. The desired state $x_r(t)$ is defined by the user and usually is constant. The PID algorithm continuously calculates the error value e(t), as:

$$e(t) = x_r(t) - x(t) \tag{5.1}$$

On each iteration, after calculating the error value, the controller is deriving a control signal u(t) based on the following equation (5.2):

$$u(t) = K_p e(t) + K_d \frac{de(t)}{dt} + K_i \int_{t_0}^{t} e(t)dt \tag{5.2}$$

where the parameters K_p, K_d, K_i, are known as the proportional, derivative and integral control gains, respectively, with each one of them aiming to counter a different aspect of the system being controlled.

Specifically:

- K_p accounts for present values of the error. Moreover, it determines the ratio of output response to the error signal. Generally, increasing the proportional gain will increase the speed of the control system response. However, if the proportional gain is too large, the process variable will begin to oscillate and in extreme conditions the system might even become unstable and oscillate out of control.
- K_d accounts for possible future values of the error. If the process variable is increasing rapidly the derivative component will cause the output control signal to decrease. Moreover, the derivative response is highly sensitive to noise in the process variable signal. This must be taken into account, otherwise the derivative response will act negatively on the system, making it ultimately unstable.

- K_t accounts for past values of the error. If the control output is not sufficient, error will accumulate over time, and the controller will respond by applying a stronger action in the next iteration. This is applied so as to remove the steady state error. But, the fact that this term is continuously increasing based on the error, generates another possibility of saturating the controller in a future output by requiring excessive control signal. This phenomenon is known as integral windup and anti-windup methods are implemented to counter it.

Considering the scenario where the position and heading of the vessel in the horizontal plane need to be fixed, the values that need to be denoted as the system states for PID design and replace x(t) are $\boldsymbol{\eta}(t) = [x(t), y(t), \psi(t)]$, as vessel's x and y coordinates in NED frame and attitude angle around z-axis, respectively. Consequently, the error is expressed as:

$$\boldsymbol{\eta}_e(t) = \boldsymbol{\eta}_r - \boldsymbol{\eta}(t) \tag{5.3}$$

where η_r denotes the desired values.

The final PID control output signal is expressed as:

$$\boldsymbol{\tau}_{PID}(t) = \boldsymbol{K}_p\boldsymbol{\eta}_e(t) + \boldsymbol{K}_d\frac{d\boldsymbol{\eta}_e(t)}{dt} + \boldsymbol{K}_i\int_{t_0}^{t}\boldsymbol{\eta}_e(t)dt \tag{5.4}$$

Due to the fact that the actuators upon which the control signal is applied are part of the vessel and also the kinetic equation regarding vessel's motions are expressed in the body-fixed coordinate frame, it is required to transform the control output from NED to BODY frame. By using the rotation matrix $\boldsymbol{J}_b^n(\psi(t))$, we obtain:

$$\boldsymbol{\tau}(t) = \boldsymbol{J}_b^n(\psi(t))^T\boldsymbol{\tau}_{PID}(t) \tag{5.5}$$

The final equation for the nonlinear PID controller is:

$$\boldsymbol{\tau}(t) = \boldsymbol{J}_b^n(\psi(t))^T\left(\boldsymbol{K}_p\boldsymbol{\eta}_e(t) + \boldsymbol{K}_d\frac{d\boldsymbol{\eta}_e(t)}{dt} + \boldsymbol{K}_i\int_{t_0}^{t}\boldsymbol{\eta}_e(t)dt)\right) \tag{5.6}$$

In the following section, the initial controller gains $\boldsymbol{K}_p$, $\boldsymbol{K}_d$, $\boldsymbol{K}_i$ will be calculated for each of the motions that need to controlled, specifically surge, sway and yaw.

5.2 Gain Parameters

The are several ways to obtain the gain parameters for a PID controller. A common approach is to tune the system in real time, when there is a physical system available, known as self-tuning or adaptive tuning. Another approach is to derive the parameters based on an internal model controller (IMC) from a table with typical system transfer functions. In this thesis, the controller gains will be obtained by pole placement technique based on the approximated mathematical vessel model. Further fine tuning will be considerd during the simulations.

According to Fossen [8], a vessel can be modeled as a mass-damper-spring system, concluding to the equations (5.7), (5.8), (5.9), for the calculation of PID gain parameters.

$$\boldsymbol{K}_p = \boldsymbol{M}\boldsymbol{\omega}_{pid}^2 \tag{5.7}$$

$$\boldsymbol{K}_d = 2\boldsymbol{\zeta}_{pid}\boldsymbol{\omega}_{pid}\boldsymbol{M} \tag{5.8}$$

$$\boldsymbol{K}_i = \frac{\boldsymbol{\omega}_{pid}}{10}\boldsymbol{K}_p \tag{5.9}$$

where M is the total mass matrix as defined in Chapter 3, ω_{pid} defines the frequencies and ζ_{pid} the relative damping ratio, of the closed loop system including the pid controller, respectively.

For typical control applications, ω_{pid} is chosen to be 2-10 times greater than the natural frequencies ω_n of the system under control. As a first estimation, it is chosen to be 5 times greater than the natural frequencies. Consequently, it is essential to define the natural frequencies of the vessel model.

Based on Chapter 3, when the parameters of the vessel in surge, sway and yaw motions where defined, three time constants T where adopted from the similar vessel Viknes 830, as an estimate for the linear viscous damping terms B_{ii}. These parameters could be used here as well for defining the natural periods of surge, sway and yaw but instead another approach will be followed.

Specifically, the linearized equation of motion (3.32) derived in Chapter 3, will be used to derive a state-space model for the vessel with no environmental disturbances. The state vector $\boldsymbol{x}$, is considered to be the vessel's velocities $\boldsymbol{\nu}$ given in the BODY frame. This yields, the following state-space model representation:

$$\boldsymbol{M}\dot{\boldsymbol{x}} + \boldsymbol{D}_L\boldsymbol{x} = \boldsymbol{\tau} \tag{5.10}$$

$$\Rightarrow \quad \boldsymbol{M}\dot{\boldsymbol{x}} = \boldsymbol{\tau} - \boldsymbol{D}_L\boldsymbol{x} \tag{5.11}$$

$$\Rightarrow \quad \dot{\boldsymbol{x}} = -\boldsymbol{M}^{-1}\boldsymbol{D}_L\boldsymbol{x} + \boldsymbol{M}^{-1}\boldsymbol{\tau} \tag{5.12}$$

From equation (5.12), we observe that the final model has the generalized state-space model form:

$$\begin{aligned} \dot{\boldsymbol{x}} &= \boldsymbol{A}\boldsymbol{x} + \boldsymbol{B}\boldsymbol{u} \\ \boldsymbol{y} &= \boldsymbol{C}\boldsymbol{x} + \boldsymbol{D}\boldsymbol{u} \end{aligned} \tag{5.13}$$

The matrices A,B,C,D are defined as:

$$\begin{aligned} \boldsymbol{A} &= -\boldsymbol{M}^{-1}\boldsymbol{D}_L \\ \boldsymbol{B} &= \boldsymbol{M}^{-1} \\ \boldsymbol{C} &= [1\,1\,1] \\ \boldsymbol{D} &= \emptyset \end{aligned} \tag{5.14}$$

where matrix C has this specific form since all states of $\boldsymbol{\nu}$ are fed back to the system from the sensors and matrix D is zero as there is no direct connection between control input $\boldsymbol{u}$ and output $\boldsymbol{y}$.

Regarding matrix A, which is representing the model dynamics (plant matrix), it will be used to compute the eigenvalues, and consequently the natural frequencies and relative damping ratios of the system.

Computation of eigenvalues λ_i is performed by solving:

$$\left|\boldsymbol{I}\lambda_i - \boldsymbol{A}\right| = 0, \qquad i \in 1, 2, 6, \qquad \boldsymbol{I} = Identity\ matrix \tag{5.15}$$

Moreover, on a generalized form, the relation between eigenvalues, natural frequencies, relative damping ratios and time constants, is given as:

$$\lambda_i = \alpha_i + i\beta_i \tag{5.16}$$

$$\omega_{n_i} = |\lambda_i| \tag{5.17}$$

$$\zeta_i = \frac{-\alpha_i}{\sqrt{\alpha_i^2 + \beta_i^2}} \tag{5.18}$$

$$T_i = \frac{1}{\omega_{n_i}\zeta_i} \tag{5.19}$$

The model is a stable mass-damper system with only real eigenvalues ($a_i < 0$, $\beta_i = 0$, $,\zeta_i = 1$). Therefore, the model natural frequencies will be of equal magnitude to the eigenvalues. The following Table 5.1 summarizes the system's natural frequencies and additionally the system pole diagram is depicted in Figure 5.2.

Table 5.1: Vessel model natural frequencies ω_n

Motion	$\omega_n[rad/s]$
Surge	0.0511
Sway	0.1177
Yaw	0.1004

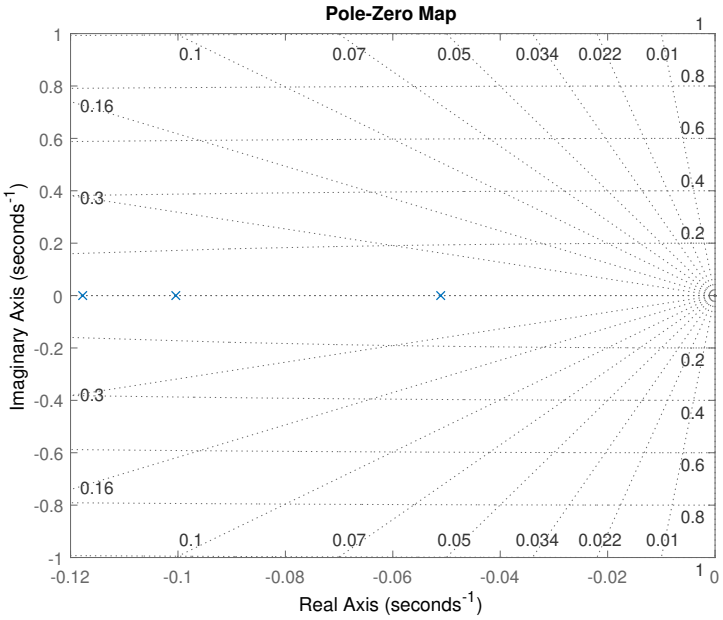

Figure 5.2: Vessel model - pole diagram

When choosing the controller bandwidth ω_{pid}, tuned by pole placement, a good selection range is to have the controller dynamics being 2 to 10 times faster than the system controlled. In this thesis, the initial controller frequencies are chosen to be 4 times larger than the vessel's, leading to the following PID frequencies and gain parameters of Table 5.2:

Table 5.2: PID controller frequencies and gains

Motion	$\omega_{pid}[rad/s]$	K_p	K_d	K_i
Surge	0.2043	210	2060	4
Sway	0.4710	1414	6004	67
Yaw	0.4016	6446	32100	259

5.3 Controller Functional Modifications

Up to this point, no modifications have been made into the algorithm of the PID controller for computing the error and outputting the control signal. But, due to specific issues that may arise during simulations, functional alternations or additions need to be done in the algorithm, which are shown below.

Reference model

For the case of low speed maneuvering, where a path is generated or whenever a new angle set-point is requested by the user, e.g the current heading is 10 degrees and the desired 60 degrees, a large error will be calculated by the controller. This will lead into an even larger output control signal, which might cause unwanted actuator behavior. To overcome this problem, the concept of a reference model is introduced, which is practically acting as a low-pass filter. In this way, no sudden changes are going to result into error amplification.

In this case, a second order reference model for position and heading is defined as:

$$\ddot{\boldsymbol{\eta}}_d + 2\boldsymbol{\zeta}\boldsymbol{\omega}_{n,d}\dot{\boldsymbol{\eta}}_d + \boldsymbol{\omega}_{n,d}^2\boldsymbol{\eta}_d = \boldsymbol{\omega}_{n,d}^2\boldsymbol{\eta}_{ref} \tag{5.20}$$

This model can be rewritten as:

$$\dot{\boldsymbol{\eta}}_d = \boldsymbol{\nu}_d \tag{5.21}$$

$$\dot{\boldsymbol{\nu}}_d = \boldsymbol{\omega}_{n,d}^2\Big(\boldsymbol{\eta}_{ref} - \boldsymbol{\eta}_d\Big) - 2\boldsymbol{\zeta}\boldsymbol{\omega}_{n,d}\boldsymbol{\nu}_d \tag{5.22}$$

where $\boldsymbol{\zeta}$ is the relative damping ratio, $\boldsymbol{\omega}_{n,d}$ is the model natural frequency and $\boldsymbol{\eta}_{ref} = [x_{ref}, y_{ref}, \psi_{ref}]$ is the reference set-point, defined by the user.

The desired reference has to change slower than the system values so as the controller output signal results in smooth vessel motions. For this reason, the natural frequencies of the reference model are set to be lower than the controller frequencies. The final setup of $\boldsymbol{\omega}_n$ and $\boldsymbol{\zeta}$ values for the reference model are given below in equations (5.23), (5.24).

$$\boldsymbol{\omega}_{n,d} = [\,0.25, 0.2, 0.1\,] \tag{5.23}$$

$$\boldsymbol{\zeta} = [\,0.45, 0.4, 0.2\,] \tag{5.24}$$

Yaw wrapping

When navigating in the NED coordinate frame, it is optimal to keep the vessel yaw angle between $\pm\pi$, with respect to the longitudinal x-axis, which is pointing towards North. This excludes the possibility of calculating a large yaw error during vessel operation. A simple example is that if a vessel turns around the z axis 3 times then the yaw angle would reach a value of 6π, resulting in a very large error for correction.

The method that will be followed to wrap the yaw angle is the modulo operation. Firstly, the modulo of 2π for the yaw angle will be derived. The result is further wrapped between $\pm\pi$ by checking if the value is larger or smaller than π and subtracting or adding 2π, respectively.

Anti-windup integration

A common issue when using a PID controller is the winding-up of the integral term. When the state won't reach the desired value fast enough, e.g when the set-point is large or when a new set-point is set and the integral error is already large, the integral term will cause the system to be saturated for a large time period or even overshoot the set-point and drive the controller to instability.

To compensate for such scenarios, a technique known as integrator clamping is used. This means that the integral term of equation (5.6) is saturated by limiting the low and upper values to be within the saturation values of the actuators used. Consequently, the calculated integral error will never exceed the physical limitations of the thrust system.

Derivative kick

Based on equation (5.6), the derivative term $\boldsymbol{K}_d \frac{d\boldsymbol{\eta}_e(t)}{dt}$, calculates the derivative of the error, which includes both the reference and the actual state. In an occasion where there is a sudden change in this error, similar to a step change, the result will be a spiked derivative. This is known as a "derivative kick". To compensate for this issue, the derivative correction of the PID controller is performed only on the actual state instead of the error, transforming the aforementioned term of equation (5.6) to $\boldsymbol{K}_d \frac{d\boldsymbol{\eta}(t)}{dt}$.

5.4 Control Allocation

After calculating the generalized control forces $\boldsymbol{\tau}$ that need to act upon the vessel in order to maintain its position and heading, it is necessary to transform them in a meaningful control input value $\boldsymbol{u}$, for the actuators installed inside the vessel, for example a specific rotational speed for an engine or angle for a rudder. This is achieved inside the control allocation block as shown in the following block diagram.

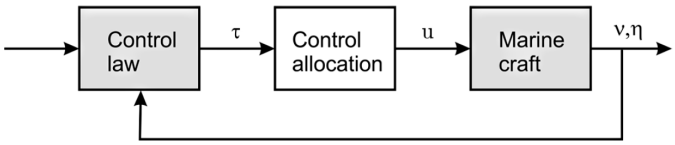

Figure 5.3: Block diagram showing control allocation in feedback system, [8]

In most cases, the computation of $\boldsymbol{u}$ from $\boldsymbol{\tau}$ is a model-based optimization problem, which can be as simple as introducing a single actuator rate saturation to highly advanced and complex, encapsulating all geometrical constraints and saturating limits and even posing specific optimization target, for example minimum usage of power for electrical thrusters or minimum fuel consumption for engines. The techniques adapted for solving such problems are many and are far beyond the scope of this project. Great research has been conducted on this subject and useful results are presented in [16], [21], [23], [5]. In this thesis, the thrust allocation problem will be simply implemented based on the aforementioned publications and at this step of the project will be based on simple rules and constraints regarding output thrust limits of the power system.

The control force due to an actuator can be written, assuming linearity, as:

$$f = ku \tag{5.25}$$

where k is the force coefficient depending on the geometrical characteristics and type of actuator and u the control input depending again on the actuator concept of producing thrust, for example rotational speed in revolutions per minute for a propeller. The above linear model can be also used to describe non-linear relation between control input and resulting force by modifying accordingly the force coefficient k.

The total forces and moments, with force vector defined as $\boldsymbol{f} = [F_x, F_y, F_z]^T$, for a vessel in 6 DOF, are expressed as:

$$\boldsymbol{\tau} = \begin{bmatrix} F_x \\ F_y \\ F_z \\ F_z l_y - F_y l_z \\ F_x l_z - F_z l_x \\ F_y l_x - F_x l_y \end{bmatrix} \tag{5.26}$$

where $\boldsymbol{r} = [l_x, l_y, l_z]^T$ are the moment arms.

Regarding dynamic positioning, where only the forces on the horizontal plane are considered, we obtain the following reduced generalized force vector matrix (5.27):

$$\boldsymbol{\tau} = \begin{bmatrix} F_x \\ F_y \\ F_y l_x - F_x l_y \end{bmatrix} \tag{5.27}$$

The actuator forces and moments relate to the control forces and moments by:

$$\boldsymbol{\tau} = \boldsymbol{T}\boldsymbol{f} = \boldsymbol{T}\boldsymbol{K}\boldsymbol{u} \tag{5.28}$$

where $\boldsymbol{T}$ is a geometrical matrix, defined as thrust configuration matrix, which is posing how each applied control force is affecting a specific motion.

Regarding the operation of the hardware equipment, system's pump is designed to operate on an on/off principle, giving no option for controlling the revolutions of the impeller. Moreover, it is stated that the maximum thrust output is fixed and always split equally between the nozzles operating at a specific time. Based on the aforementioned facts, there is no direct model for transforming the required thrust to an actual measurable unit such as revolutions. Consequently, for the simulations, it is assumed that the required thrust can be produced within pump's limits and the actuator internal model is bypassed.

As a first approach for the vessel under consideration in this project, it has been decided to make the following geometrical configuration, shown in Figure 5.4, regarding the positions of the actuators, with six total nozzles for water displacement under operation.

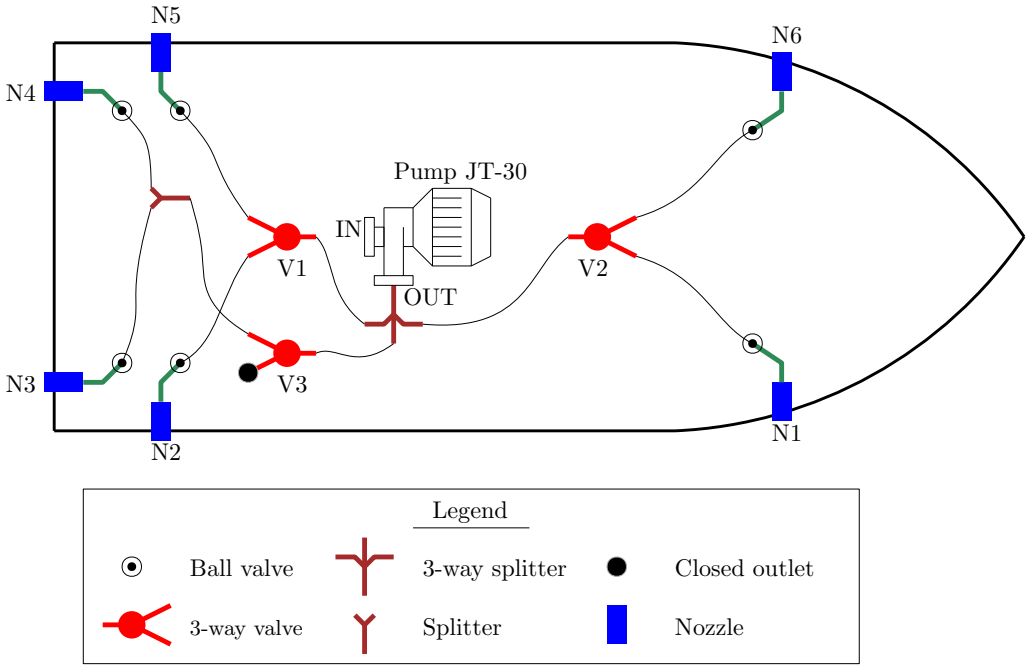

Figure 5.4: Initial nozzle configuration for thrust allocation

Specifically, two nozzles will be placed on the hull's transom, having equal distance lb from the longitudinal plane of symmetry and also equal amount of thrust will always be allocated, so as to produce only force in surge direction and not also contribute to yaw moment.

Moreover, the next two nozzles will be placed on the aft part of the hull at a distance lxa, as far as possible from the body-frame origin CO, located amidships. Lastly, the final two nozzles will be on the fore part of the hull, also at maximum possible distance lxf from the origin CO.

After inspecting hull's geometry and body plans, it was decided to simulate the vessel motions with the nozzles distances as shown in Table 5.3.

Table 5.3: Nozzle distances from body-frame origin

Distance	Value [m]
lxf	4.5
lxa	4
lb	0.75

After having defined the position of the total number of actuators (nozzles), the following Schematic 5.5, depicts the possible forces that can act on the vessel at a specific time. Based on momentum conservation principle, the direction of acting force on the hull from a nozzle is the opposite of the direction that the water is ejected.

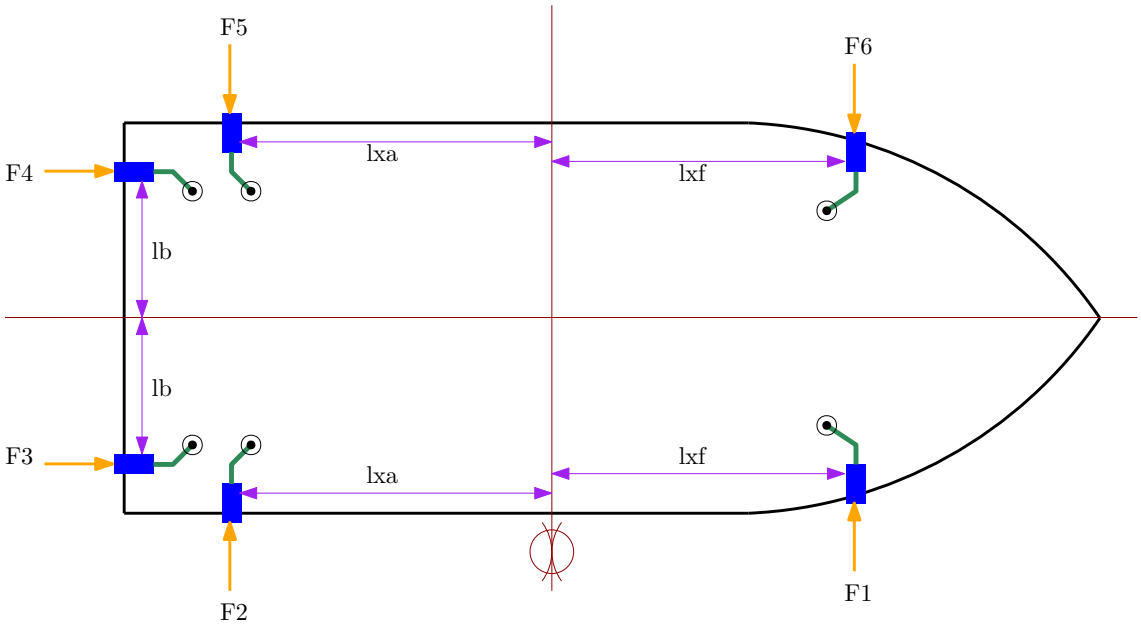

Figure 5.5: Diagram of nozzle control forces

Based on the above Schematic 5.5, the vessel can be controlled based on the following assumptions:

- Transom nozzles produce a total force F_x, acting only on the surge direction and also it can be only positive based on the defined body axes.
- Aft nozzles can produce a force F_{1y}, which can be either positive or negative. Depending on the required direction, nozzle 2 or nozzle 4 will be activated.
- Fore nozzles can produce a force F_{2y}, which can be either positive or negative. Depending on the required direction, nozzle 1 or nozzle 6 will be activated.
- Activation of either aft or fore nozzles as well as both of them, creates a moment around the body-frame z axis that can be calculated based on the equation: $M_z = F1y\, lxa + F2y\, lxf$

Finally, equation (5.27), connecting the controller thrust vector $\boldsymbol{\tau}$ to the actuator forces f, can be rewritten as:

$$\boldsymbol{\tau} = \begin{bmatrix} F_x \\ F_{1y} + F_{2y} \\ F_{1y}lxa + F_{2y}lxf \end{bmatrix} \tag{5.29}$$

The maximum thrust output for each nozzle operating at a specific time step, will be based on the number of total nozzles that are currently on use at the same time. As a result, no optimization technique is deployed to calculate actuator forces but rather a simplified algorithm based on the required thrust vector $\boldsymbol{\tau}$, which is fed by the PID controller.

The first step of the algorithm is the determination of active nozzles. This is achieved by checking if the controller output for a specific motion is non-zero. After the calculation of the total nozzle number, the maximum output actuator force is saturated with the pump's thrust output limits. Finally, the produced actuator forces are derived, as shown below.

Considering a thrust vector $\boldsymbol{\tau} = [X, Y, N]$, equation (5.29) is rewritten as:

$$\begin{bmatrix} X \\ Y \\ N \end{bmatrix} = \begin{bmatrix} F_x \\ F_{1y} + F_{2y} \\ F_{1y}lxa + F_{2y}lxf \end{bmatrix} \tag{5.30}$$

$$\Rightarrow \begin{bmatrix} F_x \\ F_{1y} \\ F_{2y} \end{bmatrix} = \begin{bmatrix} X \\ \frac{Ylxf - N}{lxf - lxa} \\ \frac{N - Ylxa}{lxf - lxa} \end{bmatrix} \tag{5.31}$$

The final force vector acting upon the vessel to control it will be:

$$\boldsymbol{F}_{control} = \begin{bmatrix} F_x \\ F_{1y} \\ F_{2y} \end{bmatrix} \tag{5.32}$$

The allocation algorithm is given in the thesis's appendix.

5.5 Observer

As explained in the previous sections, vessel position is obtained by sensors installed on board that are susceptible to noise. What's more, all the measurements include the high frequency component of wave excitation, which should not be compensated by the controller and thus needs to be excluded.

An observer should be designed so as to provide a solution to the aforementioned issues. Kalman filter is the most common approach as it provides a framework for both estimating an unknown system state and also filtering out any unnecessary wave components. But the great drawback is that it is difficult and time-consuming to tune the state estimator, since it requires fine tuning of the covariance matrices Q and R, as explained in paragraph [4.2.4], while the parameters also change, depending on the sea state.

Consequently, an alternative nonlinear passive observer design, as proposed in [8], [10] will be included in the simulations. The observer is based on the following two assumptions:

- The zero-mean Gaussian white noise terms included in wave modeling are omitted in the observer analysis
- The angle included in the rotation matrix R(ψ) is not affected by the wave-induced yaw disturbance ψ_w, since ψ_w is less than 1 degree in normal DP operations. This is depicted in the following equation (5.33), which is equation (3.34) for yaw motion:

$$y_3 = \psi + \psi_w \approx \psi \tag{5.33}$$

Under these assumptions, the DP system model for the passive observer is shown below:

$$\dot{\boldsymbol{\xi}} = \boldsymbol{A}_w \boldsymbol{\xi} \tag{5.34}$$

$$\dot{\boldsymbol{\eta}} = \boldsymbol{R}(y_3)\boldsymbol{\nu} \tag{5.35}$$

$$\dot{\boldsymbol{b}} = -\boldsymbol{T}^{-1}\boldsymbol{b} \tag{5.36}$$

$$\boldsymbol{M}\dot{\boldsymbol{\nu}} = -\boldsymbol{D}\boldsymbol{\nu} + \boldsymbol{R}^T(y_3)\boldsymbol{b} + \boldsymbol{\tau} + \boldsymbol{\tau}_{wind} \tag{5.37}$$

$$\boldsymbol{y} = \boldsymbol{\eta} + \boldsymbol{C}_w \boldsymbol{\xi} \tag{5.38}$$

where $\boldsymbol{b}$ is a bias term for including nonlinear dynamics and ocean currents coupled with a bias time constant $\boldsymbol{T}$, equations (5.35), (5.37) and (5.38) are the vessel mathematical model, as explained in previous paragraphs, with $\boldsymbol{\eta}_w = \boldsymbol{C}_w\boldsymbol{\xi}$ representing a linear wave response model. Finally, equation (5.34) is an internal equation for the wave model coupling linear response $\boldsymbol{\xi}$ and velocity $\dot{\boldsymbol{\xi}}$. Matrices $\boldsymbol{A}_w, \boldsymbol{C}_w$ are based on the wave characteristics.

The observer equations are chosen to copy the dynamics of the system presented above and are given below, (5.39) to (5.43). Moreover, the block diagram 5.6 depicts the internal structure of the observer.

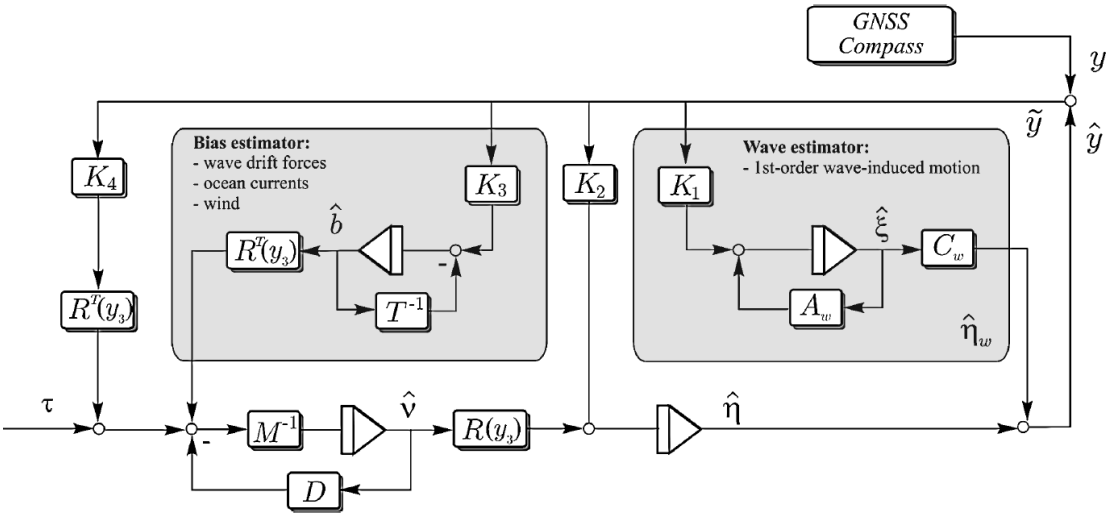

Figure 5.6: Block diagram of nonlinear passive DP observer, [8]

$$\dot{\hat{\boldsymbol{\xi}}} = \boldsymbol{A}_w\hat{\boldsymbol{\xi}} + \boldsymbol{K}_1(\omega_0)\tilde{\boldsymbol{y}} \tag{5.39}$$

$$\dot{\hat{\boldsymbol{\eta}}} = \boldsymbol{R}(y_3)\hat{\boldsymbol{\nu}} + \boldsymbol{K}_2\tilde{\boldsymbol{y}} \tag{5.40}$$

$$\dot{\hat{\boldsymbol{b}}} = -\boldsymbol{T}^{-1}\hat{\boldsymbol{b}} + \boldsymbol{K}_3\tilde{\boldsymbol{y}} \tag{5.41}$$

$$\boldsymbol{M}\dot{\hat{\boldsymbol{\nu}}} = -\boldsymbol{D}\hat{\boldsymbol{\nu}} + \boldsymbol{R}^T(y_3)\hat{\boldsymbol{b}} + \boldsymbol{\tau} + \boldsymbol{\tau}_{wind} + \boldsymbol{R}^T(y_3)\boldsymbol{K}_4\tilde{\boldsymbol{y}} \tag{5.42}$$

$$\hat{\boldsymbol{y}} = \hat{\boldsymbol{\eta}} + \boldsymbol{C}_w\hat{\boldsymbol{\xi}} \tag{5.43}$$

The presented observer equations, (5.39) - (5.43), are exactly the same as the system's equations, (5.34) - (5.38) with the only difference that four gain matrices $\boldsymbol{K}_i$, $i = 1, 2, 3, 4$ are included, which require tuning for approximating the wave model characteristics. The gain matrices are computed based on the equations (5.44) to (5.47).

$$\boldsymbol{K}_1(\omega_0) = \begin{bmatrix} diag\{K_{11}(\omega_{o1}), K_{12}(\omega_{o2}), K_{13}(\omega_{o3})\} \\ diag\{K_{14}(\omega_{o1}), K_{15}(\omega_{o2}), K_{16}(\omega_{o3})\} \end{bmatrix} \tag{5.44}$$

$$\boldsymbol{K}_2 = diag\{K_{21}, K_{22}, K_{23}\} \tag{5.45}$$

$$\boldsymbol{K}_3 = diag\{K_{31}, K_{32}, K_{33}\} \tag{5.46}$$

$$\boldsymbol{K}_4 = diag\{K_{41}, K_{42}, K_{43}\} \tag{5.47}$$

Additionally, the matrix elements are given as:

$$K_{1i}(\omega_{oi}) = -2(\zeta_{ni} - \lambda_i)\frac{\omega_{ci}}{\omega_{oi}} \tag{5.48}$$

$$K_{1(i+3)}(\omega_{oi}) = 2\omega_{oi}(\zeta_{ni} - \lambda_i) \tag{5.49}$$

$$K_{2i} = \omega_{ci} \tag{5.50}$$

where $\zeta_{ni} > \lambda_i$ is the notch of the filter and $\omega_{ci} > \omega_{oi}$ is the filter cutoff frequency. Here it is chosen to be $\zeta_{ni} = 1$ and $\omega_{ci} = 1.3\omega_{oi}$. What's more, ω_{oi} and λ_i are the wave spectrum's peak frequency and damping coefficient, as presented in Chapter 3.

Finally, the gains K_3 and K_4 are tuned based on the following requirement (5.51):

$$\frac{1}{T_i} \ll \frac{K_{3i}}{K_{4i}} < \omega_{oi} < \omega_{ci} \tag{5.51}$$

where T_i is the bias time constant of equation (5.36).

For a wave peak frequency of $\omega_0 = 0.8\ [rad/s]$, the gain matrices have the following form:

$$\boldsymbol{K}_1 = \begin{bmatrix} -diag\{1.924, 1.924, 1.924\} \\ diag\{1.184, 1.184, 1.184\} \end{bmatrix} \tag{5.52}$$

$$\boldsymbol{K}_2 = diag\{1.04, 1.04, 1.04\} \tag{5.53}$$

$$\boldsymbol{K}_3 = 0.2diag\{300, 300, 300\} \tag{5.54}$$

$$\boldsymbol{K}_4 = 0.4diag\{300, 300, 300\} \tag{5.55}$$

In the following Figures 5.7, 5.8, the actual wave disturbance and observer estimation after filtering are depicted, for a peak wave frequency of $\omega_0 = 0.8\ [rad/s]$.

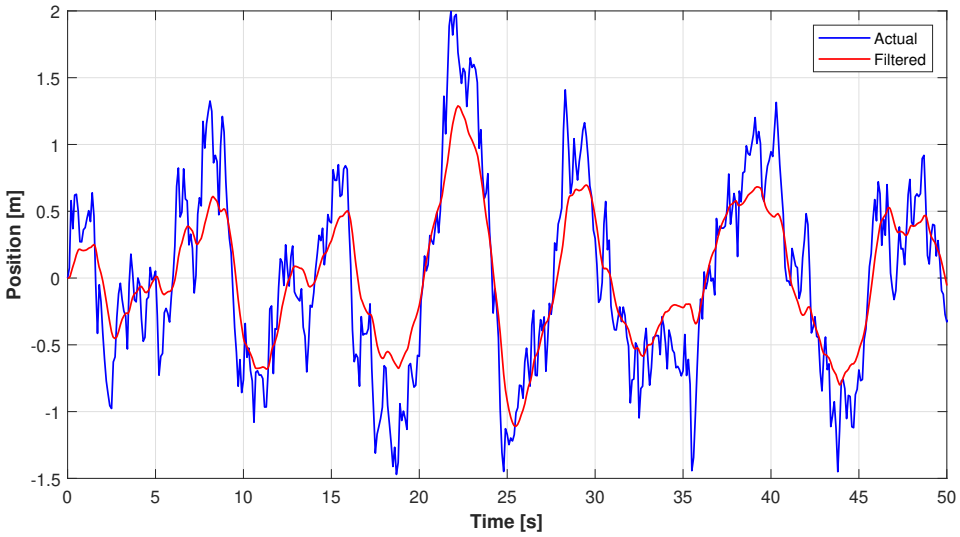

Figure 5.7: Observer estimation for wave disturbance in x and y position

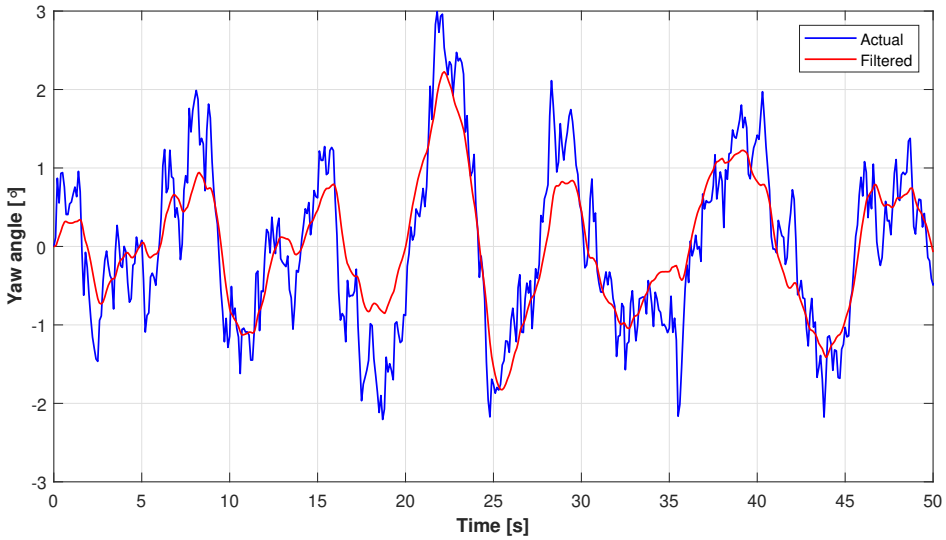

Figure 5.8: Observer estimation for wave disturbance in yaw angle

Chapter 6

Simulation and Results

6.1 Configuration

6.1.1 Parameters

Some of the parameters mentioned in the previous paragraphs, regarding vessel's geometry and loading condition, are not readily available. This includes the position of center of gravity and center of buoyancy as well as the total hull mass for the simulations. The only available drawings of the vessel are the general arrangement and body plans as shown in Figure 6.1.

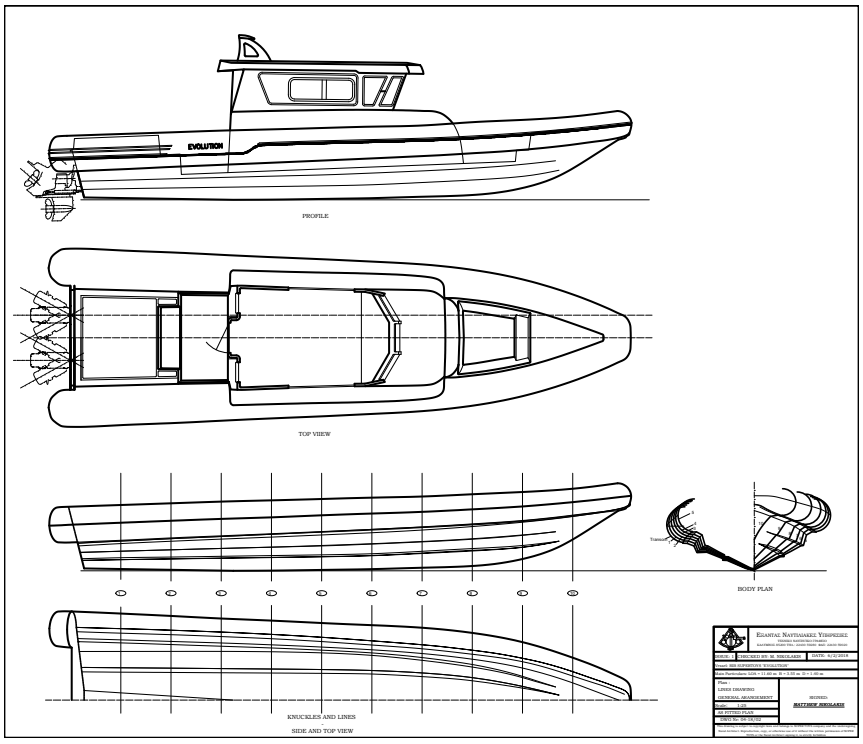

Figure 6.1: Evolution vessel - Body plans and General Arrangement

In order to estimate the vessel's center of buoyancy and further parameters, a 3-D model of the hull was designed, based on the body plans, using the 3-D CAD software Rhinoceros. The resulting hull geometry is shown in Figure 6.2.

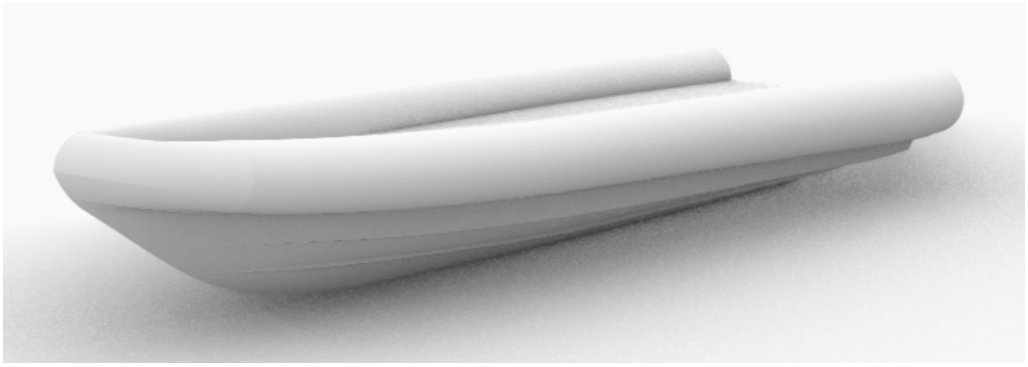

Figure 6.2: Evolution vessel - 3D CAD model rendered

The bare hull mass is given by the boat builder to be:

$$m_{hull} = 1700 \ [kg] \tag{6.1}$$

Regarding normal operations, where the vessel is considered fully equipped, with both engine fuel tanks at half-capacity, the total mass is measured to be:

$$m_{total} = 4600 \ [kg] \tag{6.2}$$

Calculation of the longitudinal center of gravity will be based on the principle of moments. The total vessel mass is distributed in groups, as shown in the following table. The center of gravity for each group is measured from the origin point located amidships. Additionally, during operations, three rescuers are considered to be the crew on board, with an average weight of 70 kg.

Table 6.1: Vessel LCG calculation based on principle of moments

	Weight [kg]	Distance [mm]	Mi [kg.mm]
Hull	1700	-1100	-1870000
Engine and Fuel	1300	-5800	-7540000
Superstructure	1300	-600	-780000
Constants	300	-2500	-750000
Crew	210	-2000	-420000

Based on Table 6.1, the longitudinal center of gravity is:

$$\text{LCG} = \text{-2.362 [m]}$$

The final parameter, required for the simulations is the longitudinal center of buoyancy. With the aid of the vessel's 3D-model, the operating waterline was varied until the displacement of the vessel was equal to the total weight given above, in calm water equilibrium with salt water density equal to $\rho = 1.025\,t/m^3$. The results derived are summarized in Table 6.2.

Table 6.2: Vessel hydrostatic parameters

Parameter	Value	Unit
Draft (from B.L.)	0.551	m
LCB	-1.109	m
LCF	-0.881	m
WSA	20.72	m^2
L_{WL}	9.592	m
C_B	0.656	-

After having defined all the necessary parameters for the matrices present in the mathematical model, the matrices used in the simulations are given below with their final values, by equations (6.3), (6.4).

$$\boldsymbol{M}^{CO} = \begin{bmatrix} 5249.7 & 0 & 0 \\ 0 & 6584.3 & -10989.5 \\ 0 & -10989.5 & 41552.2 \end{bmatrix} \tag{6.3}$$

$$\boldsymbol{D}^{CO} = \begin{bmatrix} 529.1 & 0 & 0 \\ 0 & 673.4 & 0 \\ 0 & 0 & 2299.8 \end{bmatrix} \tag{6.4}$$

6.1.2 Scenarios

The simulations will evaluate the dynamic positioning system in both station keeping and heading control. The scenarios that will be run, in order to examine the feasibility of the system developed are shown in Table 6.3. In all the scenarios, it is assumed that the vessel is facing ocean currents by the bow with a magnitude of $\nu_c = 0.5\,[m/s]$ and wind forces also by the bow with a velocity depending on the scenario. Finally, the sea state codes refer to the wave characteristics of Table 3.1.

Table 6.3: Simulation Scenarios

Case	Control state	Sea state code	Wind velocity [knots]
1	Dynamic positioning	2	7
2	Dynamic positioning	4	10
3	Dynamic positioning	5	15
4	Low-speed maneuver	5	10

6.2 Simulink Model

A general overview of the simulation model that was built using the MatLab Simulink environment is shown in Figure 6.4, and the main blocks consisting the system are further explained.

The first step of the simulation is to define the desired position and heading that the vessel should keep, through the reference block of Figure 6.4, which is shown in detail in Figure 6.3 below. This includes defining the x and y coordinate as well as the yaw angle in degrees, all in the NED frame. The second order reference model is then built, as described in Section 5.3, and finally the reference vector $\boldsymbol{\eta}_d$ is the block output.

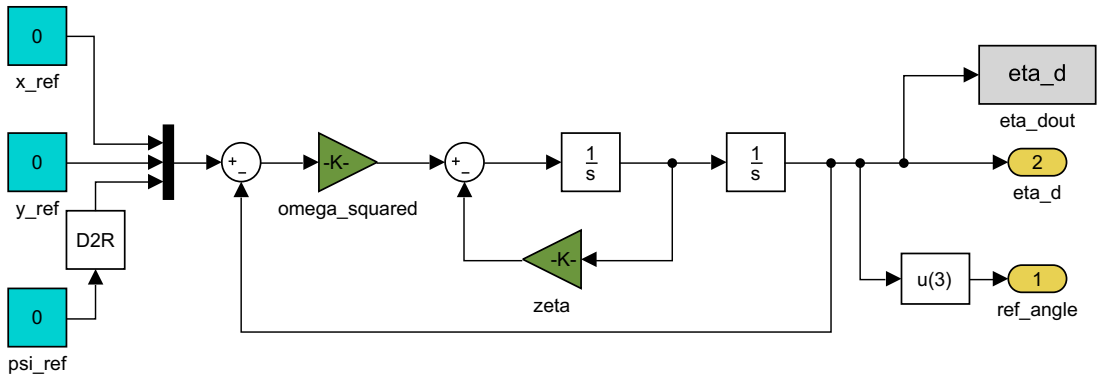

Figure 6.3: Reference model block

The reference vector, together with the actual vector of position and yaw angle that is obtained through the vessel's sensors, are then fed into the PID controller block, shown in Figure 6.6. Here, the ψ angle is wrapped between $\pm\pi$ and then the error vector is transformed into the BODY frame coordinates. After this, equation (5.6) is fully defined to finally receive the controller output signal $\boldsymbol{u}$, based on the gains K_p, K_i, K_d that have been calculated. What's more, the integral term of the equation, is clamped between thrust output limits by using a static limiter block.

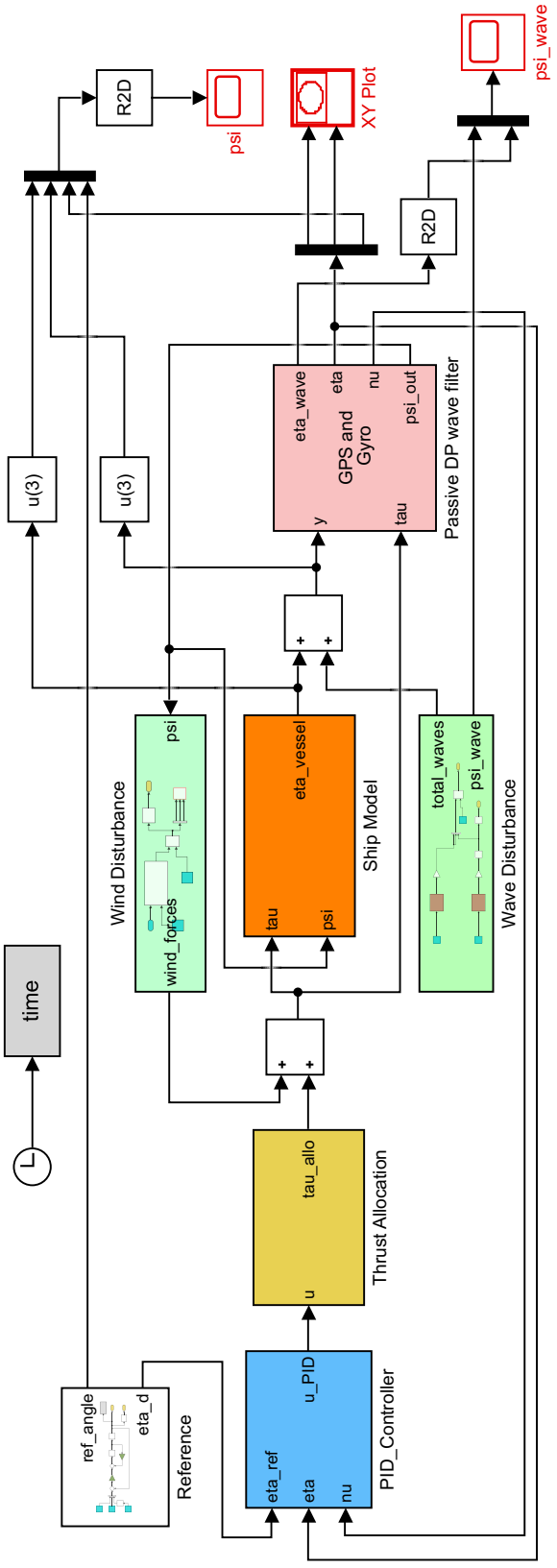

Figure 6.4: General overview of the Simulink model

The controller output signal $\boldsymbol{u}$ is then fed to the force allocation algorithm, which is given in the appendix of the thesis. At this point, the control thrust vector is bounded between the actuator's thrust limits and properly split, as explained in Section 5.4. For better visual observation, the equations of allocation are built through a function block instead of using a great number of Simulink blocks to represent them, as shown in Figure 6.5.

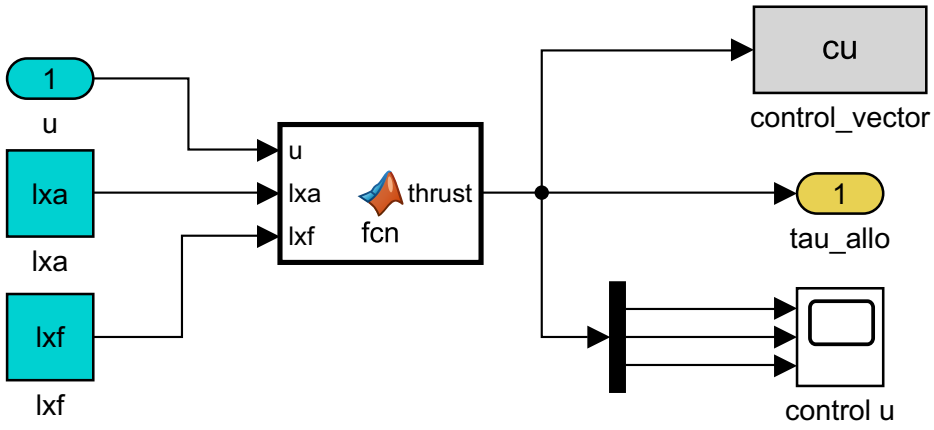

Figure 6.5: Thrust allocation block

The final allocated thrust vector $\boldsymbol{\tau}$ is then added to the wind disturbance vector $\boldsymbol{\tau}_{wind}$, and the resulting forces are acting upon a linear vessel model, representing the dynamics of the actual vessel, as formulated in Chapter 3. Inside the vessel model, equation (3.60) is defined, where also the ocean currents disturbance is included as a constant velocity deviation. The position and heading output is, finally, transformed into NED coordinates.

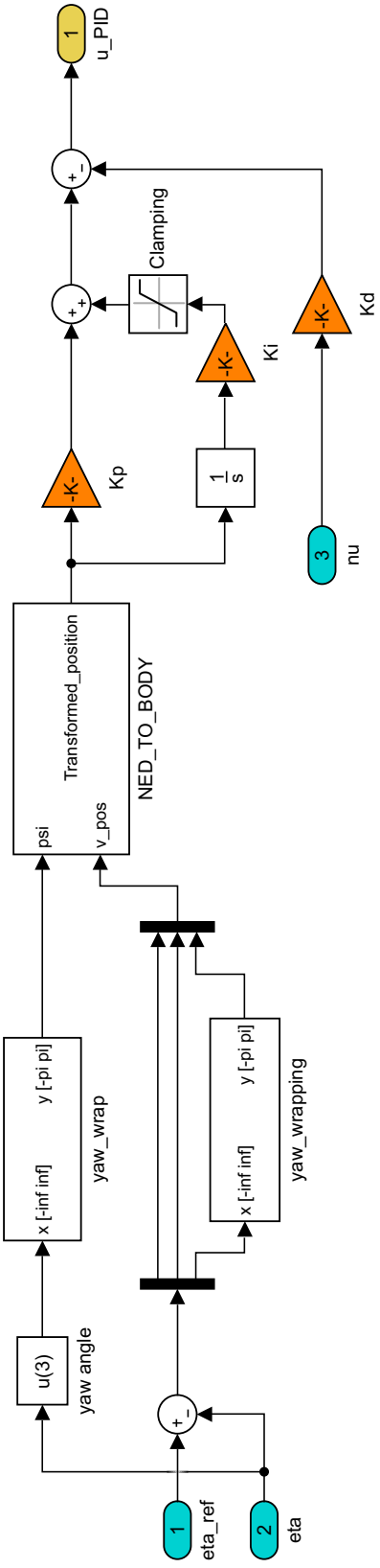

Figure 6.6: PID controller block

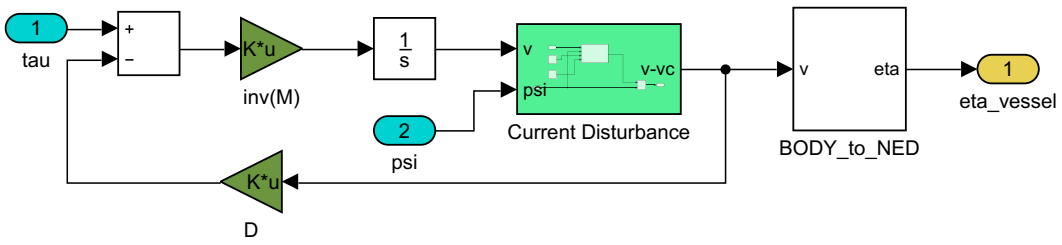

Figure 6.7: Linear vessel model block

The wind disturbance block is again formulated as a function block, which has the wind force algorithm that is given in the thesis's appendix. Between the different simulation scenarios, the wind velocity was the main parameter changed.

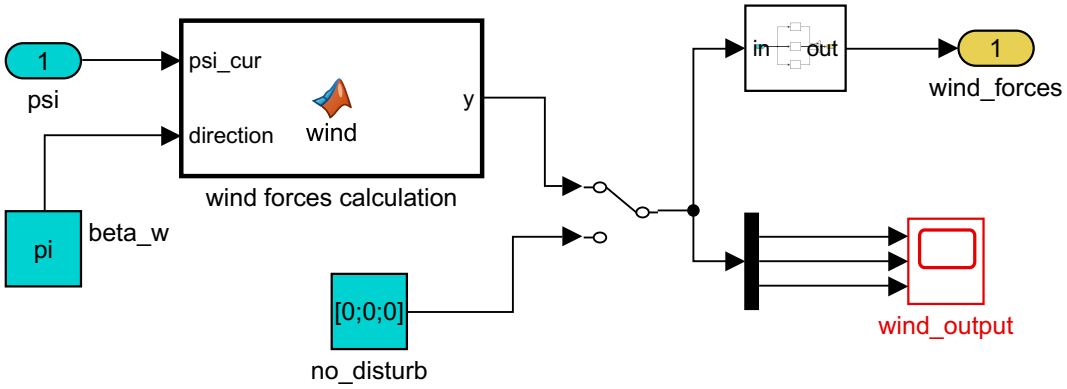

Figure 6.8: Wind disturbance block

At this point, the final environmental disturbance that needs to be included to the simulation is added up. The wave disturbance $\boldsymbol{\tau}_{wave}$ is formulated as shown in Figure 6.9, and then added to the output $\boldsymbol{\eta}$ vector of the linear vessel model. Note that there are different blocks for position and heading, due to the different requirements of K gain values. The wave model is based, as explained before, on equation (3.35). Three blocks are placed in line, starting with a zero mean Gaussian white noise, then a second order system, given by equation (3.37), with λ and σ parameters set per scenario and finally a gain block that acts as the wave gain K of equation (3.36).

As discussed in previous sections, the output vector of position and heading includes both the low and high wave frequencies. Consequently, a passive wave filter was built to feed back to the controller only the low frequency motion. The passive filter block is shown in the next Figure 6.10, and has the exact build scheme as explained in Section 5.5 and shown in Figure 5.6. The structure of this block is based on the open-source Simulink library, given by [11]. This block completes the simulation model.

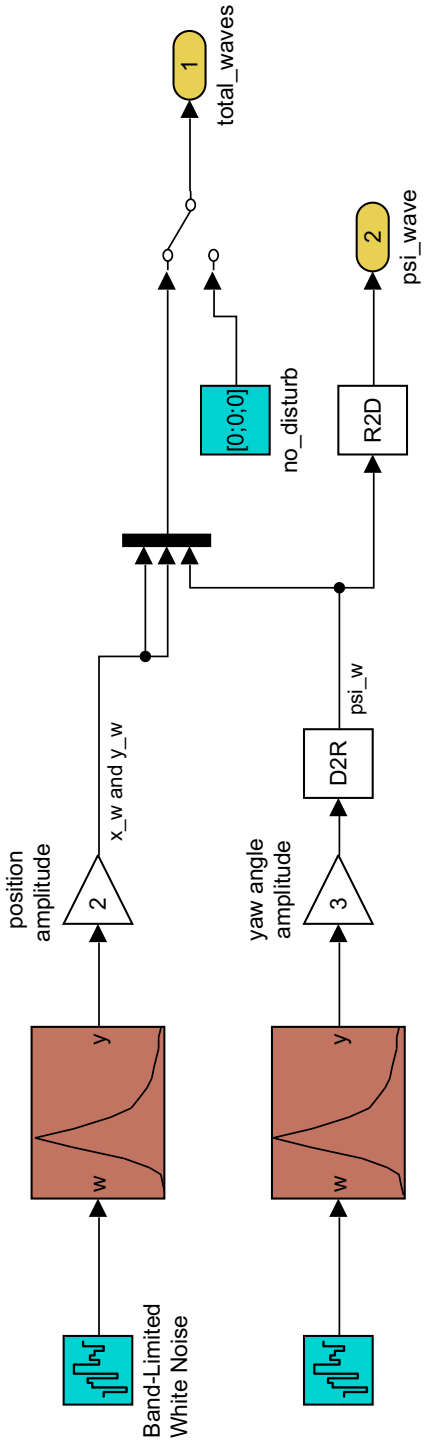

Figure 6.9: Wave disturbance block

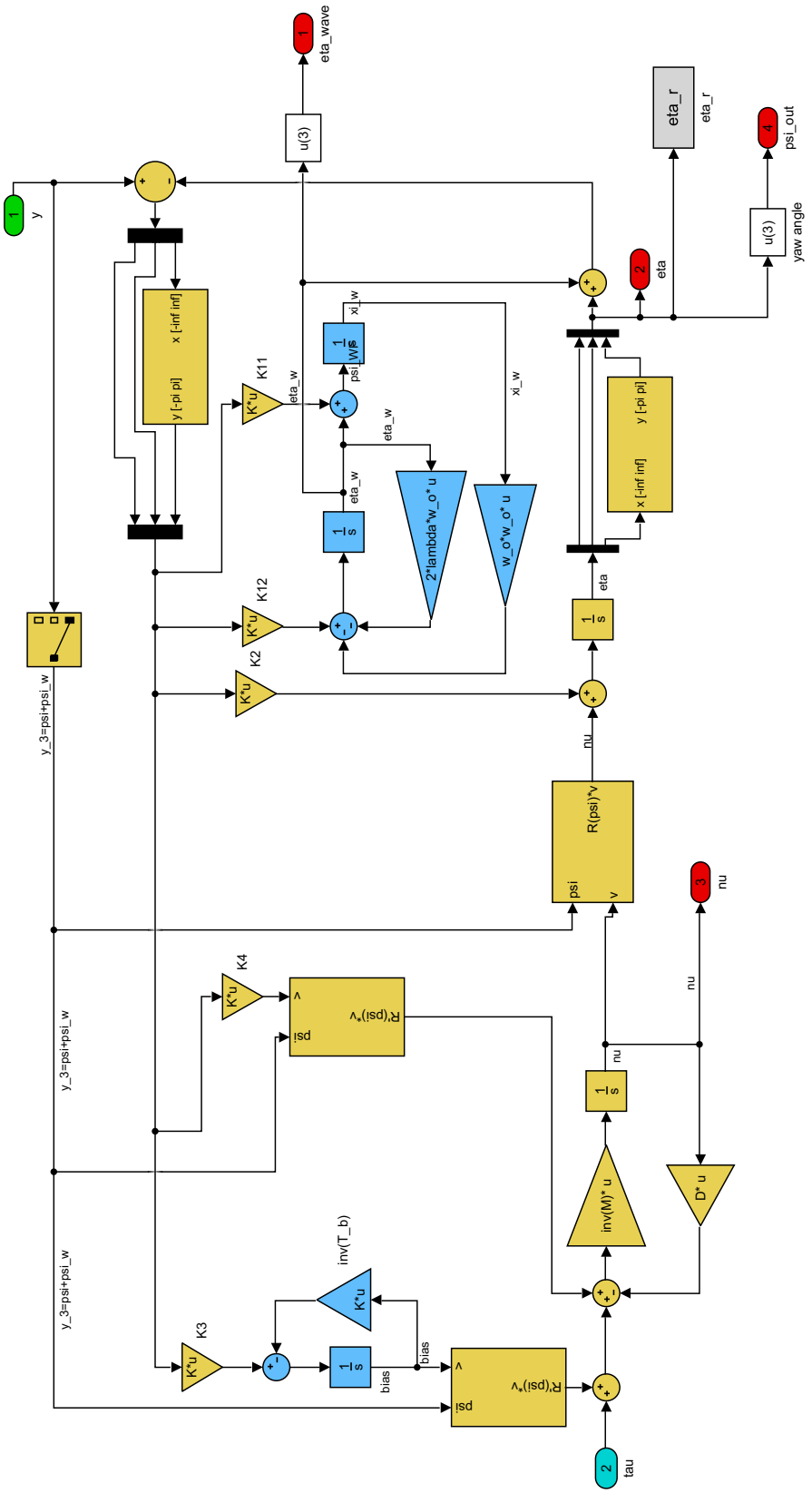

Figure 6.10: Passive DP observer filter block

6.3 Simulation Results

In this section, the results derived from the simulations of the aforementioned four scenarios of paragraph [6.1.2] are shown. For each scenario, a x-y plot shows the path the vessel is following, during DP operation. Moreover, the deviation of vessel's position and heading from the desired values is depicted. Finally, the control input $\boldsymbol{\tau}$ in terms of force and moments is shown, which is fed to the actuators by the controller. All the scenarios except case 4 were run for a total time of 100 seconds, whereas case 4 was run for 150 seconds to further evaluate low speed maneuvering.

Case 1

From the following Figures 6.11, 6.12, 6.13, it is concluded that the vessel maintains its reference position and heading within reasonable limits. For a DP system, position deviation should not be more than 1 [m] and heading deviation not more than 5 degrees. Both these limits are not exceeded. Additionally, one parameter that should be taken into consideration at this point, is the occasional saturation of sway control input. From Figure 6.13, it can be seen that the sway control input reaches its saturation point of 200 [N], but not for a great time period so as to be considered harmful for the actuators. But the fact that this occurred in a scenario with mild environmental loads, places the parameter of total system thrust as a candidate for alternation in greater sea states.

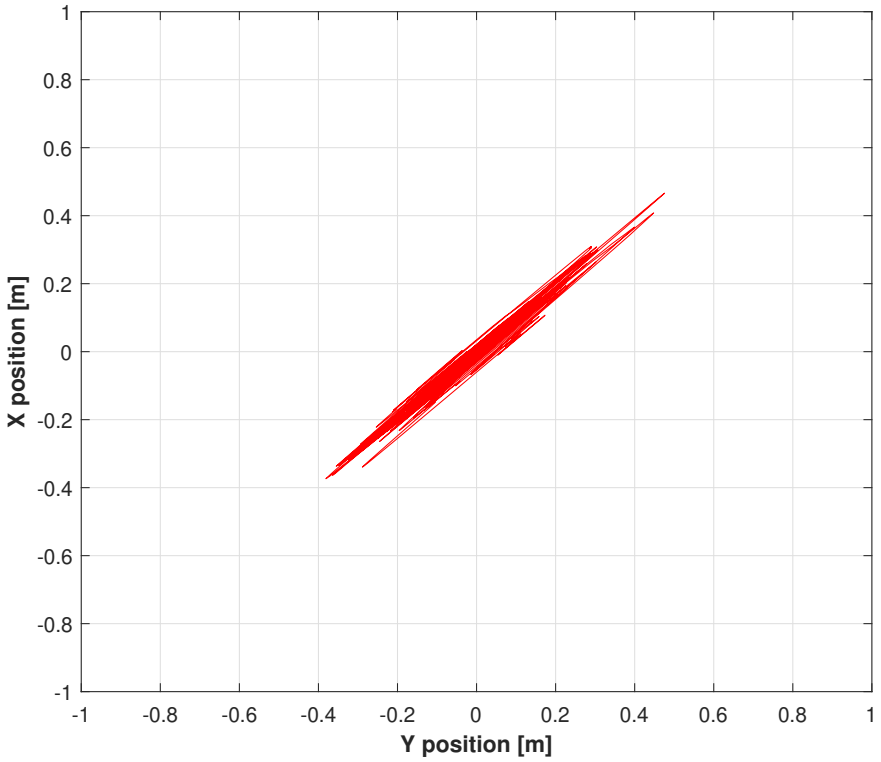

Figure 6.11: Case 1 - Vessel trajectory during DP operation

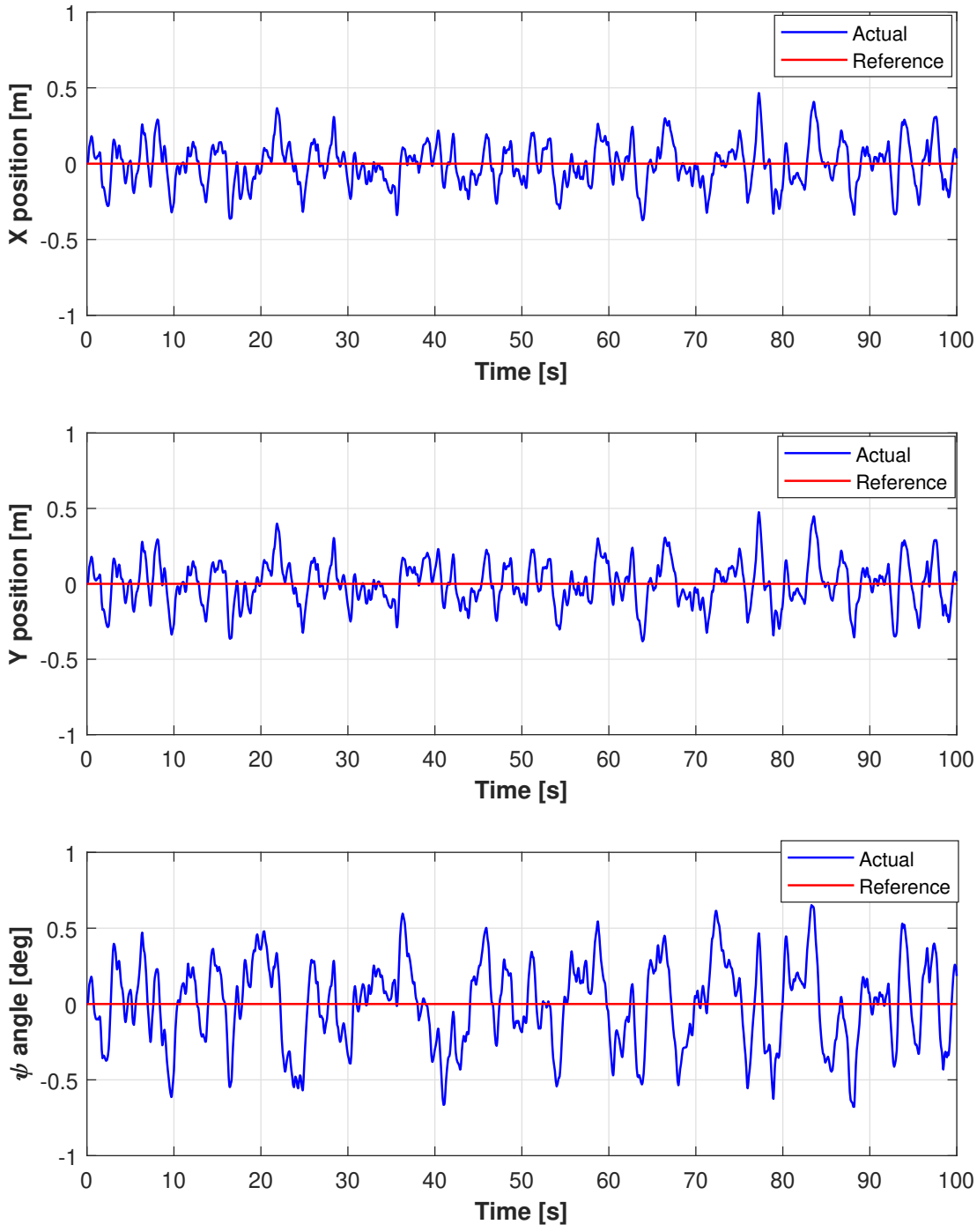

Figure 6.12: Case 1 - Vessel position and heading $\boldsymbol{\eta} = [x, y, \psi]$ in NED frame

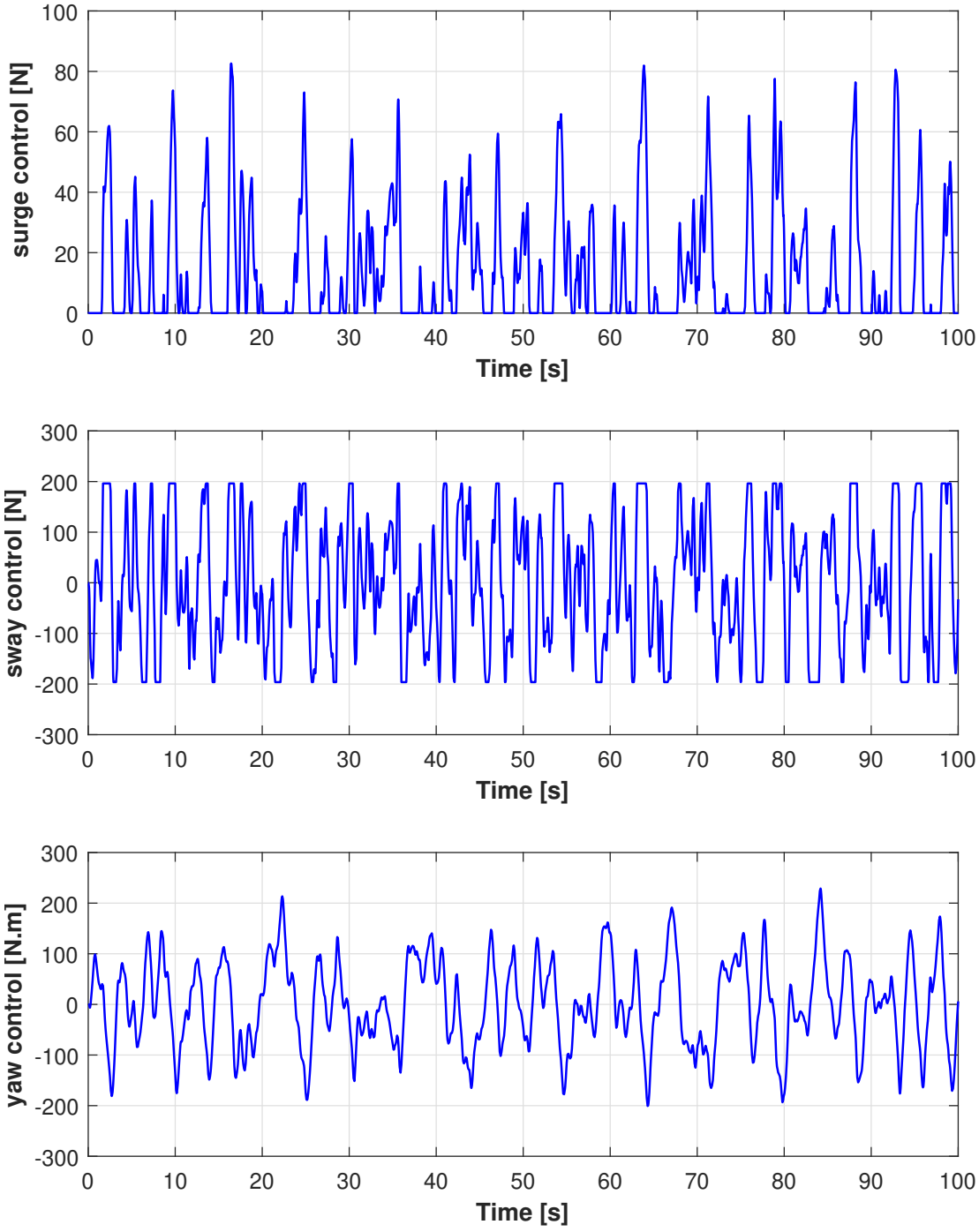

Figure 6.13: Case 1 - Control input $\boldsymbol{\tau}$ for surge, sway and yaw motions

Case 2

From the results of case 2, depicted in Figures 6.14, 6.15, 6.16, it can be seen that the vessel maintains its reference position and heading, without causing instability of the controller, but the deviation is greater than the acceptable limits. At certain time points, the vessel is more than 2 meters away from the desired fixed position and heading exceeds the 5 degrees limit. What's more, the controller output signal is highly saturated, and almost at any time interval the maximum possible thrust is fed to the system. This is clearly an unfavorable state, and thus it is decided to alternate the maximum system thrust value.

This is achieved by selecting a different pump for the system, which is producing the required thrust. From the manufacturer's catalog, the biggest possible pump is selected, that is the JT-90. The maximum thrust produced is tripled up, leading to 90 Kgf or approximately 900 N. Under these modifications, the simulation of case 2 is performed again, but now with the new thrust values.

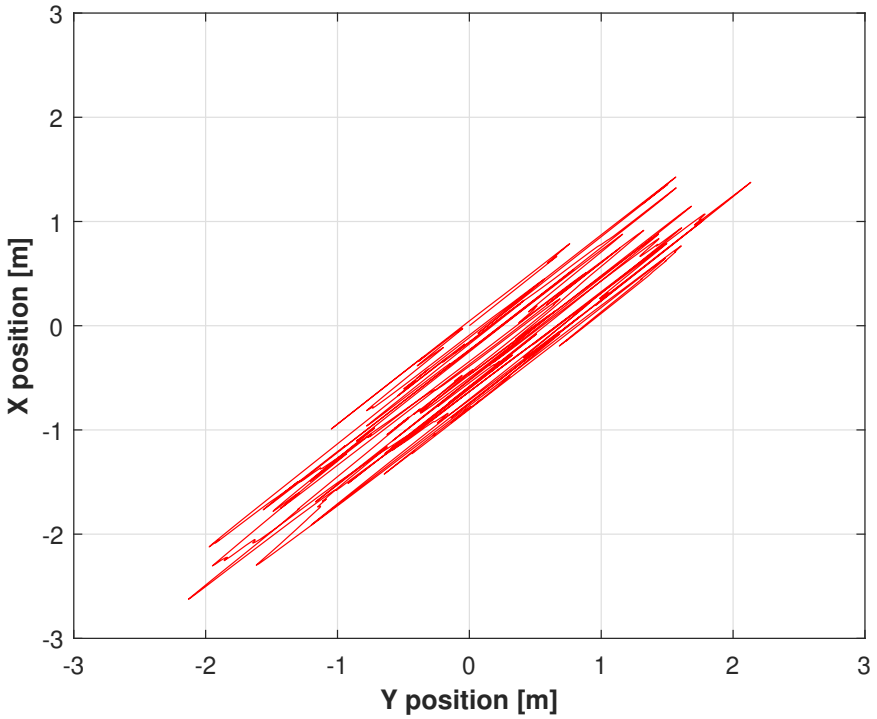

Figure 6.14: Case 2 - Vessel trajectory during DP operation

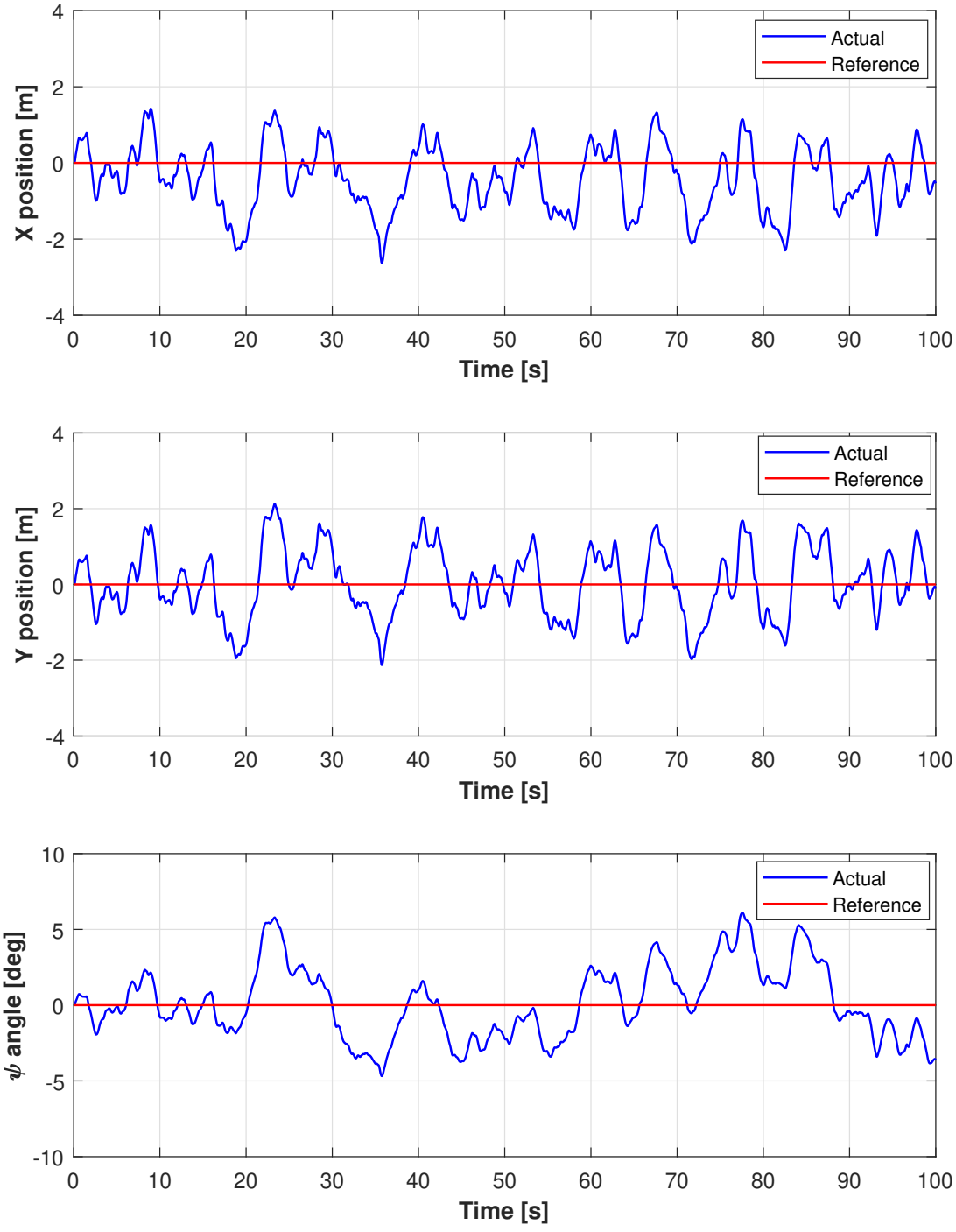

Figure 6.15: Case 2 - Vessel position and heading $\boldsymbol{\eta} = [x, y, \psi]$ in NED frame

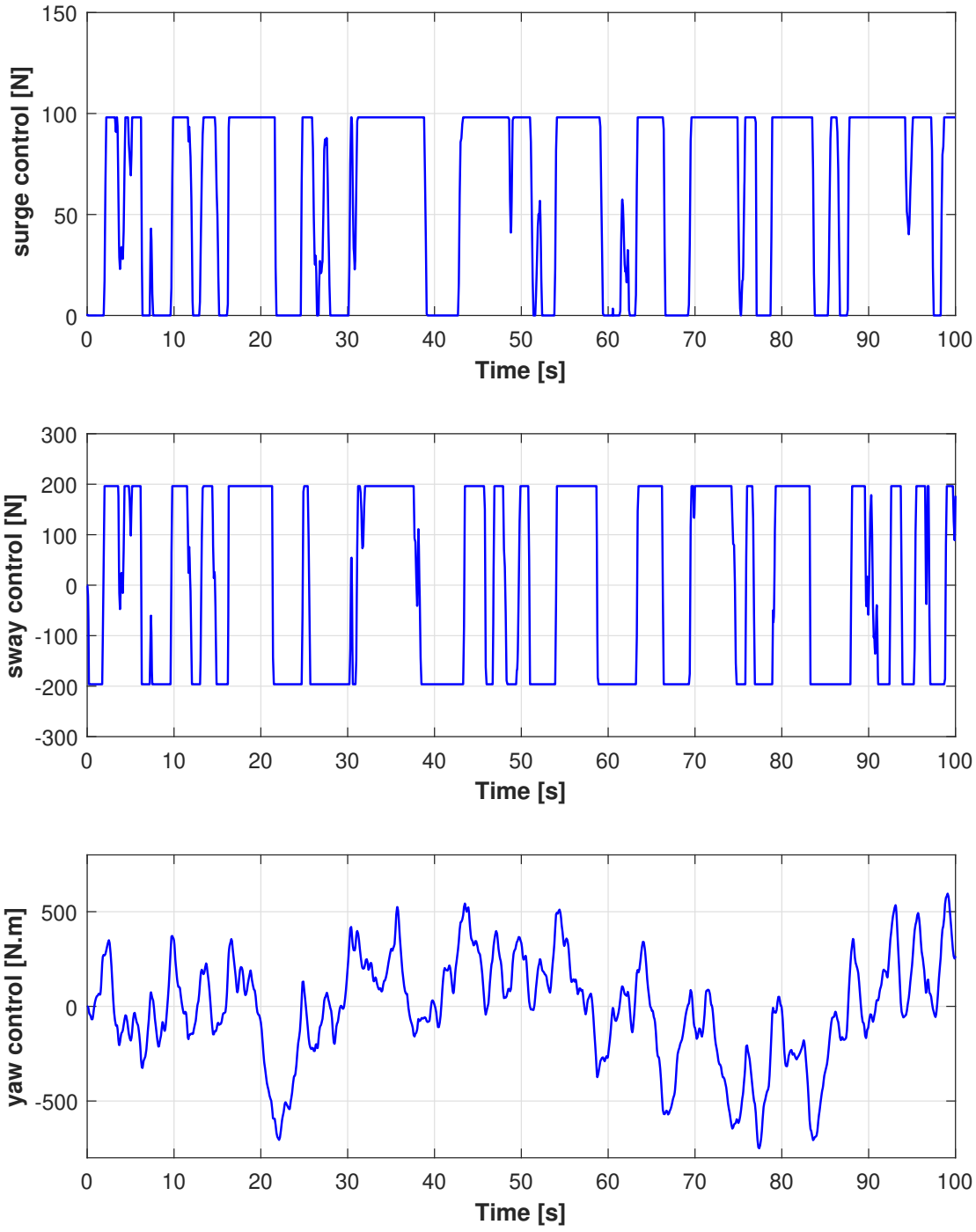

Figure 6.16: Case 2 - Control input $\boldsymbol{\tau}$ for surge, sway and yaw motions

Case 2 - New thrust limit

After modifying the maximum thrust limit, it is clear from Figures 6.17, 6.18, 6.19, that the vessel manages to hold its position and heading, and this time without exceeding the acceptable limits. Additionally, the controller is not getting unstable at any time point during simulation and the thrust output is reaching the saturation point for a limited time period and very few times, which is a sign of good system operation.

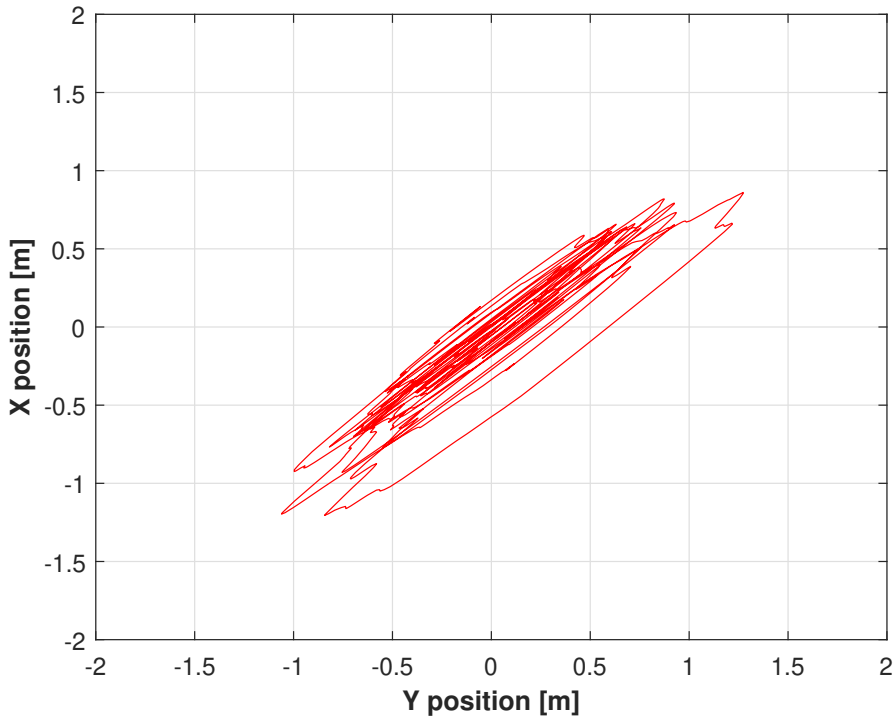

Figure 6.17: Case 2 Revised - Vessel trajectory during DP operation

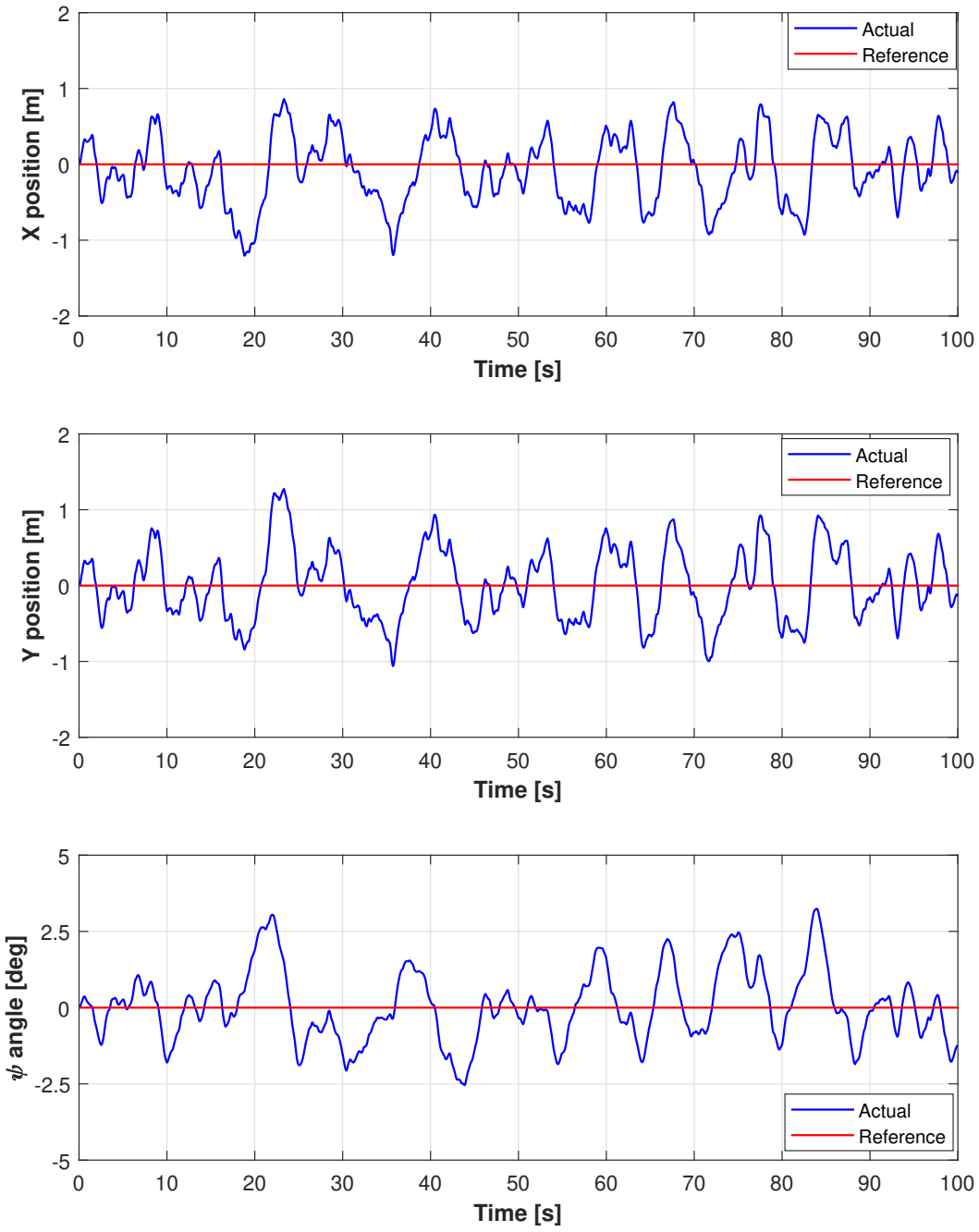

Figure 6.18: Case 2 Revised- Vessel position and heading $\boldsymbol{\eta} = [x, y, \psi]$ in NED frame

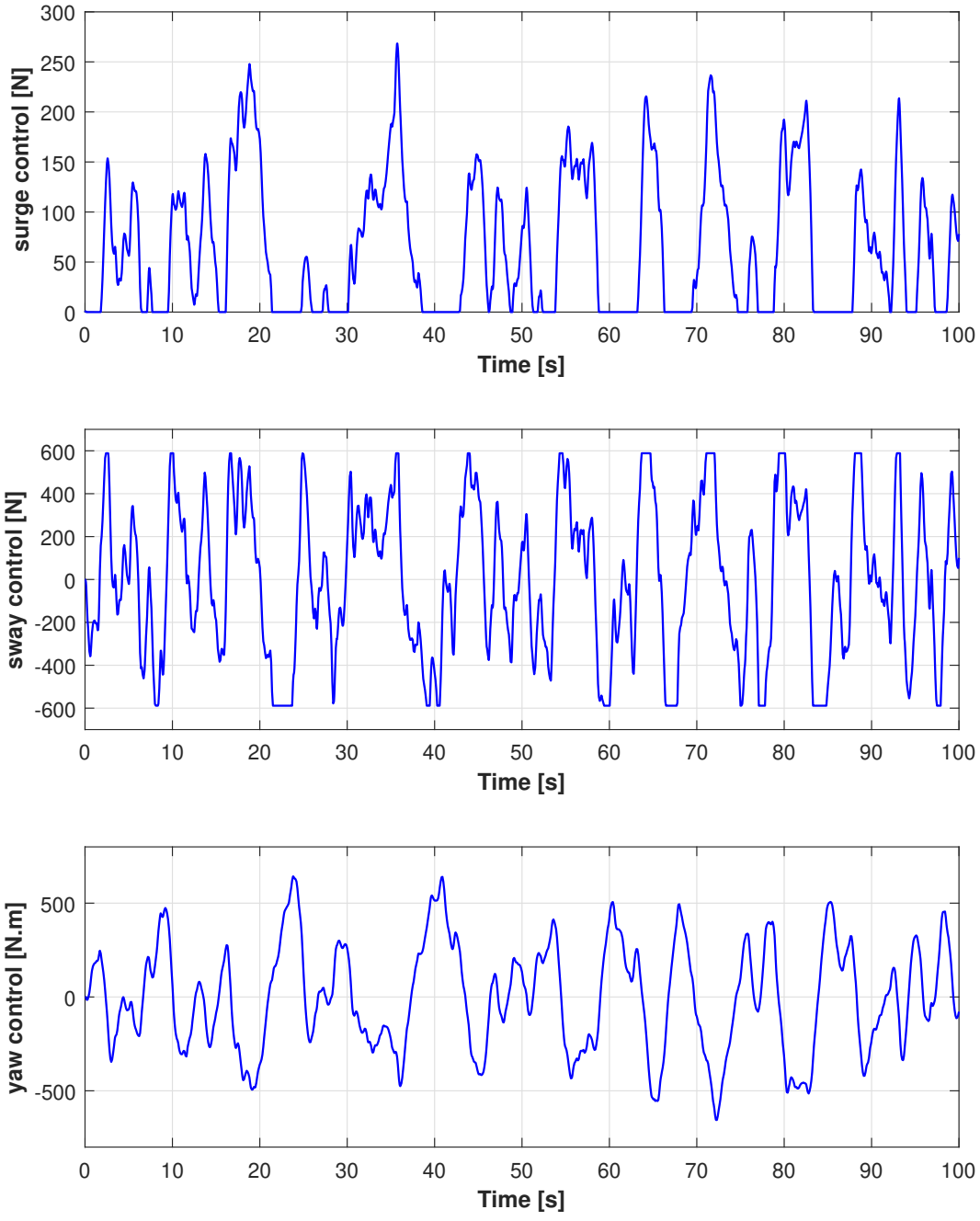

Figure 6.19: Case 2 Revised - Control input $\boldsymbol{\tau}$ for surge, sway and yaw motions

Case 3

This is the final scenario, where the vessel is considered to perform dynamic positioning. Based on Figures 6.20, 6.21, 6.22, it is again clear that the controller manages to keep the vessel stationary, with position and heading deviation inside the acceptable limits. Moreover, there is minimal thrust saturation and no controller instability is occurring. No further dynamic positioning scenarios are considered, since environmental loads, are already intense, at this final case. Concluding, the operational target is achieved for this case, which ultimately proves that dynamic positioning is feasible with this system setup.

In general, dynamic positioning is examined even with wind forces derived for 6-7 Beaufort, but based on hull geometry and thrust system setup, such scenarios are not evaluated. The final step, in order to complete the system evaluation is to ensure that the vessel is capable of performing a low speed maneuver.

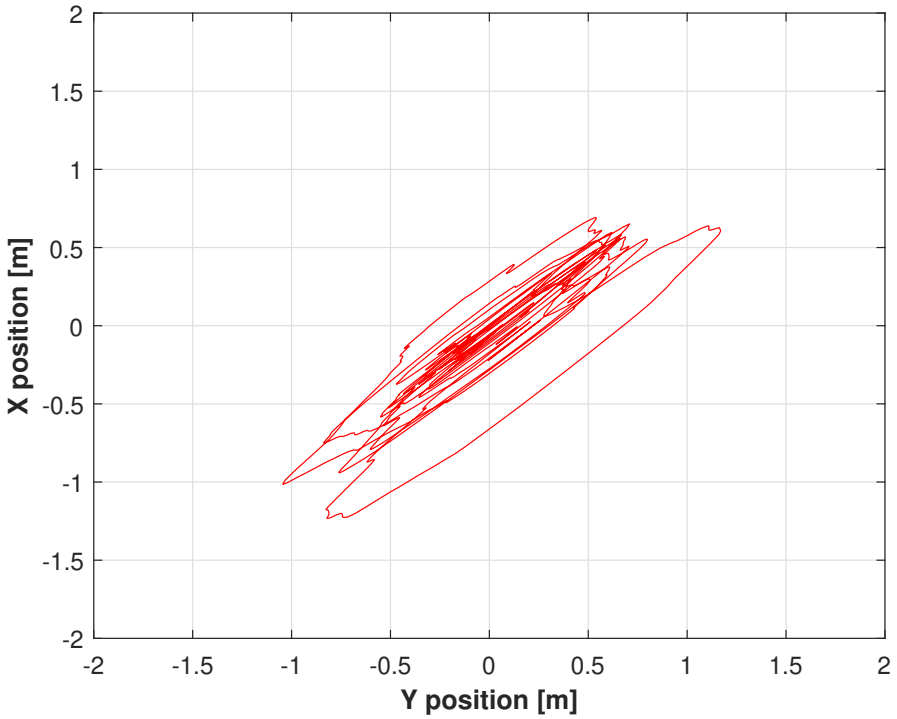

Figure 6.20: Case 3 - Vessel trajectory during DP operation

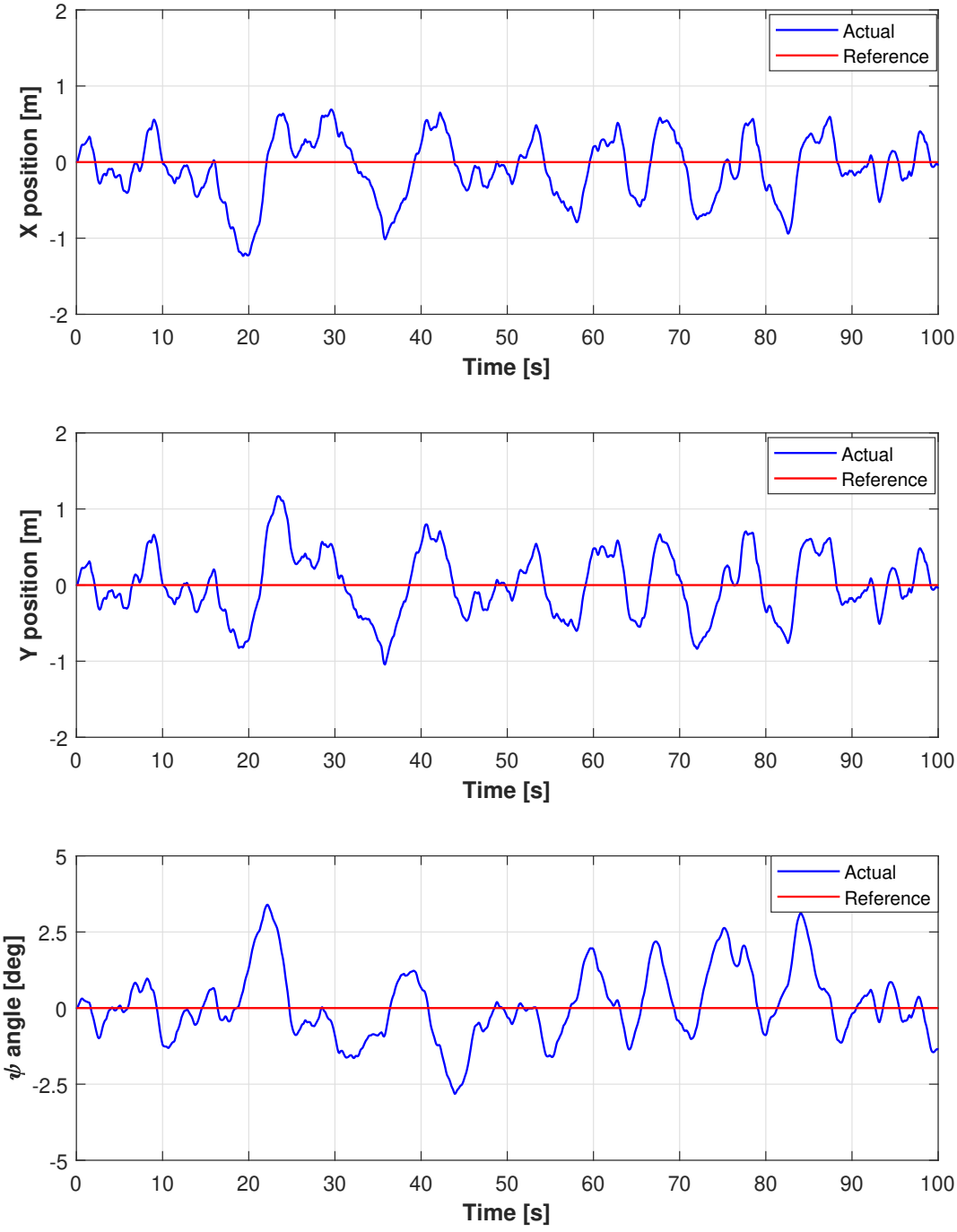

Figure 6.21: Case 3 - Vessel position and heading $\boldsymbol{\eta} = [x, y, \psi]$ in NED frame

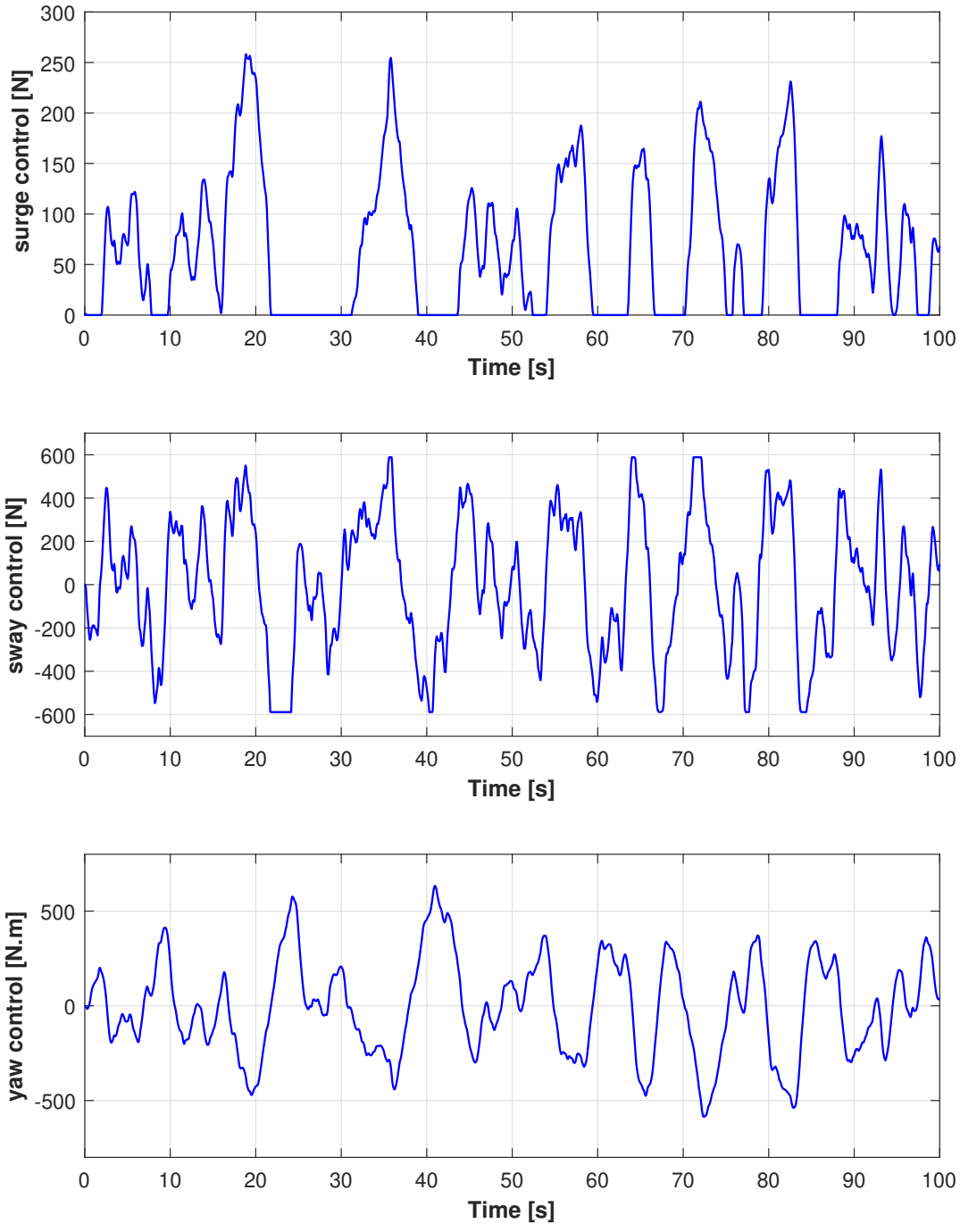

Figure 6.22: Case 3 - Control input $\boldsymbol{\tau}$ for surge, sway and yaw motions

Case 4

This scenario is performed so as to evaluate the reference model that was built for smoothing out the transitions. The vessel is considered to start the DP operation at a fixed location denoted as [0,0,0] in NED frame and the target to reach is [2,2,0]. This means that the vessel has to travel 2 meters in surge and sway direction, without final change of the heading angle, which is pointing towards North.

From Figures 6.23, 6.24, 6.25, it can be seen that the target point is reached within a reasonable time period of about 30 seconds. The vessel manages to perform a low-speed maneuver while the controller is stable at all times. Moreover, the actuators are saturated for very small time periods, and no saturation is observed for the first seconds of simulation, where the transition from one point to the other is performed. This indicates that the reference model successfully keeps the state error, which is fed to the PID controller, in low values, and thus unwanted control behavior is absent.

One drawback of the current system setup is observed for the x and y position of Figure 6.24, where it can be noted that the error in surge direction is not corrected until the target value in sway direction is achieved. This is happening because the proposed actuator setup is not providing surge force in both directions but only to move forward. As a result, based on the predefined environmental loads that are perturbing the vessel, the possible way of control is to drive one state to the target value and then do the same for the second one, but not simultaneously.

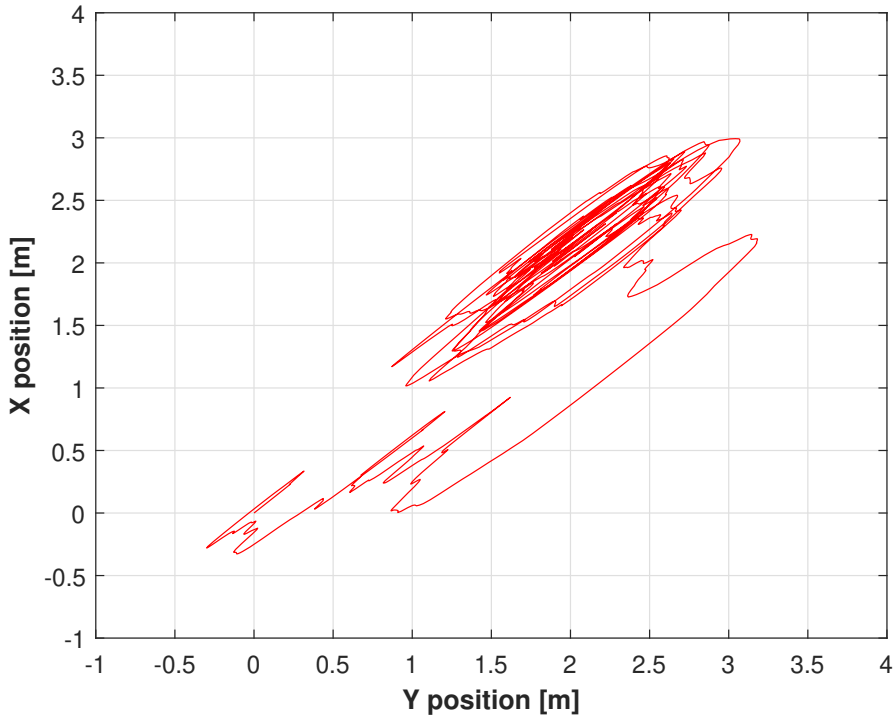

Figure 6.23: Case 4 - Vessel trajectory during a low-speed maneuver

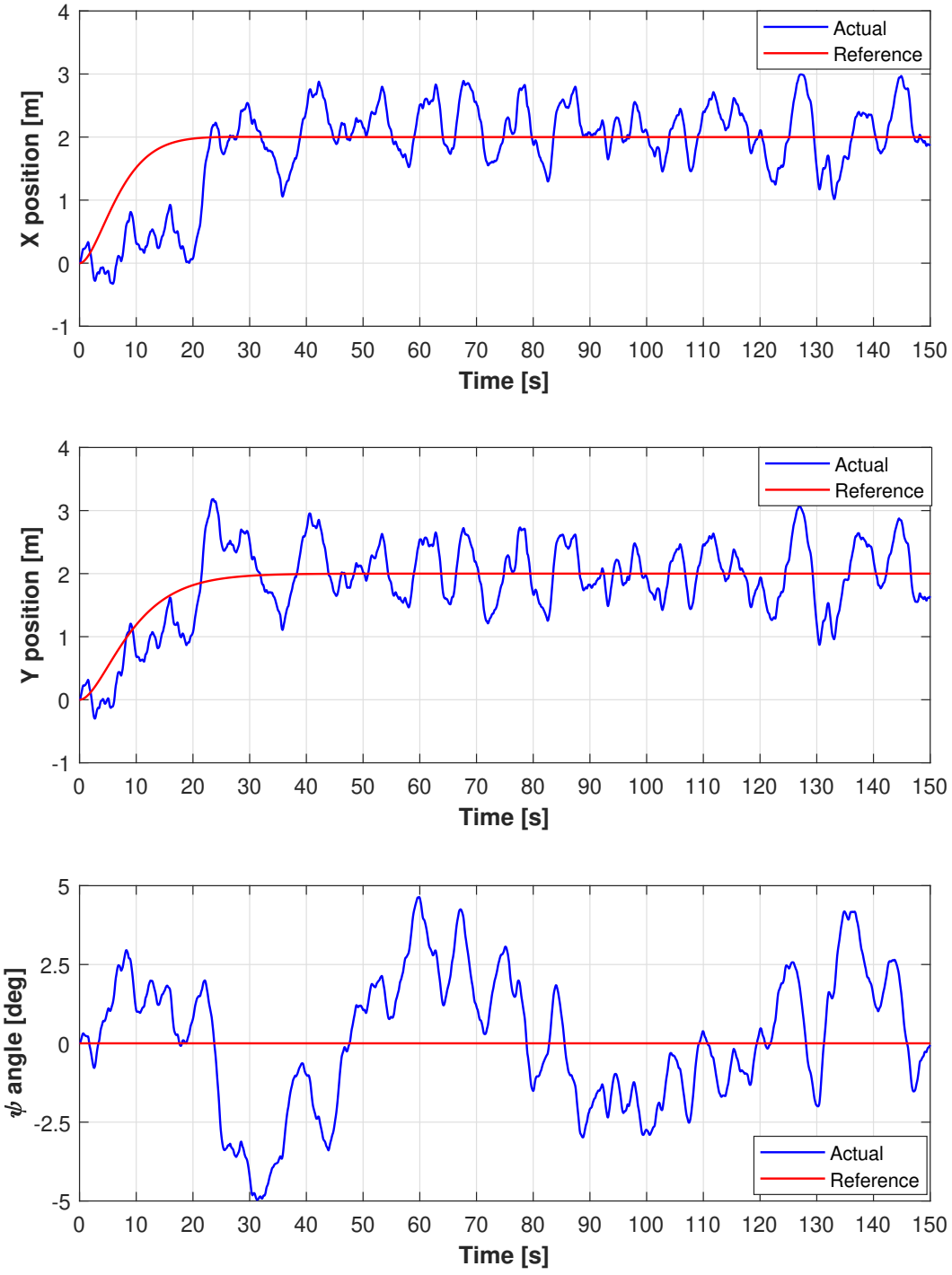

Figure 6.24: Case 4 - Vessel position and heading $\boldsymbol{\eta} = [x, y, \psi]$ in NED frame

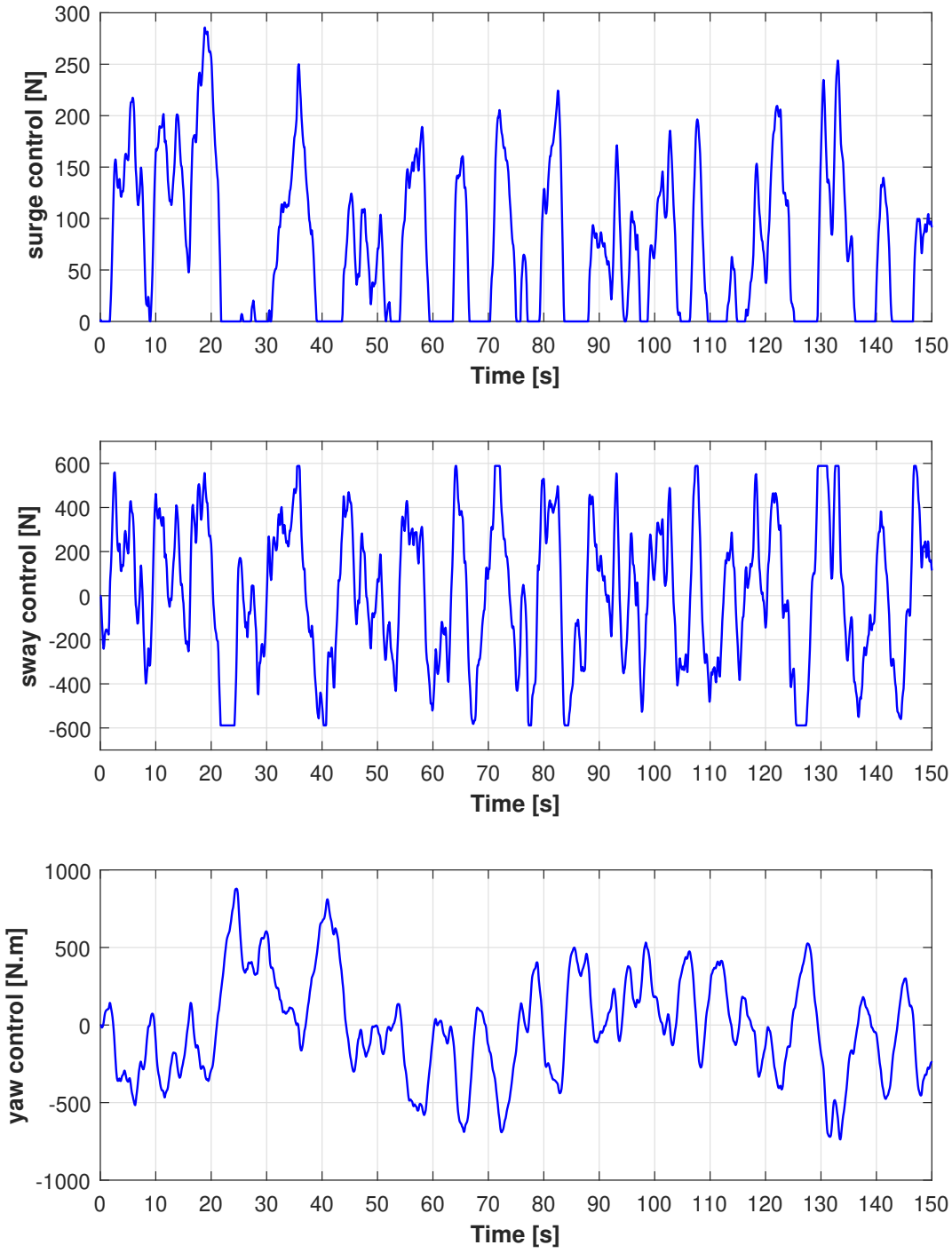

Figure 6.25: Case 4 - Control input $\boldsymbol{\tau}$ for surge, sway and yaw motions

6.4 Sea Trial Results

The final step of this thesis was to examine the functionality of the alternative dynamic positioning system in true weather and sea conditions. Consequently, a sea trial was conducted, where the system was tested to ensure proper performance. Additionally, the data logger was installed on board so as to record the pitch, roll and heading angles together with the position of the vessel. Moreover, the accelerations and angular rates for all three BODY axes were recorded. The following Figures 6.26, 6.27, depict the small vessel during sea trials.

Figure 6.26: Test boat sea trial with transom nozzles enabled

Figure 6.27: Test boat sea trial with bow and stern nozzles enabled

What's more, the following Figures 6.28, 6.29, 6.30, 6.31, depict the parameters that were recorded through the data logger. This includes the position of the vessel in the x-y horizontal plane as well as the angles of pitch, roll and heading of the vessel, in the NED frame. Moreover, the accelerations and angular rates of each axis are presented, as recorded in the BODY frame.

Regarding position results, it can be seen that the deviation in x and y axes of NED frame is within logical limits when compared to the visual observation of the vessel's position. Consequently, the IMU sensor is capable of recording the position during dynamic positioning but for a limited time period. For extended time periods, the error accumulated by the sensors is heavily drifting the results and the use of a GPS coupled with an IMU is mandatory.

Regarding the recorded angle values, a constant deviation from 0 degrees is observed in pitch and roll, apart from the oscillatory components, which is due to the fact that the center of gravity was not properly configured at this stage and both two people that were on board had random position and were also moving. These factors contributed to a permanent inclination in pitch and roll.

Finally, both accelerations and angular rates are within reasonable value limits and gravitational acceleration is clearly depicted on z axis, with values around 1g.

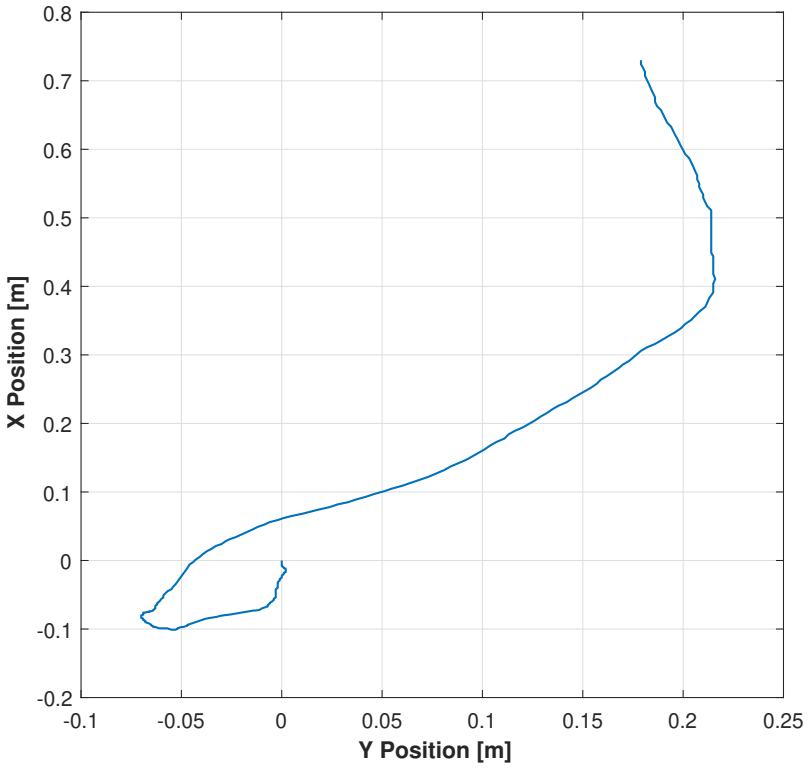

Figure 6.28: Recorded vessel position in NED frame during sea trial

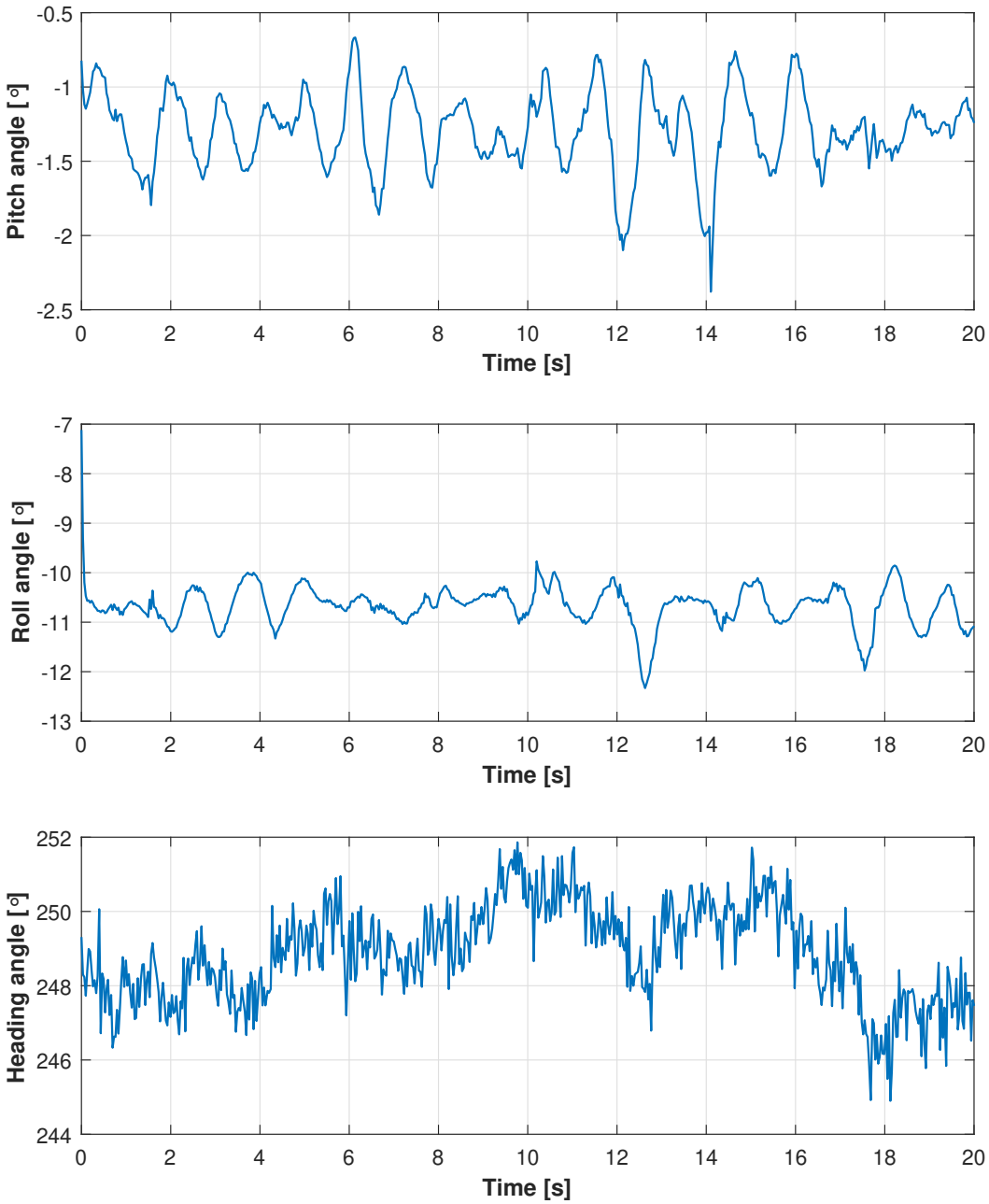

Figure 6.29: Recorded vessel pitch, roll and heading angles during sea trial

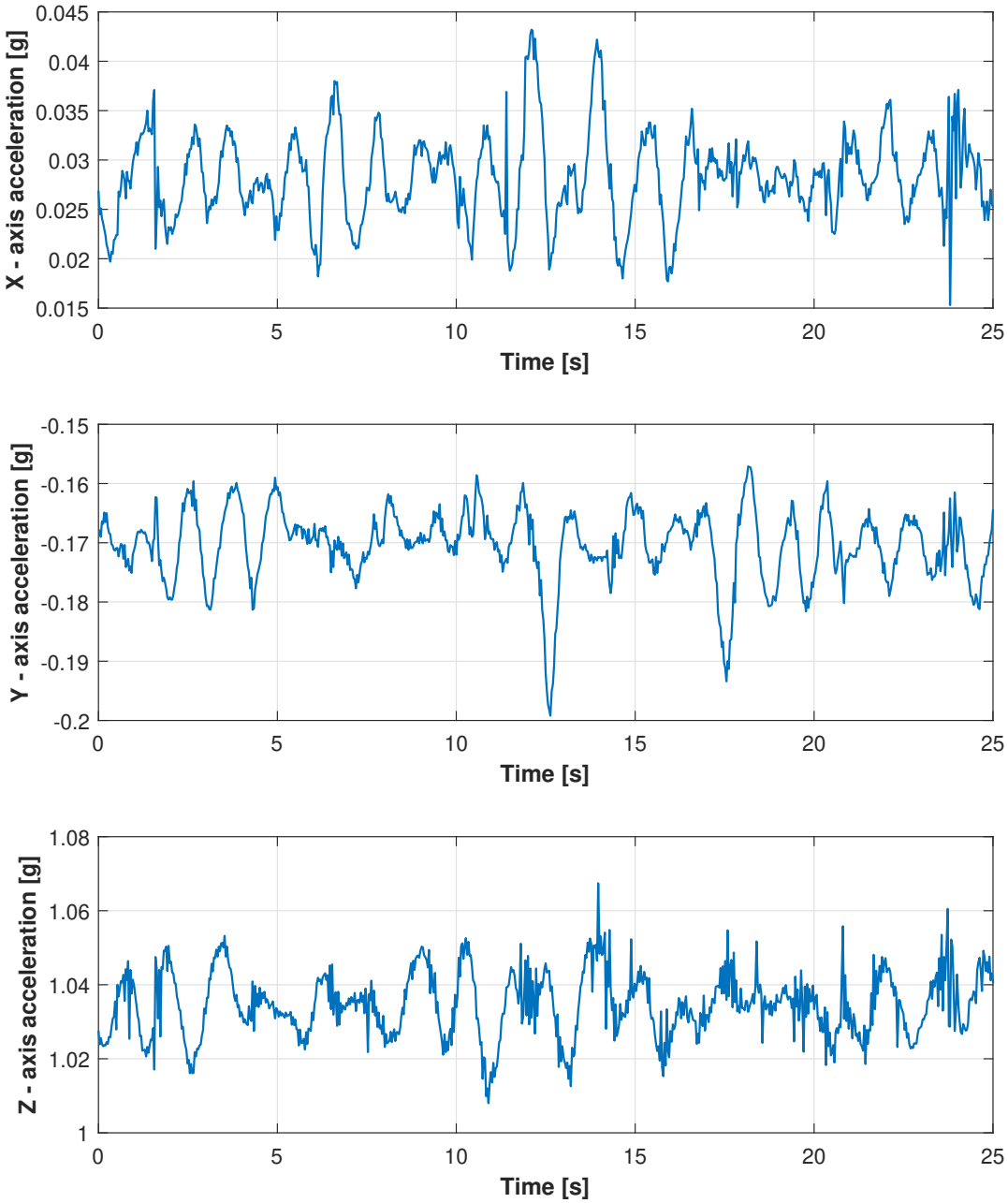

Figure 6.30: Recorded vessel accelerations on x,y,z axes during sea trial

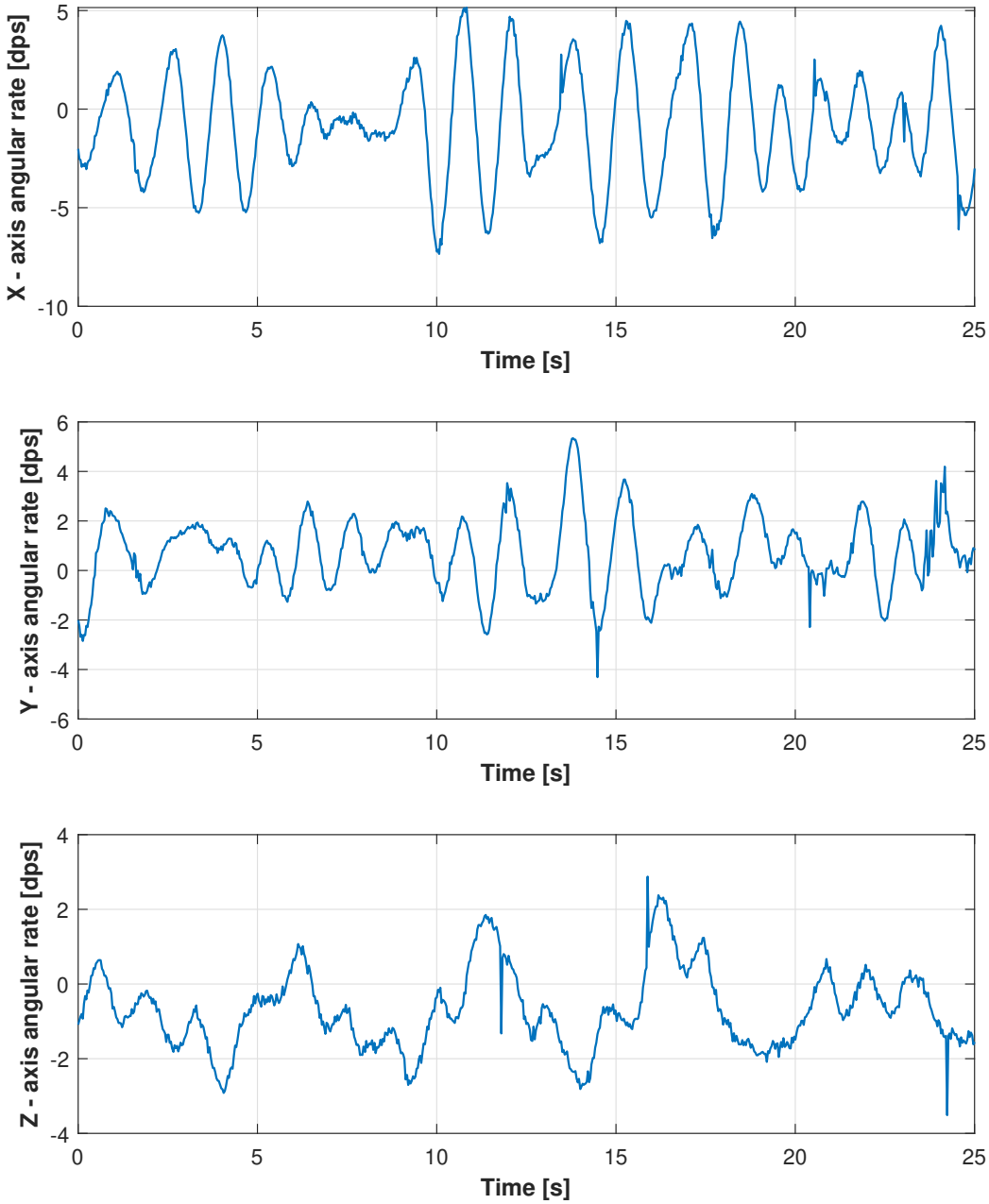

Figure 6.31: Recorded vessel angular rates on x,y,z axes during sea trial

Chapter 7

Conclusions and Future Work

Conclusions

In this thesis, the feasibility of implementing an alternative dynamic positioning system on a rescue vessel, which has no blades installed, was investigated. Specifically, a simulation model was constructed, which consisted of a linear vessel model and environmental models for waves, wind and ocean currents. Moreover, regarding the controller setup, it was decided to implement a simple nonlinear PID controller for the initial steps, accompanied by functional modifications to make the system stable. Finally, an actuator installation scheme was proposed, which gave the final system characteristic, that is the controlling vessel forces.

Dynamic positioning concept was evaluated on four different scenarios using MatLab Simulink, which included the general weather conditions that are usually encountered. The simulation results show that it is possible to install the specified DP system on the target vessel and perform DP operations within an acceptable range of environmental loads.

The second target of this thesis was to construct a measuring device, which estimates the position and heading of the vessel with the aid of an IMU solely, and will be ultimately used in future real vessel experiments. The enclosure box of the device was designed using CAD software and then 3D-printed, while all the required software was written in Python language. The results verify that it is possible to get acceptable estimations of position without using a GPS and the device performs its operational target without failures.

The final target of this thesis, was to install the proposed dynamic positioning system, consisted of a central centrifugal pump, electronically controlled ball valves and water ejection nozzles, into a smaller test boat for initial sea trials. The actuator geometrical scheme that was proposed for the simulations, was also used to install the nozzles in the boat.

Future Work

This thesis was part of a project, which is still active, and covered some of the required final targets. Consequently, based on the simulation's results, several improvements can be made to further enhance the next steps and, ultimately, achieve all the project's goals. The suggested future work is summarized in the next paragraphs.

- Controller: Although PID controllers are known for their robustness and ease of implementation, they lack knowledge of the underlying process, which can lead to limited controlling capabilities. As a result, a new controller type should be selected for controlling the vessel during sea experiments and final operation.

- Vessel parameters: In order to include a more advanced controller type, a more precise mathematical representation of vessel motions needs to be formulated. To achieve this, towing tests should be executed to obtain more precise values of the hydrodynamic vessel coefficients. Alternatively, these coefficients can be derived through CFD calculations, using the 3D hull model that is available.

- Actuator scheme: The proposed actuator positions result in a physical constraint, regarding the possible directions of vessel movement. Specifically, the vessel can only move forwards in surge direction. This leads to limitation of the possible environmental loads direction that can be countered. Consequently, a new actuator installation scheme should be considered to provide surge movement in both directions.

  Alternatively, another option is the adaptation of dynamic positioning to the concept of weathervaning. In such case, the vessel rotates around the z body axis in order to always face the environmental loads by the bow and not require reverse surge motion. This option, though, eliminates the possibility of heading control.

- Thrust allocation: The simulations required a thrust allocation scheme in order to derive the final acting forces upon the vessel for stabilization. Moreover, the internal model of each actuator that results to a specific applicable force was omitted.

  Due to the fact that the next project steps are based on a real boat, a model needs to be derived linking the required actuator force $\boldsymbol{\tau}$ to a physical parameter of the actuators. In this case, the possible parameter is the water flow inside the pipe system. A relationship between actuator force and flow should be generated, so as to complete the control concept in a real application environment.

Appendices

Appendix A

Wind Force Algorithm

```
function  y = wind(psi_cur,direction)

%------------------General constants--------------------------
rho_air = 1.225;       % air density at 15C [kg/m^3]
Loa = 11.6;            % length overall [m]
AFw = 4.61;            % frontal projected vessel area [m^2]
ALw = 14.82;           % lateral projected vessel area [m^2]
beta_w = direction;    % wind angle [deg]
bfspeed = 7;           % beaufort speed from table [knots]
height = 2;            % height for wind speed estimation
a = 1/7;               % wind profile coeff.
speed_sq = (0.5144*bfspeed*((height/10)^a))^2; % speed-squared
q =0.5*rho_air*speed_sq;                       % coefficient
gamma_w = psi_cur - beta_w - pi();             % true wind angle

%----------Blendermann - Kirchhoff plate -------------------
CDt =0.9 ;       % transverse resistance par
CDl_zero=0.55 ;  % longitudinal resistance par zero deg
CDl_pi=0.6 ;     % longitudinal resistance par pi deg
delta =0.6 ;     % cross-force parameter
sL =1.38 ;       % x-coord of centroid of AL_w from midship [m]

if abs(gamma_w) <= pi/2;
    CDl = CDl_zero*(AFw/ALw);
else
    CDl = CDl_pi*(AFw/ALw);
end

den = 1 - ((delta/2)*(1-(CDl/CDt))*(sin(2*gamma_w)^2));
CX = -CDl*(ALw/AFw)*(cos(gamma_w)/den);
CY = CDt*(sin(gamma_w)/den);
CN = ((sL/Loa)-(0.18*(gamma_w-(pi/2))))*CY;

Xwind = q*CX*AFw;     Ywind = q*CY*ALw;     Nwind = q*CN*ALw*Loa;
y = [Xwind,Ywind,Nwind];  %final wind force vector
```

Appendix B

Force Allocation Algorithm

```
function thrust = fcn(u,lxa,lxf)

pump_force = 30;           % [Kgf] pump thrust output
g = 9.81;                  % [m/s^2] gravitational acceleration
psplit = (pump_force*g)/3; %equal distribution

%-------------Force Allocation-------------------------------
xlim = psplit; % x axis nozzle force limit
ylim = 2*psplit; % y axis nozzle force limit
zlim = abs((psplit*lxa))+(psplit*lxf); % z axis nozzle force limit

%-------------Saturation of Control-------------------------
forces =[0,0,0]; % output thrust vector
%----x axis-----
if u(1)<=0
    u(1)=0; % not possible for reverse surge force
end

if abs(u(1))>= xlim
    u(1)= xlim;
end
%----y axis-----
if abs(u(2))>= ylim
    u(2)= sign(u(2))*ylim;
end
%----z axis-----
if abs(u(3))>= zlim
    u(3)= sign(u(3))*zlim;
end

forces(1)=u(1);
f2y = (u(3)-(u(2)*lxa))/(lxf-lxa);
f1y = u(2) - f2y;
forces(2)= f1y + f2y;
forces(3)= (f1y*lxa)+(f2y*lxf);
thrust = forces'; %final force vector
```

Bibliography

[1] Henrik Alfheim and Kjetil Muggerud. "Development of a Dynamic Positioning System for the ReVolt Model Ship". MA thesis. NTNU, 2017.

[2] Jens G Balchen, Nils A Jenssen, and S Sælid. "Dynamic positioning using Kalman filtering and optimal control theory". In: *IFAC/IFIP symposium on automation in offshore oil field operation*. Vol. 183. 1976, p. 186.

[3] Gary Bishop, Greg Welch, et al. "An introduction to the Kalman filter". In: *Proc of SIGGRAPH, Course* 8.27599-3175 (2001), p. 59.

[4] Werner Blendermann. "Parameter identification of wind loads on ships". In: *Journal of Wind Engineering and Industrial Aerodynamics* 51.3 (1994), pp. 339–351.

[5] Christiaan De Wit. "Optimal thrust allocation methods for dynamic positioning of ships". In: (2009).

[6] Sparkfun Electronics. *9-DOF IMU*. `https://www.sparkfun.com/products/13284`. 2018.

[7] Åsmund Våge Fannemel. "Dynamic positioning by nonlinear model predictive control". MA thesis. Institutt for teknisk kybernetikk, 2008.

[8] Thor I Fossen. *Handbook of marine craft hydrodynamics and motion control*. John Wiley & Sons, 2011.

[9] Thor I Fossen. "Marine Control System-Guidance, Navigation and Control of Ships, Rigs and Underwater Vehicles". In: *Marine Cybemetics* (2002).

[10] Thor I Fossen and Jann Peter Strand. "Passive nonlinear observer design for ships using Lyapunov methods: full-scale experiments with a supply vessel". In: *Automatica* 35.1 (1999), pp. 3–16.

[11] TI Fossen. *Marine GNC Toolbox*. `http://www.marinecontrol.org/download.html`. 2005.

[12] M Grimble, Ron Patton, and D Wise. "The design of dynamic ship positioning control systems using extended Kalman filtering techniques". In: *OCEANS'79*. IEEE. 1979, pp. 488–497.

[13] Håvard Halvorsen. "Dynamic positioning for unmanned surface vehicles". MA thesis. Institutt for teknisk kybernetikk, 2008.

[14] Øivind Kåre Kjerstad. "Weather-optimal positioning control for underactuated USVs". MA thesis. NTNU, 2010.

[15] *LINCOLN Project*. `http://www.lincolnproject.eu/`. 2016-2020.

[16] I Lindfors. "Thrust allocation method for the dynamic positioning system". In: *10th international ship control systems symposium (SCSS'93)*. 1993, pp. 3–93.

[17] John J Myers, Carl H Holm, and Raymond F McAllister. "Handbook of ocean and underwater engineering". In: (1969).

[18] Stein-Inge Torset Øien. "Dynamic Positioning for Small Autonomouse Surface Vessels". MA thesis. NTNU, 2016.

[19] Holland Marine Parts. *JT-30 Jet-Thruster*. `https://www.hollandmarineparts.nl/`. 2018.

[20] William Gerraint Price. "Probabilistic theory of ship dynamics". In: *Chapman and Hall* (1974), pp. 157–163.

[21] Martin Rindaroey and Tor Arne Johansen. "Fuel optimal thrust allocation in dynamic positioning". In: *IFAC Proceedings Volumes* 46.33 (2013), pp. 43–48.

[22] Rolls-Royce. *Autonomous Ship Project*. `https://www.rolls-royce.com/media/press-releases/2017/03-10-2017-rr-joins-forces-with-google-cloud-to-help-make-autonomous-ships-a-reality.aspx`. 2017.

[23] Eivind Ruth. "Propulsion control and thrust allocation on marine vessels". In: (2008).

[24] Steinar Saelid, N Jenssen, and J Balchen. "Design and analysis of a dynamic positioning system based on Kalman filtering and optimal control". In: *IEEE Transactions on Automatic Control* 28.3 (1983), pp. 331–339.

[25] Philip Salmony. *IMU Attitude Estimation*. `http://philsal.co.uk/projects/imu-attitude-estimation`. 2018.

[26] Per Sondre Sodeland. "Combined Dynamic Positioning and Optimal Wave Frequency Motion Damping of Surface Effect Ship". MA thesis. NTNU, 2015.

[27] Asgeir J Sørensen, Svein I Sagatun, and Thor I Fossen. "Design of a dynamic positioning system using model-based control". In: (1996).

[28] Mark W Spong, Seth Hutchinson, Mathukumalli Vidyasagar, et al. *Robot modeling and control*. Vol. 3. Wiley New York, 2006.

[29] Aleksander Veksler et al. "Dynamic positioning with model predictive control". In: *IEEE Transactions on Control Systems Technology* 24.4 (2016), pp. 1340–1353.

[30] Guoqing Xia et al. "Adaptive neural network controller applied to dynamic positioning of a remotely operated vehicle". In: *2013 MTS/IEEE OCEANS-Bergen*. IEEE. 2013, pp. 1–6.